PHOTO-INDUCED REDUCTIVE DISSOLUTION OF HEMATITE (α-Fe_2O_3) BY S(IV) OXYANIONS

Thesis by

Bruce Charles Faust

In Partial Fulfillment of the Requirements

for the Degree of

Doctor of Philosophy

California Institute of Technology

Pasadena, California

1985

(Submitted October 2, 1984)

Since brevity is the soul of wit,

And tediousness the limbs and outward flourishes.

I will be brief.

Shakespeare, Hamlet, II, 2

© 1984

Bruce Charles Faust

All Rights Reserved

ACKNOWLEDGEMENTS

Thanking all the people who contributed to this thesis would be an impossible task. I thank my advisor, Michael Hoffmann, for his continued support and advice throughout my graduate life. Thanks also to James Morgan for his advice and encouragement throughout my graduate career. I would also like to thank the members of my committee: Drs. Glen Cass, William Johnson, James Morgan, and John Seinfeld.

One cannot put in words the debt of gratitude that I owe to my friends Martha Conklin, Michael Lewy, Bill Munger, Laini Rothchild, and Costas Synolakis. The value of their constant support, encouragement, advice, and cajoling cannot be overestimated and is deeply appreciated. Thanks to Simon Davies for tolerating my numerous chemical queries and for providing me samples of goethite and lepidocrocite, and to Noel Smyth for proofreading this text. Elton Daly and coworkers provided helpful advice on numerous matters. The help of Sandy Brooks and Elaine Granger in the preparation of this document is especially appreciated. Financial support, from an S. D. Bechtel Fellowship and from the U.S. EPA is gratefully acknowledged.

Finally, it is to my parents, who have provided inestimable support throughout all of my endeavors, that I dedicate this thesis.

ABSTRACT

The kinetics and mechanism of the photo-induced reductive dissolution of hematite (α-Fe_2O_3) by S(IV) oxyanions, in aqueous suspensions of hematite, have been investigated. Experimental quantum yields for $Fe(II)_{aq}$ production are reported for deoxygenated hematite suspensions containing S(IV). Quantum yield studies together with spectroscopic information indicate that ≡Fe(III)—S(IV) surface complexes undergo a photo-induced ligand to metal charge transfer reaction resulting in the reductive dissolution of hematite and production of $Fe(II)_{aq}$.

The autoxidation of S(IV) in oxygenated hematite suspensions exhibits autocatalytic behavior. This behavior is interpreted in terms of three general processes: i) production of $Fe(II)_{aq}$ from photo-induced ligand to metal charge transfer reactions of ≡Fe(III)—S(IV) surface complexes, ii) oxidation of $Fe(II)_{aq}$ to $Fe(III)_{aq}$ and, iii) the $Fe(III)_{aq}$ catalyzed autoxidation of S(IV). A numerical model, based on these processes, is developed to predict the disappearance of S(IV) in oxygenated hematite suspensions under illumination.

TABLE OF CONTENTS

	Page
ACKNOWLEDGEMENTS	iv
ABSTRACT	v
TABLE OF CONTENTS	vi
LIST OF FIGURES	ix
LIST OF TABLES	xi
1. INTRODUCTION	1
1.1 Motivation to Study Photochemistry of Hematite and S(IV)	1
1.1.1 Atmospheric S(IV) Oxidations	1
1.1.2 Speciation of Fe(III) in Natural Waters	5
1.2 Scope and Objectives	6
2. THEORY AND BACKGROUND	7
2.1 Molecular Model of the Surface	7
2.1.1 Hematite Surface Speciation	7
2.1.2 Surface Coordination	8
2.1.2.1 Iron(III)-Anion Surface Complexes	8
2.1.2.2 Role in Dissolution	8
2.2 Photochemistry at Solid/Solution Interfaces	10
2.2.1 Models for Photo-Induced Surface Redox Reactions	10
2.2.1.1 Bulk Solid Excitation	10
2.2.1.2 Surface Complex Excitation	13
2.2.2 Observed Photochemical Behavior of Various Solids	15
2.3 Redox Chemistry of S(IV)	18

TABLE OF CONTENTS (Continued)

		Page
3.	MATERIALS AND METHODS	23
	3.1 Hematite Preparation and Characterization	23
	3.1.1 Synthesis of Hematite	23
	3.1.2 $Fe(III)_T$ Determination	23
	3.1.3 Powder X-ray Diffraction	24
	3.1.4 Particle Morphology	24
	3.1.5 Total Exchange Capacity	28
	3.1.6 Reflectance Measurements	29
	3.2 Photochemical Reactors	33
	3.2.1 Immersion Well Reactor	33
	3.2.2 Monochromatic Illumination System	33
	3.3 Materials and Reagents	38
	3.4 Analytical Techniques and Experimental Procedures	39
	3.4.1 S(IV)	39
	3.4.2 Fe(II) and Fe(III)	39
	3.4.3 Chemical Actinometry	40
	3.4.4 S(IV) Adsorption Experiments	41
	3.4.5 Deoxygenated Reactions	43
	3.4.6 Oxygenated Reactions	43
4.	RESULTS AND INTERPRETATIONS OF EXPERIMENTS	45
	4.1 Adsorption of S(IV) on Hematite	45
	4.2 Oxidation of S(IV)	51
	4.2.1 Reaction Stoichiometry	51
	4.2.2 Quantum Yields for Fe(II) Production in Deoxygenated Hematite Suspensions	53
	4.2.2.1 Reductive Dissolution of Hematite	53
	4.2.2.2 Excitation of Bulk Solid	64
	4.2.2.3 Excitation of Surface Complexes	66

TABLE OF CONTENTS (Continued)

		Page
4.2.3	Effect of Reaction Variables on Rate of S(IV) Oxidation by Molecular Oxygen	72
4.2.3.1	S(IV)	72
4.2.3.2	Total Surface Area	76
4.2.3.3	Oxygen	78
4.2.3.4	pH	78
4.3	Reaction Model	81
4.3.1	Kinetic Model for S(IV) Oxidation	81
4.3.1.1	General Model Description	81
4.3.1.2	Kinetic Model for Hematite Reductive Dissolution	82
4.3.1.3	Induced Oxidation of Fe(II) and S(IV)	83
4.3.1.4	Fe(III) Catalyzed Autoxidation of S(IV)	84
4.3.2	Model Predictions	84
4.3.3	Band Model Interpretation	89
5.	SUMMARY AND CONCLUSIONS	94
5.1	Reductive Dissolution of Hematite	94
5.2	S(IV) Oxidation	95
5.3	Roles of Surface Photo-redox Reactions in Natural Waters	95
	LITERATURE CITED	101
A.	EXPERIMENTAL DATA	108

LIST OF FIGURES

Figure		Page
1.1	Solubility of hematite as a function of pH.	4
2.1	Band formation in solids.	12
3.1	Scanning electron micrograph of hematite particles (Batch 1).	27
3.2	Reflectance spectra of hydroxylated and dry hematite (Batch 2).	30
3.3	Reflectance spectra of hematite (Batch 2), goethite, and lepidocrocite.	31
3.4	Reflectance spectra of hematite preparations dried at 20-25°C.	32
3.5	Immersion well reactor.	34
3.6	Spectrum of the ultraviolet filter.	35
3.7	Monochromatic illumination system.	37
3.8	Photochemical and thermal production of SCN^- in aqueous solutions of Reinecke's salt.	42
4.1	Adsorption kinetics of S(IV) on hematite.	46
4.2	Adsorption isotherms of S(IV) on hematite.	47
4.3	Photochemical and thermal solubilization of hematite in deoxygenated aqueous hematite suspensions containing S(IV).	54
4.4	i) Experimental quantum yields for aqueous Fe(II) production in deoxygenated hematite suspensions containing S(IV), and ii) charge transfer absorption band of an aqueous Fe(III)-S(IV) complex (λ = 367 nm).	57
4.5	i) Experimental quantum yields for aqueous Fe(II) production in deoxygenated hematite suspensions containing S(IV), ii) reflectance spectrum of hematite, and iii) absorption coefficients of hematite, after Marusak et al. (1980).	58

LIST OF FIGURES (Continued)

Figure		Page
4.6	Conceptual model of Fe(III) reduction in hematite suspensions containing S(IV).	63
4.7	A possible mechanism for the photo-induced reductive dissolution of hematite by S(IV).	71
4.8	Rate of S(IV) autoxidation as a function of [S(IV)].	73
4.9	Autocatalytic autoxidation of S(IV).	74
4.10	Effect of visible light on S(IV) autoxidation.	75
4.11	Pseudo-order rate constant for S(IV) autoxidation as a function of hematite concentration.	77
4.12	Reduction of molecular oxygen by S(IV).	79
4.13	Experimental rate constants for S(IV) autoxidation as a function of pH.	80
4.14	Experimental results and model predictions of S(IV) autoxidation rates, with monochromatic illumination.	85
4.15	Experimental results and model predictions of S(IV) autoxidation rates, with polychromatic illumination.	87
4.16	Experimental results and model predictions of S(IV) autoxidation rates for different oxygen partial pressures, with polychromatic illumination.	88
4.17	Conceptual model of the redox chemistry of oxygenated hematite suspensions containing S(IV).	90
4.18	A possible mechanism for S(IV) autoxidation in illuminated hematite suspensions.	93

LIST OF TABLES

Table		Page
3.1	X-Ray diffraction patterns of hematite reference standards and experimental preparations.	25
3.2	X-Ray diffraction reference and experimental data.	26
3.3	Ultraviolet-visible spectral distribution of the Hg-vapor lamp corrected for absorption by the UV filter.	36
4.1	Experimental quantum yields for aqueous Fe(II) production in deoxygenated hematite suspensions containing S(IV).	56
5.1	Band gap energies of some binary semiconductor compounds.	97

CHAPTER 1

INTRODUCTION

1.1 Motivation to Study Photochemistry of Hematite and S(IV)

1.1.1 Atmospheric S(IV) Oxidations

In urban atmospheres sulfuric acid is a major source of acidity in hydrometeors, clouds, and fogs (Waldman et al., 1982; Liljestrand and Morgan, 1981; Munger et al., 1983). A quantitative understanding of the rates of S(IV) to S(VI) transformation, for various pathways, is necessary for accurate predictions of the rate of acidity production in atmospheric water droplets (i.e., haze aerosol, fog, clouds, rain). The oxidation of S(IV) to S(VI) may occur in both gas and aqueous phases. Gas phase oxidation alone, by reactive radicals such as $^{\bullet}OH$, is insufficient to quantitatively account for observed tropospheric SO_2 oxidation rates (Sidebottom et al., 1972; Calvert et al., 1978; Calvert and Stockwell, 1984). This has served to focus attention on aqueous-phase oxidation of S(IV) by a variety of oxidants, such as O_3 (Erickson et al., 1977; Penkett et al., 1979; Maahs, 1983; Martin, 1984), H_2O_2 (Penkett et al., 1979; McArdle and Hoffmann, 1983; Martin and Damschen, 1981; Kunen et al., 1983), O_2 (Fe(III) catalyzed autoxidation) (Hoffmann and Jacob, 1984; Aubuchon, 1976; Martin, 1984) and oxidations by transition metal oxides (Bassett and Parker, 1951).

Oxidations involving molecular oxygen are very slow in the absence of specific catalysts, which are thought to "activate" either dioxygen or the reductant to a more reactive state than their

respective ground states (Valentine, 1973). Metals with at least two readily accessible formal oxidation states (Fe(III)/Fe(II), Mn(IV)/Mn(III)/Mn(II), and Cu(II)/Cu(I)) that can be reversibly reduced or oxidized by coordination to S(IV) and/or O_2 are likely to be effective catalysts in S(IV) autoxidation (Hoffmann and Boyce, 1983; Boyce et al., 1983; Hoffmann and Jacob, 1984). The catalytic autoxidation of S(IV) is inhibited by metal sequestration with ethylenediaminetetraacetate (EDTA) (Boyce, et al., 1983; Huss et al., 1978). By occupying all of the coordination sites on the metal, EDTA may prevent the coordination of either molecular oxygen or S(IV), and therefore the formation of an "activated" species — thereby reducing the reaction rate. The wide variety of mechanisms which are postulated to explain the metal catalyzed autoxidation of S(IV) classify into two major categories (Hoffmann and Boyce, 1983): i) two-electron polar reactions which invoke ternary complexes comprised of S(IV), O_2, and the transition metal (Bassett and Parker, 1951), and ii) one-electron radical chain mechanisms based on the mechanisms first suggested by Bäckström (1934) and Haber et al. (1931).

The aqueous phase photochemistry of S(IV) has been examined previously (Hayon, et al., 1972; Luňák and Vepřek-Šiška, 1976). The photochemical oxidation of S(IV) by O_2 can proceed by two general pathways: i) direct excitation of $SO_2 \cdot H_2O$, $HOSO_2^-$, SO_3^{2-}, or $S_2O_5^{2-}$, and ii) excitation of ligand to metal charge transfer bands in transition metal–S(IV) complexes. Aquated SO_2, $HOSO_2^-$, SO_3^{2-} and

$S_2O_5^{2-}$ have absorption maxima at 280, 190, <190 and 255 nm respectively (Hayon et al.. 1972; Golding, 1960); thus direct photochemical excitation of these S(IV) species can only be achieved with ultraviolet (UV) light. If oxygen is present, the excited S(IV) species react rapidly with O_2 to produce sulfate (Hayon et al., 1972). Photochemical reactions involving the direct excitation of S(IV) species are interesting but irrelevant to tropospheric transformations of S(IV) to S(VI), because as Zepp and Cline (1977) point out, essentially no light is transmitted to the surface of the earth at wavelengths (λ) < 295 nm and because $SO_2 \cdot H_2O$, $HOSO_2^-$, SO_3^{2-}, and $S_2O_5^{2-}$ all have absorption maxima at λ < 295 nm. The second photochemical pathway for the aqueous oxidation of S(IV) involves excitation of ligand to metal charge transfer bands in transition metal--S(IV) complexes (Luňak and Veprek-Šiška, 1976; Veprek-Šiška and Luňak, 1974; El-Wakil et al., 1983; Veprek-Šiška et al., 1974).

The roles of photochemical reactions occurring at solid/solution interfaces in the autoxidation of S(IV) in atmospheric water droplets have not been fully explored (Calvert, 1956). Frank and Bard (1977) reported results from a preliminary investigation of the oxidation of S(IV) on the surfaces of a variety of semiconductor solids, including one experiment with $[Fe_2O_3]$ = 10 g/L. Iron oxides such as hematite, because of their relative abundance and intrinsic insolubility (Figure 1.1), may have important roles in such transformations.

Foster (1969) found that α-Fe_2O_3 comprised 5-15 wt% of fuel ash

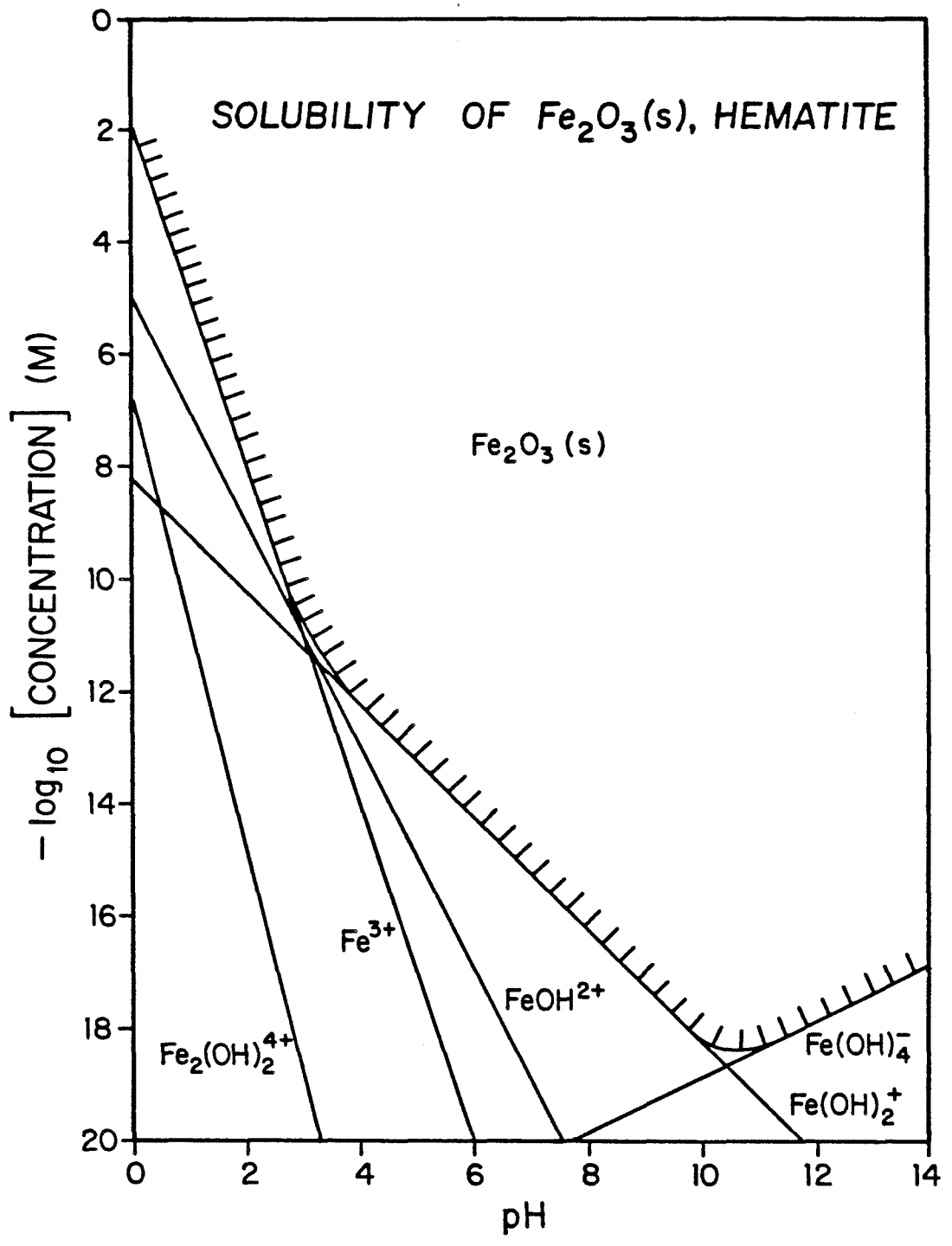

Figure 1.1. Solubility of hematite as a function of pH.

from power stations while Taylor and Flagan (1981) reported that Fe_2O_3 comprised a significant fraction of the ash from laboratory coal combustion experiments. Fukasawa et al. (1980) have specifically identified hematite, by X-ray diffraction analysis, as a component of airborne particulates. Munger et al. (1983) have measured total iron concentrations in fogs and clouds that exceed 10^{-4} M. Iron oxides also constitute substantial fractions of sand or soil dust in certain regions (Schrauzer, 1983). Given the relative abundance of Fe(III) (hydrous) oxides in aerosols and atmospheric waters, an investigation of their photo-redox behavior is warranted.

1.1.2 Speciation of Fe(III) in Natural Waters.

Most early limnological studies of lakes have concluded that the geochemistry of iron in epilimnions is dominated by the speciation of Fe(III), and that Fe(II) has a very small role in iron geochemistry of surface waters (Hutchinson, 1957). Although early studies reported apparent total Fe(II) concentrations in lake waters of approximately 1-3 μM (Muller, 1932; Hutchinson, 1957), the analytical techniques for Fe(II) were criticized for being subject to positive interferences from Fe(III), and therefore not specific for Fe(II). However, McMahon (1969) and Collienne (1983) have reported significant concentrations (1-6 μM) of $Fe(II)_{aq}$ in the epilimnions of several acidic lakes. They also reported that $Fe(II)_{aq}$ concentrations fluctuated in a diurnal and annual pattern.

Colliene reported increases of [$Fe(II)_{aq}$] in the empilimnion of 0.2 to 6 μM from February to June, which coincided with decreases in "particulate iron" and $Fe(III)_{aq}$ concentrations and which were not attributable to lake inflows. Furthermore, sterilizing agents did not inhibit the reduction process. Colliene concluded that photo-induced reductions of "soluble" and "particulate" iron were primarily responsible for increases in $Fe(II)_{aq}$ in the empilimnion. Waite (1983) has demonstrated that illumination of aqueous suspensions of γ-FeOOH containing citrate results in the reductive dissolution of the oxide.

1.2 Scope and Objectives

From the preceding discussion, it appears that photo-induced reductions of Fe(III) (hydrous) oxides, such as hematite, by adsorbed reductants (e.g. S(IV), organics) may play important roles in the geochemical cycling of iron in surface and atmospheric waters. The role of light in photo-induced reductions of iron (hydrous) oxides has not been elucidated. Additionally, photochemical reactions involving Fe(III) and S(IV) may be significant pathways for the oxidation of S(IV) in atmospheric droplets. For these reasons this study was initiated with the objectives of i) obtaining, through an experimental approach, information on the role of light in the oxidation of S(IV) on hematite, and ii) discussing the applicability of various theories of surface photochemical reactions in light of these results.

CHAPTER 2

THEORY AND BACKGROUND

2.1 Molecular Model of the Surface

2.1.1 Hematite Surface Speciation

As with other metal oxides, hematite has an amphoteric surface, the acid-base properties of which can be formalized by three different surface species (Schindler, 1981): i) a neutral species ($\equiv FeOH^{o}$), ii) a negatively charged one ($\equiv FeO^{-}$), and iii) a positively charged species ($\equiv FeOH_2^{+}$). Within limitations, the surface speciation can be represented as a diprotic acid with two "acid dissociation" reactions (Stumm and Morgan, 1981).

$$\equiv FeOH_2^{+} \rightleftharpoons \equiv FeOH + H^{+} \qquad K_{a1}^{s} \qquad (2.1)$$

$$\equiv FeOH \rightleftharpoons \equiv FeO^{-} + H^{+} \qquad K_{a2}^{s} \qquad (2.2)$$

Thus at the pH of zero net surface charge (pH_{zpc}), $[\equiv FeO^{-}] = [FeOH_2^{+}]$ in the absence of any other specifically adsorbable ions. Parks and de Bruyn (1962) report the zero point of charge for hematite to be $pH_{zpc} = 8.5$. For the pH range of experiments reported here (1-3), virtually all surface hydroxyl groups of hematite will be protonated in the absence of any other specifically adsorbable ions.

2.1.2 Surface Coordination

2.1.2.1 Iron(III)-Anion Surface Complexes

A number of anions (SO_4^{2-}, HPO_4^{2-}, SeO_3^{2-}, AsO_4^{2-}, HCO_3^-, $H_2SiO_4^{2-}$ and F^-) are adsorbed at goethite/water interfaces (Sigg and Stumm, 1980; Hingston et al., 1971). Furthermore, it has been suggested, on the basis of infrared spectra, that both SO_4^{2-} and PO_4^{3-} form binuclear bridging complexes ($<\equiv Fe>_2O_2XO_2$) with surface iron on goethite (Parfitt and Smart, 1977; Atkinson et al., 1970). From bond distances and bond angles of SO_3^{2-} (Strömberg et al., 1983), SO_4^{2-} (Parfitt and Smart, 1977), and FeO_6^{9-} (Tossel et al., 1973; Marusak et al., 1980), one calculates approximate Fe-Fe distances in hematite of 0.28 - 0.29 nm, compared with O-O distances in free SO_4^{2-} of 0.24 nm and in free SO_3^{2-} of 0.25 nm. This suggests that SO_3^{2-}, and possibly $HOSO_2^-$ may also form binuclear bridging complexes with surface iron in hematite.

2.1.2.2 Role in Dissolution

The rate of hematite dissolution is exceedingly slow in the pH range of most surface and atmospheric waters. Chang and Matijević (1983) studied the effects of a variety of aminocarboxylates on the rate of hematite dissolution. At pH = 3.0 in a 0.3 mM solution of EDTA, they found that hematite dissolved at a rate of 8.5×10^{-11} mole Fe/m^2-min at 25°C. Sidhu et al. (1981) reported a hematite dissolution rate of 3.9×10^{-9} mole Fe/m^2-min in 0.5 M HCl at 25°C. Furthermore, the dissolution rate of various iron (hydrous) oxides (magnetite, maghemite, hematite, goethite, lepidocrocite, and

akaganeite) was found to have a direct dependence on $[H^+]$ in solutions of $HClO_4$ and to be proportional to the quantity $[H^+][Cl^-]$ in chloride solutions. Thus there are at least two pathways for the dissolution of metal (hydrous) oxides (Grauer and Stumm, 1982): i) direct attack of the proton on hydroxylated surface metal species, and ii) proton attack of a surface complex. The second pathway dominates in the dissolution of iron (hydrous) oxides in chloride solutions. The dissolution rate expression can then be formulated in terms of ≡Fe(III)-Cl surface complexes, whose concentration can be expressesd in terms of a Langmuir adsorption isotherm (Cornell et al., 1976; Grauer and Stumm, 1982). Two explanations have been offered for the role that Cl^- plays in accelerating dissolution (Sidhu et al., 1981). Formation of ≡Fe-Cl surface complexes may polarize and therefore weaken bonds between Fe^{3+} and O^{2-}, and therefore reduce the activation energy of the bond breaking step(s). Another possibility is that specific adsorption of Cl^- (at low pH) reduces the net positive charge of the surface, and therefore reduces the electrostatic repulsion between protons and the surface.

The adsorption of a reductant onto iron (hydrous) oxides may enhance the rate of dissolution by an additional pathway, the reduction of lattice Fe(III) to Fe(II) followed by lattice detachment and desorption. Magnetite (Fe_3O_4) and maghemite (γ-Fe_2O_3) have similar crystal structures, except that in maghemite one ninth of the metal sites in the Fe_3O_4 spinel structure are

vacant (Murray, 1979). Sidhu et al. (1981) found that magnetite dissolved more rapidly than maghemite despite the fact that one ninth of the cation sites occupied by Fe in magnetite are vacant in maghemite. Cation vacancies are vacant coordination sites and generally unfavorable energetically, and could therefore enhance dissolution rates. Evidently the presence of Fe^{2+} cations in magnetite plays a more important role in dissolution than do cation vacancies in maghemite. One possible explanation of this phenomenon is that Fe^{2+} has a larger ionic radius (0.74 Å) than does Fe^{3+} (0.64 Å), which results in a longer and weaker iron-oxygen bond for Fe^{2+} than for Fe^{3+} (Sidhu et al., 1981). Since dissolution of iron oxy-hydroxides involves breakage of iron-oxygen bonds, bond weakening would reduce the activation energy for the dissolution process. Based on these observations, one might postulate that surface redox reactions of Fe(III) (hydrous) oxides, which produce lattice Fe(II), will enhance the dissolution rate of the oxide. Surface photo-induced reduction reactions of hematite would therefore result in increased dissolution rates of the oxide.

2.2 Photochemistry at Solid/Solution Interfaces

2.2.1 Models for Photo-Induced Surface Redox Reactions

2.2.1.1 Bulk Solid Excitation

Crystal field theory and/or the band model, are generally used to explain the electronic properties of many solids. The basic difference in the models is the degree to which charge carriers in

the solids are considered to occupy energy levels localized on the lattice atoms.

The band model (Morrison, 1980; Bard, 1979; Gerischer, 1979; Gerischer, 1977) considers that a three dimensional array of atoms have overlapping orbitals which form two energy "bands" (Figure 2.1) of delocalized molecular orbitals: i) lower energy bonding orbitals (valence band), and ii) higher energy anti-bonding orbitals (conduction band). This results in the formation of two distinct "bands" of closely spaced discrete energy levels separated by a characteristic "band gap" energy, E_G (hematite E_G = 2.34 eV). Generally electrons will occupy the lowest energy orbitals available, thereby filling the valence band orbitals and leaving vacant the conduction band orbitals. This does not facilitate electron movement (conduction) within the solid because filled and empty orbitals do not exist at the same energy level. When thermal or light energy greater than the band gap energy is supplied to the solid, low energy valence band electrons are promoted to higher energy states in the conduction band thereby creating vacancies (holes) in the valence band. This greatly enhances conduction within the solid because now both filled and empty orbitals exist at approximately equal energy levels. Rates of surface redox reactions may be accelerated by increased conduction in the solid.

Within the framework of the band model, surface photo-redox reactions may be viewed, in a simple way, as occurring in two steps (Gerischer, 1983). The first step involves absorption of light by

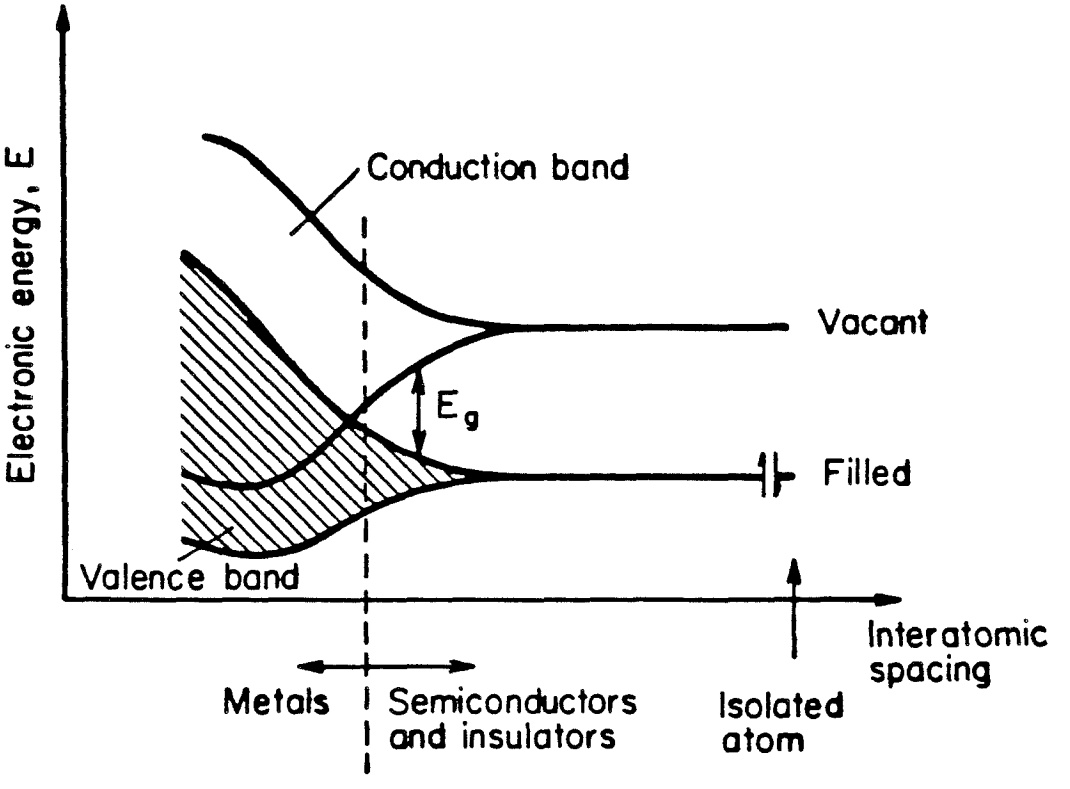

A. J. Bard and L. R. Faulkner,
Electrochemical Methods (1980)

Figure 2.1. Band formation in solids.

the solid and excitation of valence band electrons to higher energy conduction band orbitals. The second step is actually a competition between several processes: i) radiative and/or non-radiative decay of conduction band electrons to the valence band and, ii) electron transfer from adsorbed reductants to low energy valence band vacancies, and/or transfer of electrons from high energy conduction band orbitals to adsorbed oxidants.

Surface atoms have a different coordination environment than do bulk solid atoms, and may have higher energy levels which are located within the band gap. Electron transfer to or from the valence band may occur via these intermediate energy states (Kautek and Gerischer, 1982). Illuminated semiconductor solids function as catalysts or sensitizers, but only when both a solution phase oxidant and reductant are present, and then only when the rates of the two surface "half reactions" are equal. In all other cases net oxidation or reduction of the solid will occur (Gerischer, 1980).

2.2.1.2 Surface Complex Excitation

Theories applicable to solution phase charge transfer complexes may be applicable to surface complexes. In all likelihood, Fe(III) surface complexes on hematite, when illuminated with light of energy equivalent to the charge transfer transition, may undergo internal ligand to metal charge transfer resulting in more negative charge residing on the metal center.

No data exist on the charge transfer spectra of surface

complexes. Therefore, caution must be exercised in using information available from analogous solution phase charge transfer spectra, because charge transfer spectra of complexes will be slightly altered by their coordination environment at solid/solution interfaces. For a metal oxide such as hematite, two possible types of charge transfer reactions may be postulated to occur on the surface: i) charge transfer of surface hydroxyl species ($\equiv$Fe(III)—OH $\longrightarrow$ $\equiv$Fe(II) + OH$^{\cdot}$), and ii) charge transfer of surface complexes ($\equiv$Fe(III)—L $\longrightarrow$ $\equiv$Fe(II)+ P) where L and P represent a reductant (ligand) and product respectively. Solution complexes $FeOH^{2+}$ and $Fe_2(OH)_2^{4+}$ have charge transfer bands located at 300 and 335 nm respectively (Carey and Langford, 1975; Langford and Carey, 1975; Feeya and David, 1976). The positions of these charge transfer bands may reasonably approximate those of the $\equiv$FeOH surface complex. Aqueous phase charge transfer bands of $Fe(III)_{aq}$ complexes range from 283 nm for $Fe(oxalate)_3^{3-}$ to 510 nm for Fe(sulfosalicylate) (Lever, 1974; Agren, 1954). Thus $\equiv$Fe(III)—surface complexes, under illumination, may undergo a charge transfer reaction resulting in the production of Fe(II).

Illumination of solids with adsorbed reactants will promote two general processes: i) excitation of the bulk solid which may increase rates of surface redox reactions, and ii) direct excitation of the surface complexes which promotes charge transfer reactions. The relative contributions of the two pathways will depend on the solid and reactants of interest.

Observed Photochemical Behavior of Various Solids

Although some of the solids to be discussed in this section are not significant components of surface or atmospheric waters, observations on their photochemical reactivity may provide insight into the mechanisms of surface photo-redox reactions.

Becquerel (1839) was perhaps the first to report the phenomenon of photo-induced surface redox reactions when he observed that an electric current was produced upon irradiation of one of two similar electrodes immersed in dilute acid. Early research on surface photo-redox reactions was motivated by the possibility of using the visible and near ultraviolet portion of the solar spectrum to assist in the "splitting" of water into H_2 and O_2. However, Calvert et al. (1954), and Markham and Laidler (1953) reported that oxygenated aqueous suspensions of solids, such as ZnO, when illuminated with visible light gave H_2O_2 as the product, not hydrogen and oxygen. Additionally, small amounts of a variety of organic compounds increased the yield of hydrogen peroxide (Rubin et al., 1953; Calvert et al., 1954; Markham and Laidler, 1953). In particular, the work of Calvert et al. (1954) with ZnO, demonstrated several points. Through the use of O^{18} labelled oxygen and water they determined " that the oxygen in the hydrogen peroxide originates entirely from the oxygen gas for systems containing any of the additives studied (sodium formate, phenol, potassium oxalate, toluene, acetanilide) or in the additive-free solutions." They also found a direct correspondence between the experimental quantum yield

for hydrogen peroxide production and the region of light absorption by ZnO.

Surface photo-redox reactions of the various forms of TiO_2 have mainly been interpreted in terms of the band model, with localization of charge on surface states. Bahnemann et al. (1984), from flash photolysis studies of TiO_2 suspensions, report that "holes" or electrons are trapped at the oxide/water interface in the presence of adsorbed oxidants or reductants, respectively. They report a transient broad band spectrum, with a maximum at 430 nm, which they assume to be due to trapped holes (O^- lattice ion). However, Ti^{3+}_{aq} has an absorption band located at 500 nm; therefore surface ≡Ti(III) could be responsible for the observed absorption spectrum. Gravelle et al. (1971) report that illumination (200-600 nm) of TiO_2 (anatase or rutile) produces surface Ti(III), as determined from electron spin resonance spectra. Adsorption of $O_2(g)$ leads to O_2^- formation on the surface.

Herrmann and Pichat (1980) report that in illuminated and oxygenated suspensions of TiO_2 (anatase), I^- is oxidized at a rate approximately 80 times that of Br^-, while Cl^- apparently is not oxidized. Furthermore they demonstrate that the rate of I^- oxidation exhibits a saturation value with respect to $[I^-]$, consistent with their Langmuir adsorption model. Halide ions are known to form complexes with Ti^{4+}_{aq} (Cotton and Wilkinson, 1962), so formation of complexes with surface ≡Ti(IV) is quite plausible. The standard oxidation potentials for I^-, Br^-, and Cl^-

($2X^- \rightleftharpoons X_2 + 2e^-$) are -0.54, -1.09, and -1.36 volts, respectively (Latimer, 1952). Note that the oxidation rate of the halide ion increases as its standard oxidation potential increases, suggesting that the reaction rate may be related to the overall free energy change of the charge transfer reaction for this homologous series of reactions. Additionally, the standard potential for Cl^- oxidation by O_2 giving Cl_2 and H_2O as products is unfavorable (E^o = -0.13 V), which may explain the lack of observed reactivity for Cl^- oxidation.

The photochemistry of ZnS and CdS has also been interpreted in terms of the band model. Harbour and Hair (1977) have detected superoxide ion (O_2^-) upon illumination of oxygenated CdS suspensions. They also noted that addition of reductants to the solution increased the photoproduction of O_2^-. Becker and Bard (1983) have observed distinct photoluminescence bands upon irradiation of ZnS colloidal suspensions with energy greater than the band gap. They suggest that transitions of conduction band electrons back to the valence band give rise to the luminescence.

Kennedy and Friese (1978) studied the efficiency of current generation, in aqueous citrate solutions, of an illuminated Fe_2O_3 electrode to which a potential had been applied. For the same experimental conditions they found that increases in current efficiency corresponded to increases in citrate concentration until a "saturation" value of citrate was reached, upon which the efficiency remained constant. Furthermore, for a specified applied potential, the current efficiency in citrate solutions increased

significantly in the spectral region 504 to 360 nm. McGregor et al. (1979) reported that current efficiencies of an illuminated Fe_2O_3 electrode, at different applied potentials, exhibited pronounced peaks in the range of 360-390 nm. The lowest energy charge transfer band ($O^{2-} \longrightarrow Fe^{3+}$) in hematite, at 375 nm (Tossell et al., 1973; Marusak et al., 1980), corresponds quite well with the peak in current efficiency curves. This correspondence suggests that charges may be localized on lattice ions and surface states in hematite.

In his analysis of the oxides of first row transition metals, Morin (1959) suggested that when the 3d band (valence band) becomes very narrow, the 3d charge carriers can be considered to occupy energy levels localized on the cations. Further, he suggested that this is the likely case for α-Fe_2O_3.

2.3 Redox Chemistry of S(IV)

Reactions of ground state molecular oxygen with S(IV) species proceed at very slow rates in the absence of light or specific catalysts (Hoffmann and Boyce, 1983; Hoffmann and Jacob, 1984). The overall stoichiometry of these reactions is:

$$H_nO_2SO^{n-2} + 1/2\ O_2 \longrightarrow SO_4^{2-} + nH^+ \qquad (2.3)$$

where n = 0,1, or 2. In the pH range (1-3) of experiments reported here bisulfite ($HOSO_2^-$, n = 1) is a dominant species. The overall

standard free energy change of the reaction (ΔG^{o}_{rxn}) with bisulfite as the reductant is ΔG^{o}_{rxn} = -216.9 kJ/mole.

Transition metal ions which are capable of coordinating S(IV) and/or O_2, such as Fe^{3+}, accelerate the rate of S(IV) autoxidation. The mechanisms invoked to explain transition metal catalyzed S(IV) autoxidations can generally be classified into two categories: i) one-electron free radical reactions involving $SO_3^{\cdot-}$ and $SO_5^{\cdot-}$ as chain carriers and, ii) two-electron polar reactions involving ternary complexes comprised of the transition metal, S(IV), and molecular oxygen (Hoffmann and Boyce, 1983; Hoffmann and Jacob, 1984).

Backström (1934) proposed the following free radical mechanism, which is given here for the case of initiation (thermally and photochemically) by Fe(III):

$$\text{INITIATION} \quad FeOSO_2^{+} \xrightarrow{\Delta \text{ or } h\nu} SO_3^{\cdot-} + Fe^{2+} \qquad (2.4)$$

$$SO_3^{\cdot-} + O_2 \longrightarrow SO_5^{\cdot-} \qquad (2.5)$$

$$\text{PROPAGATION} \quad SO_5^{\cdot-} + SO_3^{2-} \longrightarrow SO_5^{2-} + SO_3^{\cdot-} \qquad (2.6)$$

$$SO_3^{2-} + SO_5^{2-} \longrightarrow 2\ SO_4^{2-} \qquad (2.7)$$

$$\text{TERMINATION} \quad 2\ SO_3^{\cdot-} \longrightarrow S_2O_6^{2-} \text{ and/or } SO_3 + SO_3^{2-} \qquad (2.8)$$

$$SO_3^{\cdot-} + SO_5^{\cdot-} \longrightarrow S_2O_6^{2-} + O_2 \qquad (2.9)$$

Hayon et al. (1972) have proposed an alternative chain propagation sequence involving sulfate radical ($SO_4^{\cdot-}$):

PROPAGATION

$$SO_5^{\bullet-} + SO_3^{2-} \longrightarrow SO_4^{\bullet-} + SO_4^{2-} \qquad (2.10)$$

$$SO_4^{\bullet-} + SO_3^{2-} \longrightarrow SO_4^{2-} + SO_3^{\bullet-} \qquad (2.11)$$

where reactions 2.10 and 2.11 can be viewed as alternatives to reactions 2.6 and 2.7. Molecular oxygen reacts rapidly with $SO_3^{\bullet-}$ ($k > 10^9$ M^{-1} sec^{-1}) to produce $SO_5^{\bullet-}$ (Hayon et al., 1972; Huie and Neta, 1984). Karraker (1963) has estimated that the rate of scavenging of $HOSO_2^{\bullet}$ by molecular oxygen is about thirty times faster than by Fe(III).

The rate limiting step in the Fe(III) catalyzed thermal autoxidation of S(IV) could be the initiation step (reaction 2.4). The formation constant for $FeOSO_2^+$ is $10^{7.2}$ M^{-1} (Kao, 1979), and the standard reduction potentials for the Fe^{3+}/Fe^{2+} and $SO_3^{\bullet-}/SO_3^{2-}$ couples are 0.77 and 0.63 V (versus N.H.E.) respectively (Latimer, 1952; Huie and Neta, 1984). Based on this thermodynamic information the standard free energy change for the reaction:

$$FeOSO_2^+ \rightleftharpoons Fe^{2+} + SO_3^{\bullet-} \qquad (2.12)$$

is ca. ΔG^o_{rxn} = +27.4 kJ/mole (E^o_{rxn} = -0.28 V). The unfavorable energetics of this step suggest that it could be the rate limiting step in the overall reaction sequence for thermally initiated Fe(III) catalyzed S(IV) autoxidation. This is consistent with kinetic observations of Fe(III) catalyzed S(IV) autoxidations, none of which exhibit an oxygen dependence. The general form of the rate expression for Fe(III) catalyzed S(IV) autoxidation (pH < 4) is:

$$\frac{d[S(IV)]}{dt} = k[Fe(III)][SO_3^{2-}] \qquad (2.13)$$

(Martin, 1984; Fuzzi, 1978; Aubuchon, 1976; Brimblecombe and Spedding, 1974).

Photochemical autoxidations of S(IV) may be initiated by either direct excitation of $SO_2 \cdot H_2O$, $HOSO_2^-$, SO_3^{2-} (Mason and Mathews, 1926; Mathews and Weeks, 1917; Hayon et al., 1972; Haber and Wansbrough-Jones, 1931) or by excitation of transition metal-S(IV) complexes. Excitation of SO_3^{2-} and/or $HOSO_2^-$ is generally thought to give rise to $SO_3^{\cdot-}$ and/or $HOSO_2^{\cdot}$, and e_{aq}^- (Hayon et al., 1972).

Photo-induced redox reactions of coordination compounds generally involve one-electron transfers because usually only one electron is transferred per absorbed photon (Kutal, 1983). Thus, for Fe(III)-S(IV) complexes, a photo-induced one-electron charge transfer reaction which produces $SO_3^{\cdot-}/HOSO_2^{\cdot}$ and Fe(II) seems plausible (Luňak and Vepřek-Šiška, 1976; El-Wakil et al., 1983). Surface ≡Fe(III)-S(IV) complexes may undergo similar charge transfer reactions. Photo-generated $SO_3^{\cdot-}/HOSO_2^{\cdot}$ radicals may then react with O_2 as described in reactions 2.5-2.9.

An alternative to the free radical mechanism, which postulates the existence of ternary complexes of Fe(III), S(IV), and O_2, is:

$$Fe^{3+} + HOSO_2^- \rightleftharpoons FeOSO_2H^{2+} \qquad (2.14)$$

$$FeOSO_2H^{2+} + SO_3^{2-} \rightleftharpoons Fe(OSO_2)_2H \qquad (2.15)$$

$$Fe(OSO_2)_2H + O_2 \rightleftharpoons Fe(OSO_2)HO_2 \qquad (2.16)$$

$$Fe(OSO_2)HO_2 + H^+ \longrightarrow Fe^{3+} + SO_4^{2-} + H_2O \qquad (2.17)$$

(Freiberg, 1975).

The reductive dissolution of hematite by S(IV) may proceed with the following stoichiometries:

$$\alpha\text{-}Fe_2O_3 + H_nO_2SO^{n-2} + (4-n)H^+ \longrightarrow 2Fe^{2+} + SO_4^{2-} + 2H_2O \qquad (2.18)$$

and/or:

$$\alpha\text{-}Fe_2O_3 + 2H_nO_2SO^{n-2} + (6-2n)H^+ \longrightarrow 2Fe^{2+} + S_2O_6^{2-} + 3H_2O \qquad (2.19)$$

where n can take values 0,1,2. The overall standard free energy change of reactions 2.4 and 2.5 with bisulfite ($HOSO_2^-$, n = 1) as the reductant are -106.3 and -38.1 kJ/mole, respectively. In the presence of oxygen, radical intermediates such as $SO_3^{\cdot-}$ and $HOSO_2^{\cdot}$ will react to give $SO_5^{\cdot-}$ and $HOSO_4^{\cdot}$ respectively, as first suggested by Bäckström (1934). Additionally, in the presence of oxygen, Fe(II) may be oxidized to Fe(III) with the following stoichiometry:

$$Fe^{2+} + 1/4\ O_2 + H^+ \longrightarrow Fe^{3+} + 1/2\ H_2O \qquad (2.20)$$

Thus iron may not undergo any net change in formal oxidation state. The rate of this reaction may be significantly accelerated by ligands which stabilize Fe(III) relative to Fe(II) (Kurimura et al., 1968; Tamura et al., 1976).

CHAPTER 3

MATERIALS AND METHODS

3.1 Hematite Preparation and Characterization

3.1.1 Synthesis of Hematite

Hematite was synthesized by the method of Matijević et al. (1978). The synthesis involved rapid mixing of 6.5 L of Q-H_2O (Section 3.3) pre-heated to 100°C with 0.5 L of an aqueous solution of $FeCl_3$/HCl or $Fe(ClO_4)_3$/$HClO_4$. Final concentrations of Fe(III) and H^+, after dilution, were ca. 0.035 M and 0.050 M respectively. The Fe(III) solution was then covered to prevent evaporation of H_2O and heated at 100°C for 24 hours. After 24 hours the solution, containing hematite, was decanted and the remaining suspension was "soaked" with 0.01 M $HClO_4$ for at least one day. The solution was then decanted and the washing procedure was repeated a minimum of three more times. This was done to remove Cl^- and any amorphous iron (hydrous) oxide coatings that might be present in the suspension.

3.1.2 $Fe(III)_T$ Determination

Total analytical iron concentrations of hematite stock suspensions, $Fe(III)_T$, were determined gravimetrically (Skoog and West, 1969). An aliquot of a well mixed hematite stock suspension was placed in a small pre-weighed porcelain crucible. The crucible containing the sample was then placed in an oven at 100°C until "dry", and then roasted at 950°C for two days. After removal from

the oven, the crucible was stored in a dessicator over $CaSO_4$ and allowed to cool to room temperature before weighing. Roasting the sample one additional day resulted in no additional loss of weight.

3.1.3 Powder X-ray Diffraction

Powder X-ray diffraction patterns were obtained with a Norelco vertical diffractometer using Cu($K\alpha$) radiation. Diffraction patterns of the synthetic hematite, along with reference patterns for hematite and other Fe(III) (hydrous) oxides, are presented in Tables 3.1 and 3.2. The observed patterns of the synthetic hematite are quite similar to the standard pattern for hematite. Peaks for other Fe(III) (hydrous) oxides are not observed in the hematite diffraction patterns. The X-ray diffraction patterns strongly suggest that the bulk composition of the iron oxide is indeed hematite. There is no evidence, in the X-ray diffraction patterns, of hematite to goethite surface weathering as observed by Bedarida and Pedemonte (1971).

3.1.4 Particle Morphology

A scanning electron micrograph (SEM) of Batch 1 hematite particles is presented in Figure 3.1. The particles are hexagonal platelets with approximate edge dimensions of 0.12 x 0.015 μm (Figure 3.1). The observed hexagonal platelet particle morphology is consistent with the rhombohedral crystal structure of hematite. Given the density of hematite as 5.24 g/cm^3

Table 3.1 X-ray diffraction patterns of hematite reference standard, and experimental preparations. Lattice spacings (d) and relative peak intensities (I/I_1) of the eleven most intense hematite standard peaks and the corresponding peaks for the hematite preparations used in this work.

Hematite Standard*		Hematite Preparations			
		Batch 1		Batch 2	
d (Å)	I/I_1	d (Å)	I/I_1	d (Å)	I/I_1
3.66	25	3.72	22	3.69	44
2.69	100	2.72	100	2.70	98
2.51	50	2.53	79	2.52	100
2.201	30	2.220	29	2.210	35
1.838	40	1.850	46	1.840	46
1.690	60	1.702	74	1.697	53
1.596	16	1.607	23	1.604	16
1.484	35	1.489	40	1.487	35
1.452	35	1.458	53	1.456	42
1.310	20	1.310	22	—	—
0.908	25	—	—	—	—

* Joint Committee on Powder Diffraction Standards "high reliability" rating

Table 3.2 X-Ray diffraction reference and experimental data.

Mineral or Compound	JCPDS* card	Most intense d-spacings (Å) (Relative intensity)							
Batch 1 Hematite α-Fe_2O_3	--	3.72 (22)	2.72 (100)	2.53 (79)	2.220 (29)	1.850 (46)	1.702 (74)	1.489 (40)	1.458 (53)
Batch 2 Hematite α-Fe_2O_3	--	3.69 (44)	2.70 (98)	2.52 (100)	2.210 (35)	1.840 (46)	1.697 (53)	1.487 (35)	1.456 (42)
Hematite α-Fe_2O_3	13-534	3.66 (25)	2.69 (100)	2.51 (50)	2.201 (30)	1.838 (40)	1.690 (60)	1.484 (35)	1.452 (35)
Goethite α-FeOOH	17-536	4.18 (100)	2.69 (30)	2.49 (16)	2.452 (25)	2.192 (20)	1.721 (20)	1.564 (16)	
Lepidocrocite γ-FeOOH	8-98	6.26 (100)	3.29 (90)	2.47 (80)	1.937 (70)	1.732 (40)	1.524 (40)	1.367 (30)	1.075 (40)
Akaganeite β-FeOOH	13-157	7.40 (100)	5.25 (40)	3.31 (100)	2.61 (40)	2.543 (80)	1.944 (60)	1.635 (100)	1.438 (80)
Maghemite γ-Fe_2O_3	5-615	5.95 (60)	3.75 (100)	3.42 (65)	2.950 (100)	2.521 (100)	2.089 (100)	1.702 (100)	1.608 (100)
Magnetite Fe_3O_4	19-629	4.85 (8)	2.967 (30)	2.53 (100)	2.424 (8)	2.096 (20)	1.715 (10)	1.616 (30)	1.485 (40)
b-FeOOH	13-87	4.61 (20)	2.545 (100)	2.25 (100)	1.685 (100)	1.471 (100)	1.271 (20)	1.223 (20)	

* Joint Committee on Powder Diffraction Standards

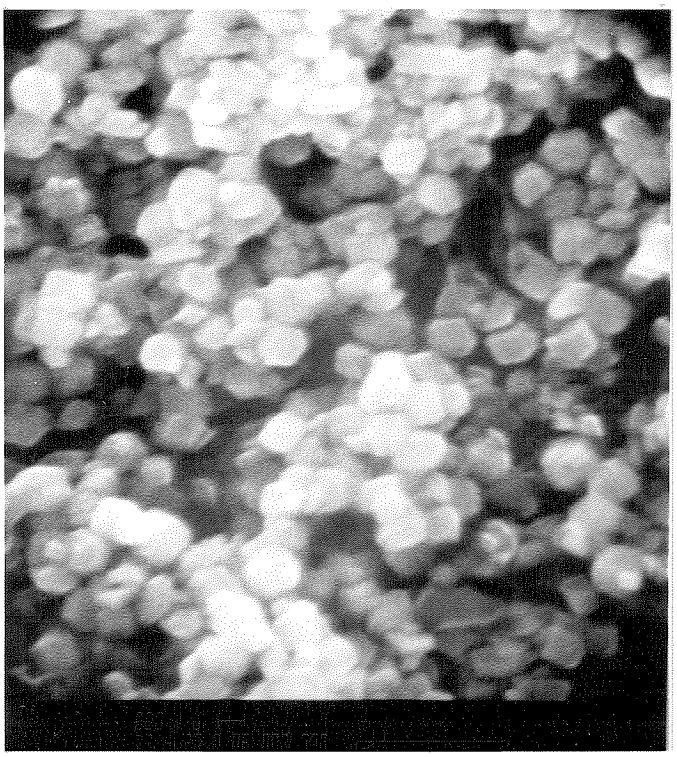

Figure 3.1. Scanning electron micrograph of hematite particles (Batch 1).

(Weast and Astle, 1980-81), and an average of 9 surface hydroxyl groups per 100 $(\text{Å})^2$ of hematite surface (Morimoto et al., 1969; Dana and Ford, 1960), the fraction of iron atoms present as surface sites, for the hexagonal platelets of hematite, is ca. 1.5%. There is no evidence, in the scanning electron micrograph (Figure 3.1), for the formation of goethite crystals on the surface of hematite particles as observed by Bedarida et al. (1973).

3.1.5 Total Exchange Capacity

The total exchange capacity of hematite was determined by fluoride desorption measurements of hematite which had previously been equilibrated in a 0.05 M NaF solution at pH = 3.6 ($HClO_4$). High concentrations of fluoride were used to insure that nearly all surface hydroxyl groups were exchanged for F^-. Fluoride adsorption experiments were carried out at pH = 3.6 because fluoride adsorption onto α-FeOOH was found to exhibit an adsorption maximum between pH 3-4 (Hingston, 1981). After a 15-30 minute adsorption period the solution was filtered and the solid was rinsed with a small volume of dilute $HClO_4$ (pH = 4.0). Fluoride was desorbed from the hematite particles in 50 ml. of a pH = 8.5 buffer (242 g tris-(hydroxymethyl)-aminomethane, 230 g sodium tartrate ($Na_2C_4H_4O_6 \cdot 2H_2O$), and 84 ml concentrated HCl, diluted to 1.0 liter with Q-H_2O). Following a 15-30 minute desorption period, the solution was filtered and the fluoride activity of the filtrate was measured with a specific fluoride electrode, using standards

prepared from the same buffer with dried (120°C) NaF. This gives. for Batch 2 hematite, [Total exchange sites]/[α-Fe_2O_3] = 0.09 i.e. approximately 4.5% of the total iron is present as surface sites.

3.1.6 Reflectance Measurements

Reflectance spectra were obtained with a Beckman UV 5240 spectrophotometer equipped with an integrating sphere. Reflectance spectra of α-Fe_2O_3 (both dry and hydroxylated), α-FeOOH (goethite), and γ-FeOOH (lepidocrocite) are presented in Figures 3.2 - 3.4. Except for the one dry sample of hematite, all solids prepared for reflectance measurements were stored in a humidified atmosphere at approximately 20-25°C to insure that surface sites remained hydroxylated. Little difference exists between the reflectance spectra of hydroxylated and dry hematite samples, as illustrated in Figure 3.2. The similarity of reflectance spectra suggests that, for hematite particles of the size used in this investigation, hydroxylation of surface sites has little effect on the ultraviolet-visible spectrum of the bulk sample. This is consistent with the fact that surface sites represent only 1.5-4.5% of the total iron for hematite used in this investigation. Figure 3.3 illustrates that absorption edges for α-Fe_2O_3, α-FeOOH, and γ-FeOOH all occur in the region 520-570 nm which demonstrates that the presence of hydroxyl groups in the solid, even at stoichiometric levels, does not cause a large shift in the absorption edge. As evidenced in Figure 3.4, reflectance spectra of Batch 1 and Batch 2

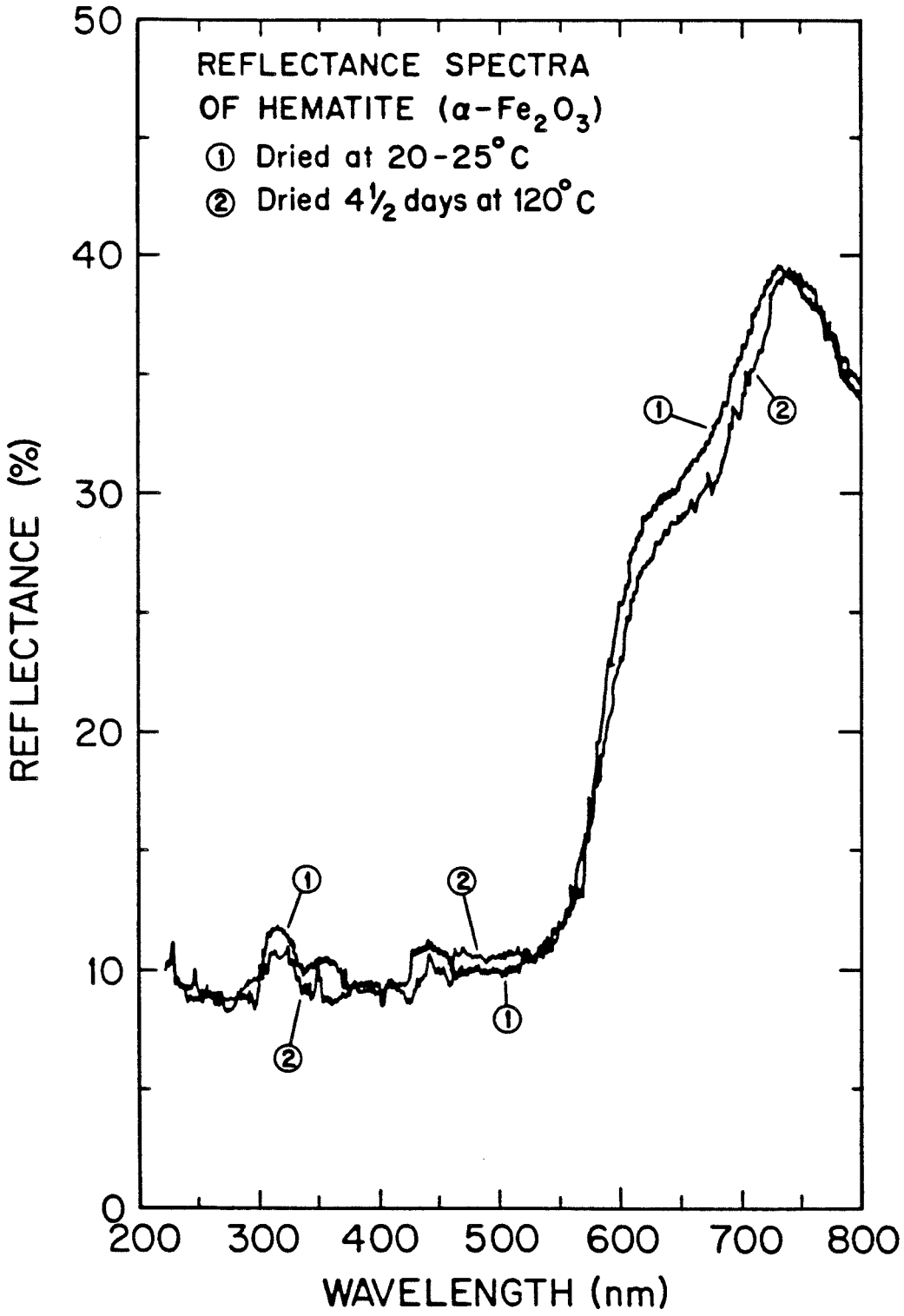

Figure 3.2. Reflectance spectra of hydroxylated and dry hematite (Batch 2).

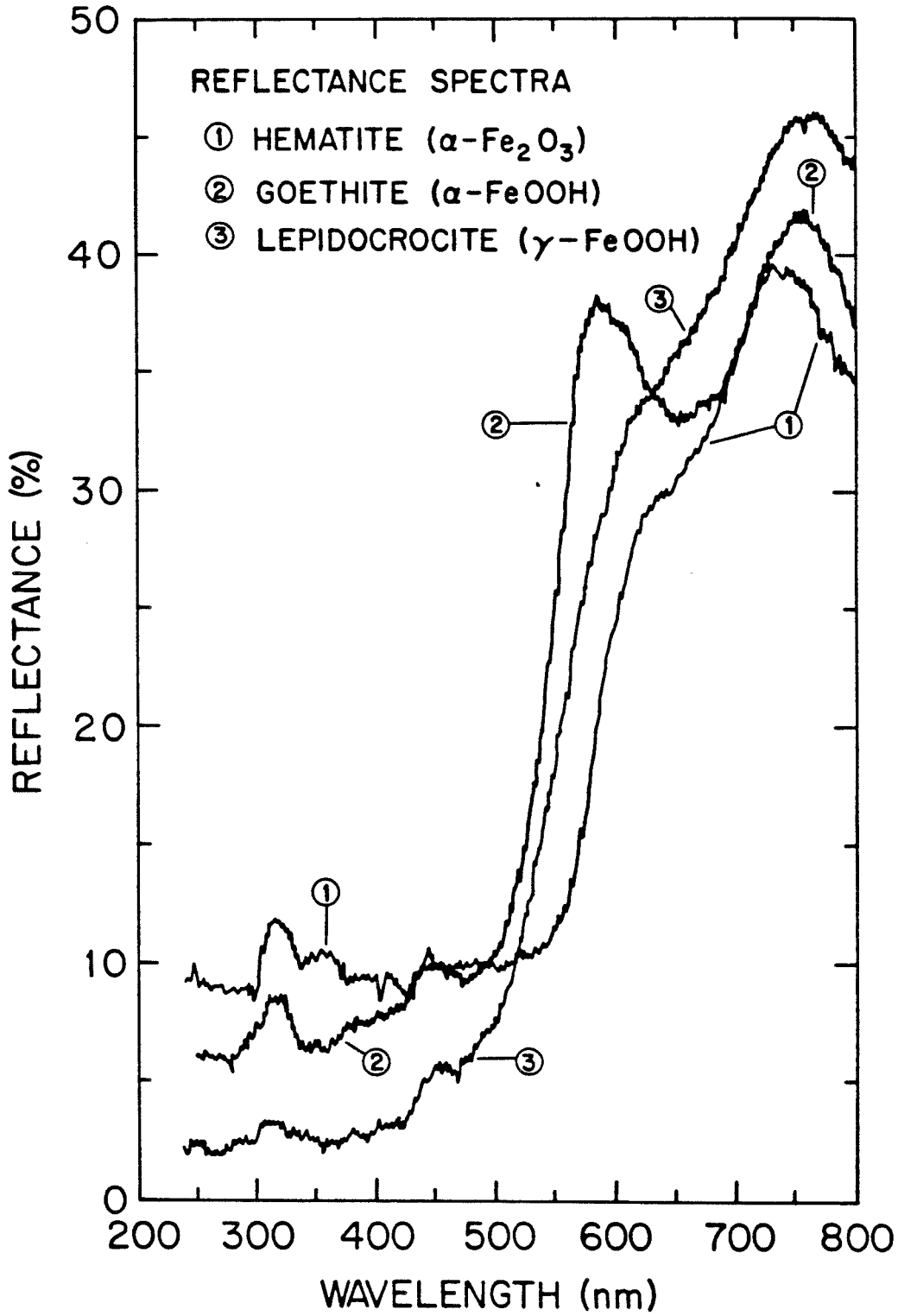

Figure 3.3. Reflectance spectra of hematite (Batch 2), goethite, and lepidocrocite. All solids were dried at 20-25°C.

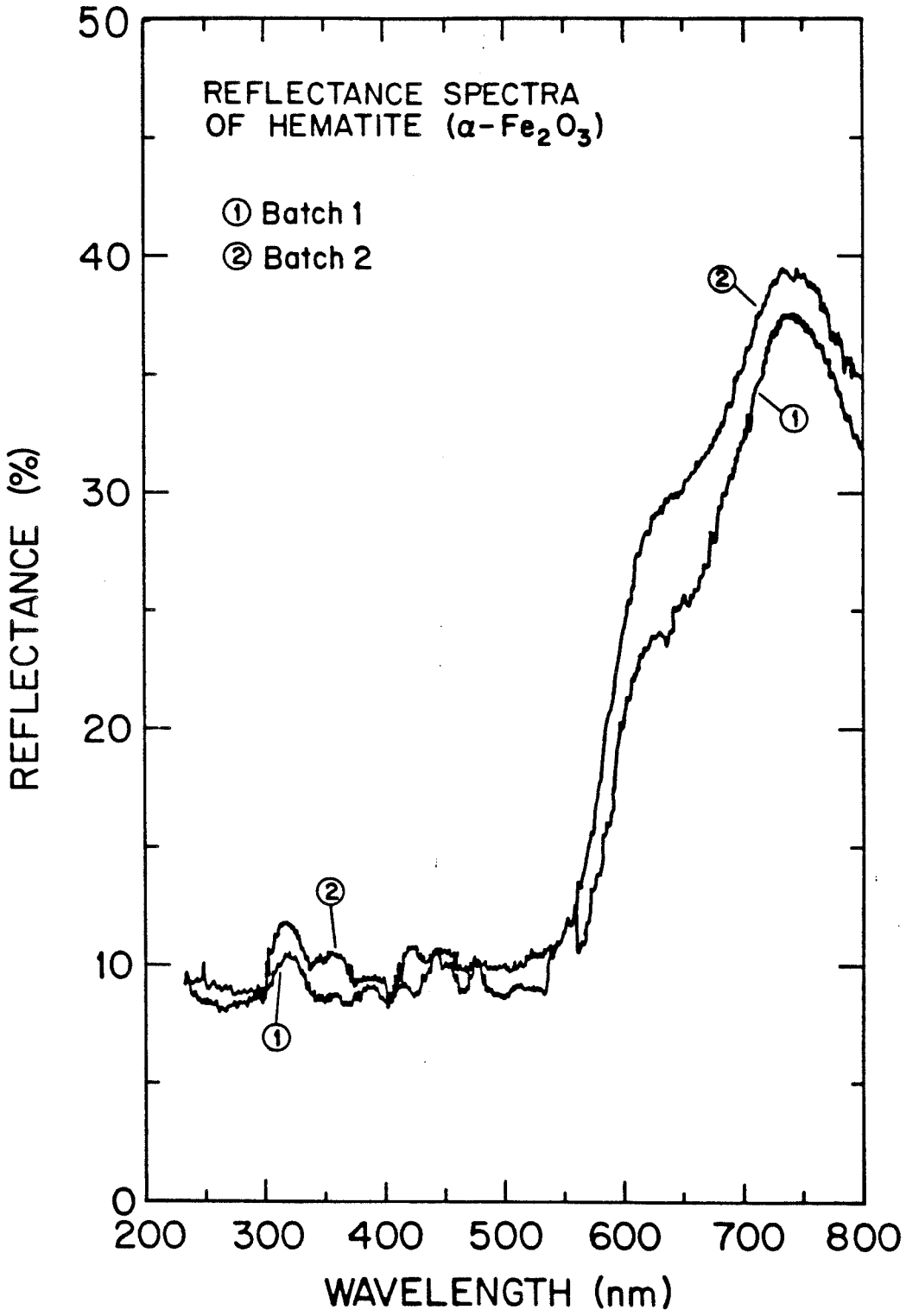

Figure 3.4. Reflectance spectra of hematite preparations dried at 20-25°C.

hematite samples are similar.

3.2 Photochemical Reactors

3.2.1 Immersion Well Reactor

An immersion well reactor (IWR), equipped with a 450 W Hg-vapor lamp and an ultraviolet (UV) filter was used for experiments not requiring monochromatic light. The reactor volume is 0.75 L and the light path length is 1.0 cm. Figures 3.5 and 3.6 illustrate the immersion well reactor and the ultraviolet/visible absorption spectrum of the filter respectively. The spectral distribution of the Hg-vapor lamp, corrected for absorption by the UV filter, is presented in Table 3.3. Note, from Figure 3.6, that the filter has essentially zero transmittance for wavelengths < 330 nm. The use of this filter for all experiments utilizing the immersion well reactor precludes the possibility of direct excitation of $SO_2 \cdot H_2O$, $HOSO_2^-$, SO_3^{2-}, and $S_2O_5^{2-}$, all of which exhibit absorption maxima at wavelengths < 300 nm.

3.2.2 Monochromatic Illumination System

The monochromatic illumination system (MIS) that was used is illustrated in Figure 3.7. Monochromatic light was generated by focussing light from a 450 W Xe light source (Osram) through an infrared (water) filter into a 100 mm focal length holographic grating monochromator, and through an appropriate order sorting filter. The collimated beam was then used to illuminate a tubular

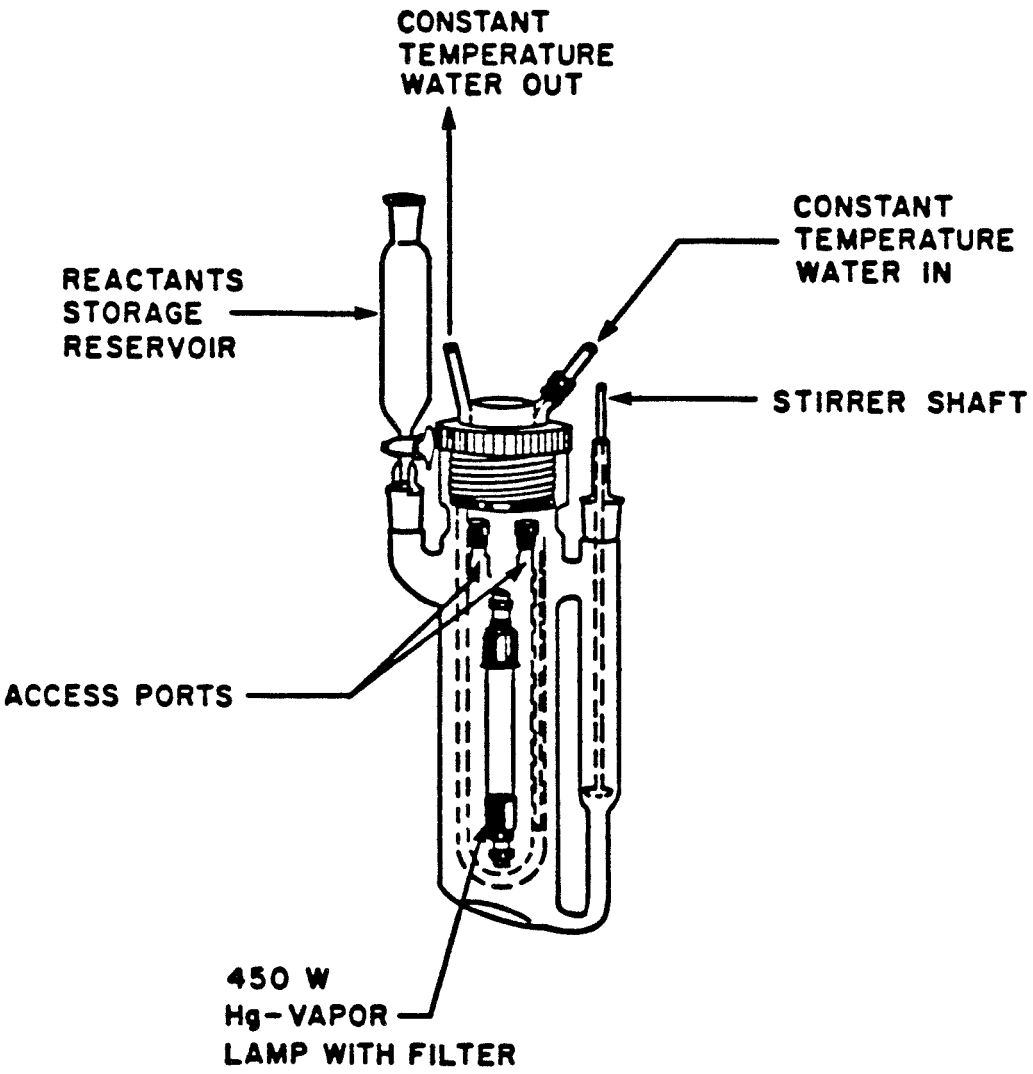

Figure 3.5. Immersion well reactor.

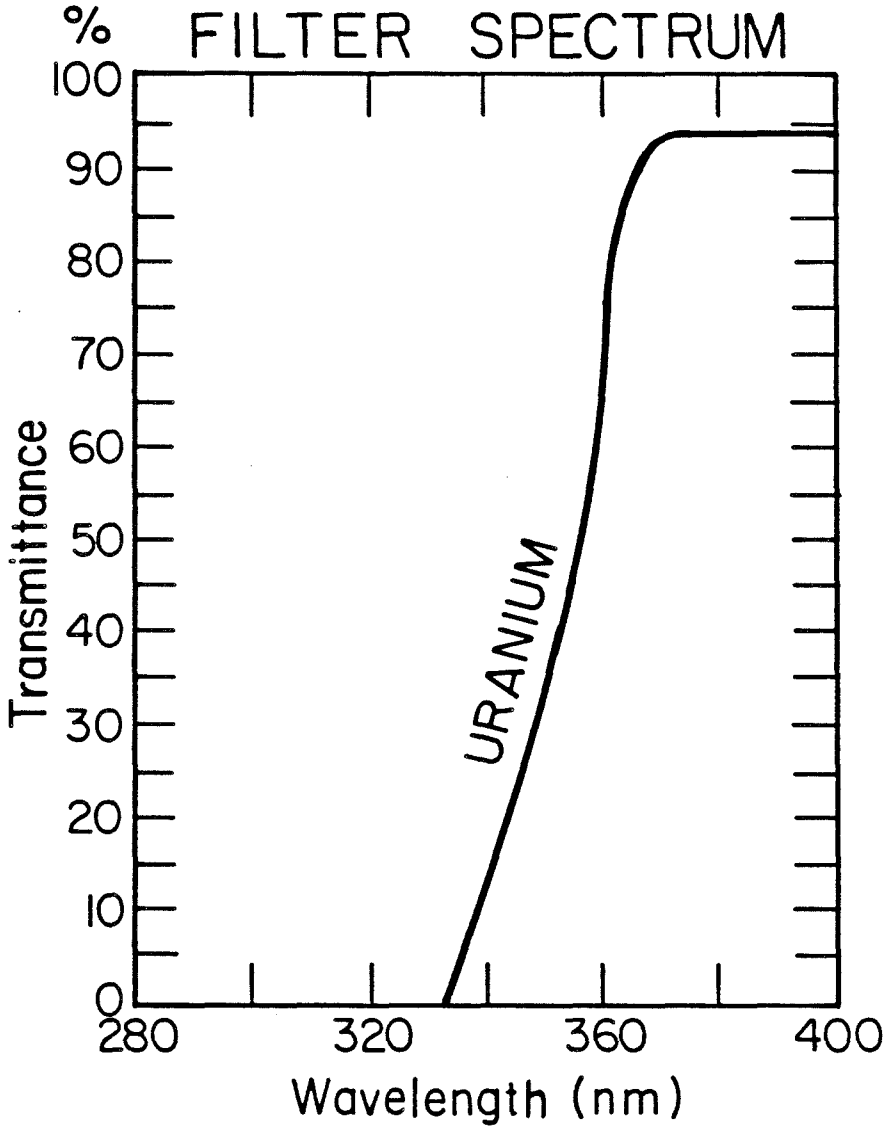

Figure 3.6. Spectrum of ultraviolet filter.

Table 3.3 Ultraviolet-visible spectral distribution of the Hg-vapor lamp corrected for absorption by the UV filter.

Wavelength (nm)	Intensity m(einstein)/min
366.0	4.3
404.5	2.1
435.8	4.2
546.1	6.3
578.0	5.4

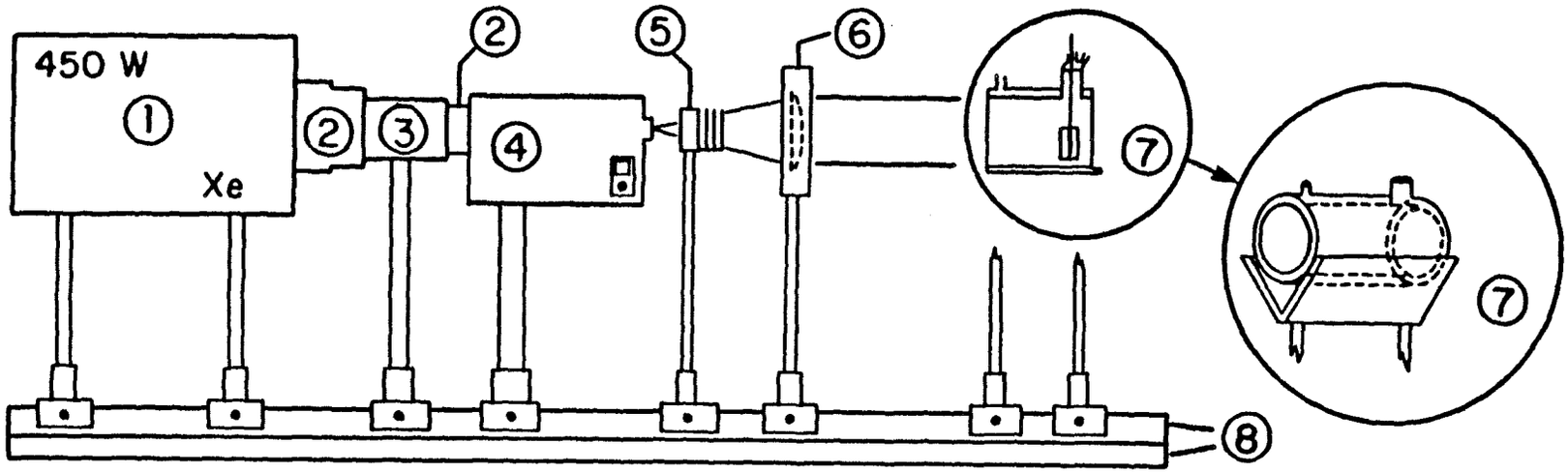

Figure 3.7. Monochromatic illumination system. 1. 450 W Xe lamp and housing. 2. Light shields. 3. Liquid (infrared) filter. 4. 100 mm holographic grating monochromator. 5. Optical filter holder. 6. Collimating lens. 7. Reaction vessel and holder.

pyrex reactor (10 cm path length, 0.37 L volume) equipped with optical pyrex glass faces at both ends. The bandwidth, with 4 mm slitwidths, is approximately 25 nm.

3.3 Materials and Reagents

All solutions were prepared from analytical grade reagents and high purity water ("Q-H_2O," resistivity > 18 Mohm-cm) which was produced by passing either tap or deionized water sequentially through a reverse osmosis membrane, carbon filter, two ion exchange membranes, and a 0.22 μm filter (Millipore). One molar S(IV) stock solutions were prepared from dried anhydrous Na_2SO_3 and standardized with IO_3^-/I^- as the primary standard (Vogel, 1961). The first S(IV) stock solution was found to be identical, within experimental error, to the direct weighing of Na_2SO_3 when corrected for the lot analysis. Subsequent standard S(IV) stock solutions were prepared gravimetrically from dried Na_2SO_3 and corrected for the lot analysis. All S(IV) stock solutions were stored under nitrogen gas in an unpressurized glove box. Filtered (0.2 μm Nuclepore) $NaClO_4$ (G. Frederick Smith) solutions (4.0 M) were used to adjust the ionic strength to 0.1 M.

A constant temperature of 25 ± 1°C for all experiments was maintained with a temperature controlled recirculating water bath. All pH measurements were made with an Altex Φ-71 pH meter equipped with a Radiometer combination glass electrode, using at least three standards bracketing the actual pH of the sample. For all kinetics

experiments and S(IV) adsorption experiments, the ionic strength was adjusted to 0.1 M with $NaClO_4$.

3.4 Analytical Techniques and Experimental Procedures

3.4.1 S(IV)

Throughout kinetics experiments, samples were periodically taken and filtered through 0.2 μm Nuclepore filters. Samples for S(IV) analyses were preserved by addition of an aliquot of the filtrate to a small known volume of a solution containing NaH_2PO_4/Na_2HPO_4, NaOH, and the disodium salt of ethylenediaminetetraacetate (EDTA), giving total phosphate and EDTA concentrations, after dilution, of 0.05 M and 10^{-3} M respectively, and a final pH of 6.8-8.0. Samples were then stored in the dark at $5^{o}C$ until they were analyzed for either S(IV) or $Fe(II)_{aq}$. Decreases in [S(IV)], in samples preserved by this method, were less than 7% over a period of 34 days.

The spectrophotometric method of Humphrey et al. (1970), using 5,5'-dithiobis-(2-nitrobenzoic acid) (DTNB) as the "color forming" reagent, was used for S(IV) determinations. Stock solutions of DTNB were prepared by dissolving the solid in 95% ethanol. DTNB reacts with $SO_3^{=}$ producing 2-nitro-5-sulfhydrylbenzoic acid, which has an absorption peak at 408 nm that was monitored and found to obey the Lambert-Beer law with respect to [S(IV)].

3.4.2 Fe(II) and Fe(III)

Samples were preserved for $Fe(II)_{aq}$ analyses by acidifying an

aliquot of the filtrate to pH ≈ 1 with H_2SO_4, and purging them with nitrogen gas to remove all S(IV) and thus quench further redox reactions, such as the rapid electron transfer that occurs between $Fe(III)_{aq}$ and S(IV) in the presence of 1,10-phenanthroline (Carlyle, 1972).

Analyses for $[Fe(II)_{aq}]$ used the modified 1,10-phenanthroline technique of Tamura et al. (1974), with fluoride added to complex Fe(III) and thereby prevent its interference in the $[Fe(II)_{aq}]$ measurement. For measurements of total aqueous iron ($[Fe(aq)]_T$ = $[Fe(II)_{aq}] + [Fe(III)_{aq}]$), 0.1 M hydroxylamine sulfate was substituted for the NH_4F to reduce all $Fe(III)_{aq}$ to $Fe(II)_{aq}$, which was then measured using 1,10-phenanthroline.

3.4.3 Chemical Actinometry

Reinecke's salt, $KCr(NH_3)_2(NCS)_4$, was used as a chemical actinometer (Wegner and Adamson, 1966). The potassium form of Reinecke's salt was used for actinometry because it is more soluble than the ammonium form of the salt. Preparation of the potassium salt involved dissolving 100 grams of $NH_4Cr(NH_3)_2(NCS)_4$ in one litre of pre-heated (50-60°C) Q-H_2O. All operations for the preparation of the K-form of the salt were performed under red light. Because the thermal aquation reaction occurs at a moderate rate at 50-60°C, it is important to rapidly dissolve the solid. A small amount of impurity will, however, not dissolve. After the salt has dissolved, 150 grams of KNO_3 is rapidly added to the mixture and dissolved. At

this point the solution may be rapidly filtered or decanted to remove solid impurities, cooled rapidly to 0-5°C, and kept at this temperature until precipitation and settling of the solid have occurred. The solution is then decanted, the solid washed with 5°C Q-H_2O, and then filtered to remove most of the water. The solid is then dried in a vacuum dessicator, over P_2O_5, until dry.

The aqueous complex, $Cr(NH_3)_2(NCS)_4^-$, undergoes a ligand exchange reaction in which SCN^- is exchanged for H_2O. The ligand substitution reaction is accelerated when the complex is illuminated with visible or ultraviolet light. Solutions of Reinecke's salt, in 0.1 M $HClO_4$, were photolyzed and the released SCN^- was determined immediately by a colorimetric method which involved adding $Fe(III)_{aq}$ in ten-fold excess and measuring the absorbance, at 450 nm, of the $Fe(SCN)^{2+}$ complex. $[Fe(III)]_{aq}/[SCN^-]$ ratios greater than ten insured that the 1:1 complex predominated under analytical conditions. The corresponding release of SCN^- from the thermal (dark) aquation reaction was also monitored and the results were used to determine a thermal aquation rate which was subtracted from the photochemical aquation rate. Examples of the thermal and photo-induced aquation reactions are presented in Figure 3.8. Chemical actinometry, when required, was performed immediately prior to the experiment of interest.

3.4.4 S(IV) Adsorption Experiments

Batch S(IV) adsorption experiments, at constant pH, were carried

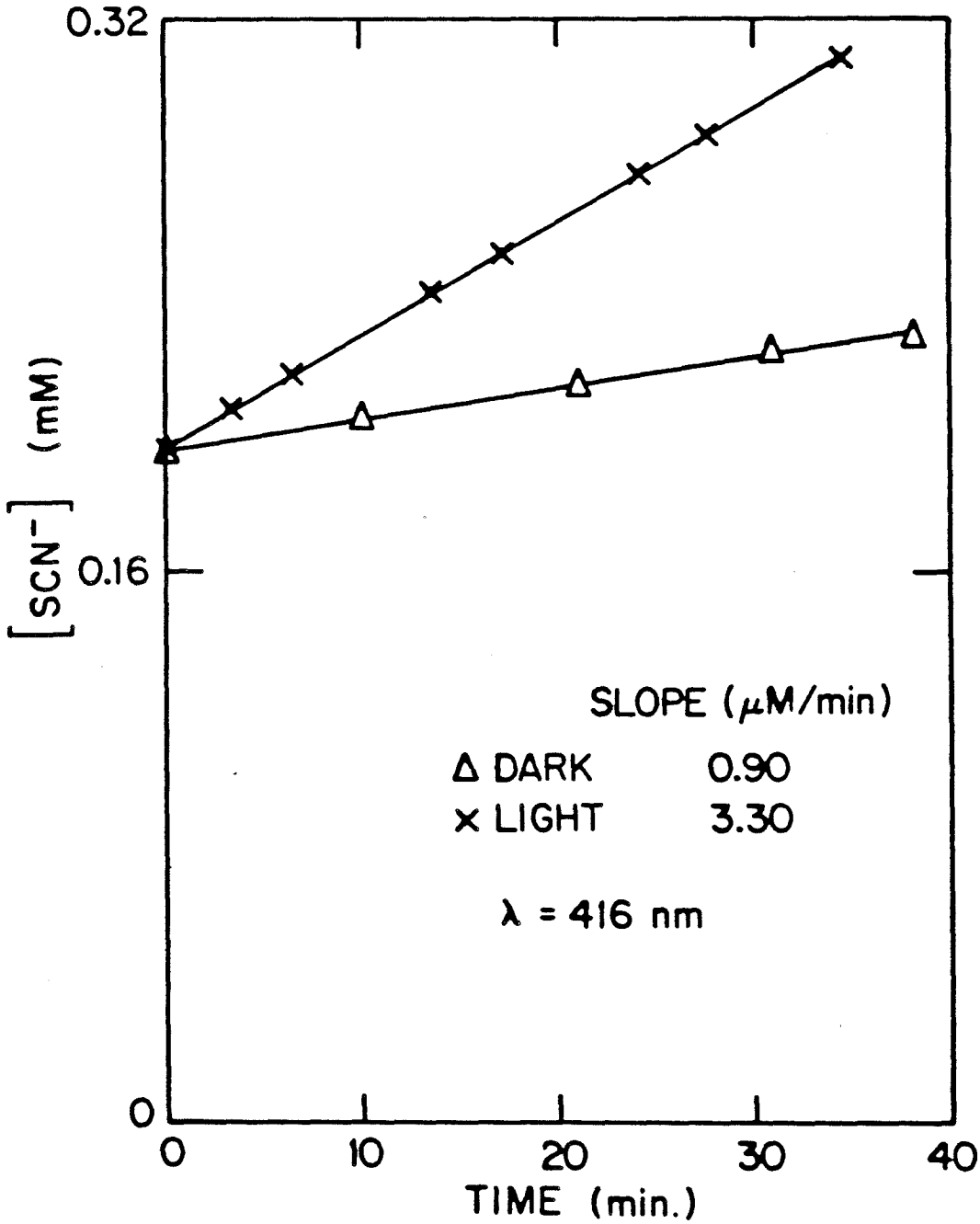

Figure 3.8. Photochemical and thermal production of SCN^- in aqueous solutions of Reinecke's salt.

out by addition of aliquots of a S(IV) stock solution to 25 ml of a hematite suspension. The samples were continuously mixed on a shaker in the dark for 90 minutes, after which sample aliquots were filtered and preserved for S(IV) analyses.

3.4.5 Deoxygenated Reactions

Deoxygenated solutions were prepared by purging them with nitrogen gas. Residual oxygen in the nitrogen gas was removed by passing the nitrogen through acidified solutions of V(II) which rapidly reduce oxygen (Skoog and West, 1969). Reactant solutions with low $[O_2(aq)]$ were prepared by purging a hematite suspension with N_2 for a minimum of one hour. After deoxygenation, an aliquot of Na_2SO_3 stock solution was transferred into the suspension. The reactants were then transferred to the reactor which had previously been purged with nitrogen. All reagent transfers were performed under nitrogen in an unpressurized N_2 glove box. Experiments which required solutions to have low $[O_2(aq)]$ were carried out under nitrogen gas, which was flowed continuously over the surface of the reacting solution throughout the course of the experiment.

3.4.6 Oxygenated Reactions

For oxygenated reactions, an aqueous solution of $HClO_4/NaClO_4$ was purged with O_2/N_2 mixtures of specific partial pressure for at least one hour. After oxygenation, aliquots of stock Na_2SO_3 and α-Fe_2O_3 solutions were added, in the order listed. The solution was gently,

but thoroughly mixed, and then introduced into the immersion well reactor, with the Hg-vapor lamp and UV filter in place. The Hg-vapor lamp had been operating for at least 30 minutes prior to the introduction of the reactants into the reactor. Periodically throughout the experiment samples were withdrawn, filtered through 0.2 μm filters, and preserved for S(IV) analyses by the method previously described.

CHAPTER 4

RESULTS AND INTERPRETATIONS OF EXPERIMENTS

4.1 Adsorption of S(IV) on Hematite

Results of adsorption kinetics experiments, presented in Figure 4.1, indicate that S(IV) adsorptive equilibrium is attained in a few minutes. Isotherms for S(IV) adsorption on α-Fe_2O_3 are presented in Figure 4.2, along with model calculations for a two site Langmuir adsorption model. Both pH and [α-Fe_2O_3] for the adsorption experiments are identical to those used in quantum yield experiments. As evidenced in Figure 4.2, there appear to be two different surface complexes with significantly different formation constants.

The results of the adsorption experiments are modeled using a two-site Langmuir adsorption isotherm:

$$[S(IV)]_{ADS} = \frac{K_I X_1 [S(IV)]_{aq}}{1 + K_I [S(IV)]_{aq}} + \frac{K_{II} X_2 [S(IV)]_{aq}}{1 + K_{II} [S(IV)]_{aq}} \qquad (4.1)$$

where X_1 and X_2 are the molar concentrations of the two types of sites, $[S(IV)]_{aq}$ and $[S(IV)]_{ADS}$ are the molar concentrations of all aqueous and adsorbed S(IV) species respectively, and K_I, K_{II} are the stability constants of the surface complexes. Note that the adsorption data did not fit a one site model. The functional relationship between specific surface area, A_s (m^2/g), and molar concentration of surface sites, $X_T = X_1 + X_2$, is given by

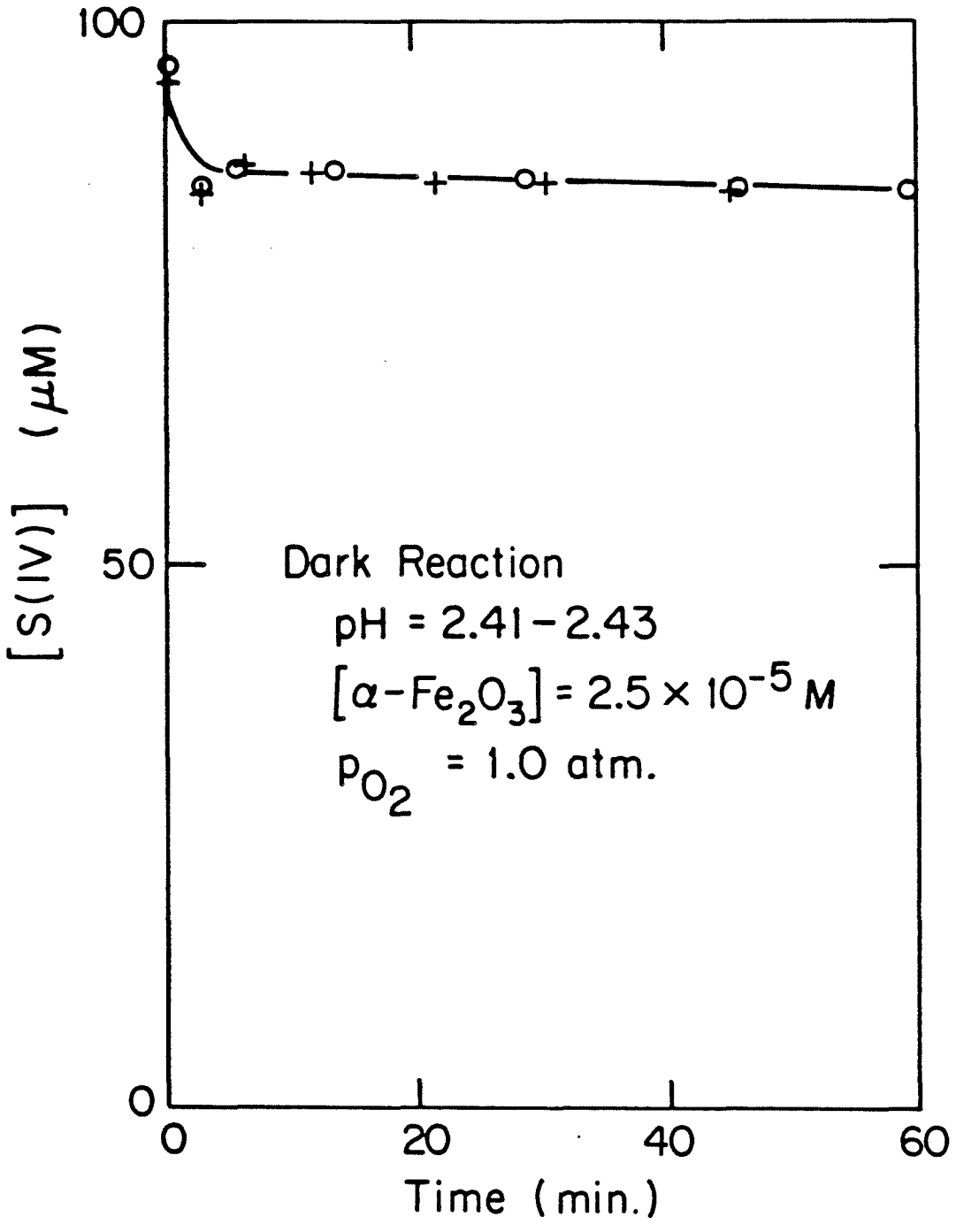

Figure 4.1. Adsorption kinetics of S(IV) on hematite.

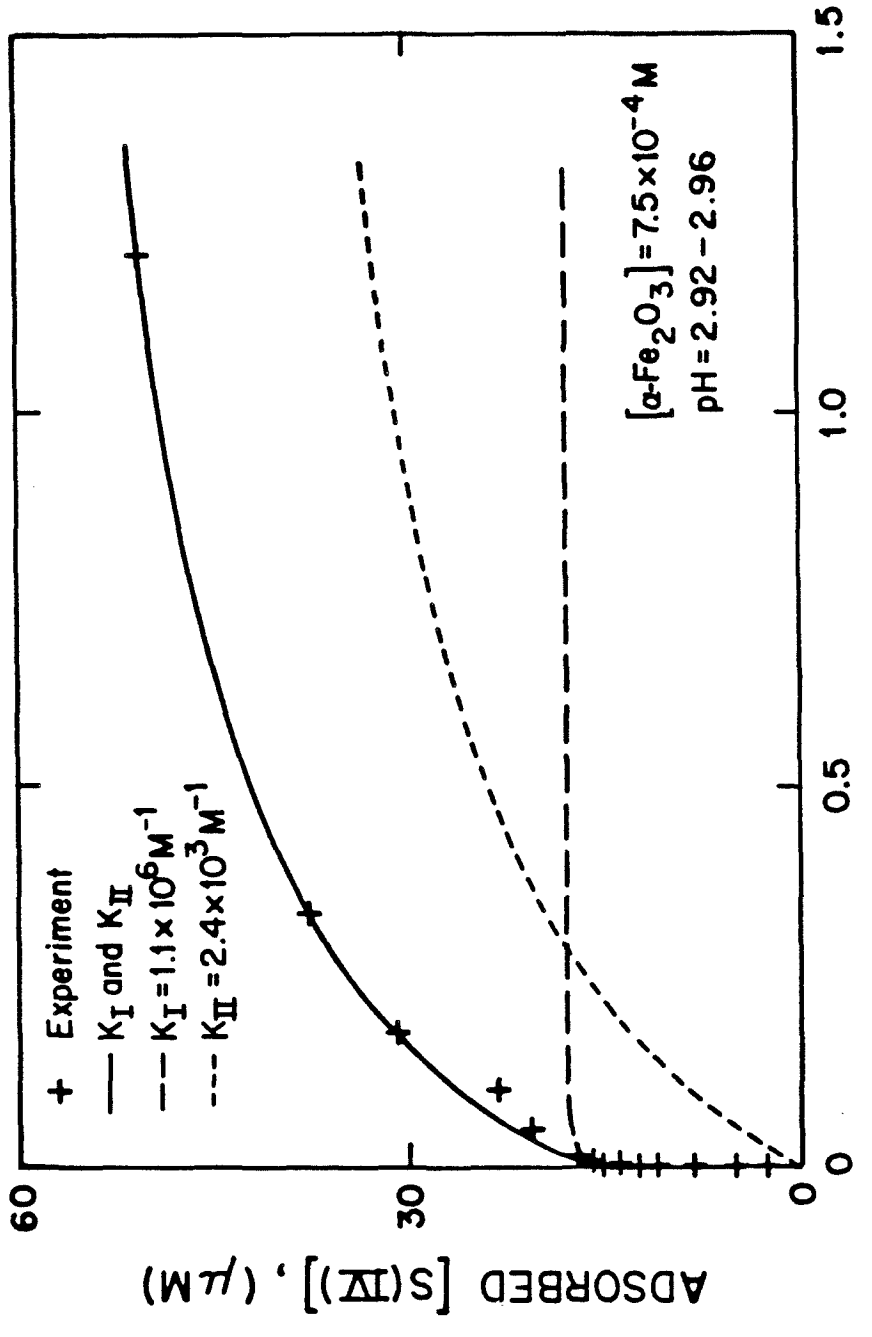

Figure 4.2. Adsorption isotherms of S(IV) on hematite. Adsorption in the dark, with $p_{O_2} = 0.21$ atm.

equation 4.2:

$$A_s = X_T/CM\Gamma \tag{4.2}$$

where C is the solids concentration (M), M is the solid molecular weight (g/mole), and Γ is the site density (moles of sites/m^2). Inverting equation 4.1 one obtains:

$$\frac{1}{[S(IV)]_{ADS}} =$$

$$\frac{(1 + K_I[S(IV)]_{aq})(1 + K_{II}[S(IV)]_{aq})}{[S(IV)]_{aq}(K_IX_1(1 + K_{II}[S(IV)]_{aq}) + K_{II}X_2(1 + K_I[S(IV)]_{aq}))} \tag{4.3}$$

In order to evaluate K_I and K_{II} several assumptions will be made which can be validated based on the calculated values of K_I, K_{II}, X_1, and X_2. For low surface coverages, $K_{II}[S(IV)]_{aq} \ll 1$, equation 4.3 simplifies to:

$$\frac{1}{[S(IV)]_{ADS}} \simeq \frac{1 + K_I[S(IV)]_{aq}}{[S(IV)]_{aq}(K_IX_1 + K_{II}X_2 + K_IK_{II}X_2[S(IV)]_{aq})} \tag{4.4}$$

It is further assumed that $K_{II}X_2 \ll K_IX_1$ and that $K_{II}X_2[S(IV)]_{aq} \ll X_1$. Equation 4.4 then simplifies to:

$$\frac{1}{[S(IV)]_{ADS}} \simeq \frac{1}{K_IX_1[S(IV)]_{aq}} + \frac{1}{X_1} \tag{4.5}$$

From a linear least squares analysis of $1/[S(IV)]_{ADS}$ versus $1/[S(IV)]_{aq}$, for $[S(IV)]_{aq} < 1.3 \times 10^{-5}$ M, $K_I = 1.1 \times 10^6$ M^{-1} and $X_1 = 1.8 \times 10^{-5}$ M are obtained. To evaluate K_{II} and X_2, data at higher surface coverages, where $K_I[S(IV)]_{aq} >> 1$, are used. Under these conditions equation 4.1 simplifies to:

$$[S(IV)]_{ADS} \simeq X_1 + \frac{K_{II}X_2[S(IV)]_{aq}}{1 + K_{II}[S(IV)]_{aq}} \qquad (4.6)$$

which can be reformulated as:

$$\frac{1}{[S(IV)]_{ADS} - X_1} \simeq \frac{1}{K_{II}X_2[S(IV)]_{aq}} + \frac{1}{X_2} \qquad (4.7)$$

From a linear least squares analysis of $1/([S(IV)]_{ADS} - X_1)$ versus $1/[S(IV)]_{aq}$, for $[S(IV)]_{aq} > 0.17$ mM, one obtains $K_{II} = 2.4 \times 10^3$ M^{-1} and $X_2 = 4.4 \times 10^{-5}$ M. Based on the values of K_I, K_{II}, X_1, and X_2 it is evident that the previously stated assumptions are valid for the conditions under which they were applied. Note that the two surface complexes have vastly different stabilities, i.e. $K_I >> K_{II}$. This could be due to: i) different stabilities of monodentate complexes formed between S(IV) and surface iron in two different coordination environments (implicitly assumed in the model calculations), or ii) formation of monodentate and bidentate (i.e. $<\equiv Fe(III)>_2O_2SO$) surface complexes which would be expected to have

different stabilities. The model calculation, which assumes monodentate complexes, predicts a total surface site concentration, $X_T = X_1 + X_2$, of 6.2×10^{-5} M. This compares favorably with $X_T = 6.7 \times 10^{-5}$ M, as determined independently by fluoride desorption measurements.

S(IV) is adsorbed onto hematite in significant quantities for the experiments reported here, and is presumably coordinated to surface ≡Fe(III). Motschi (1984) has established that complexes of Cu(II) undergo direct inner sphere coordination with some oxide surfaces, and inner sphere surface complexes of anions with hydrous oxide surfaces have been postulated by Stumm et al. (1980). Results of these experiments suggest that $HOSO_2^-$ or SO_3^{2-} may form surface complexes on α-Fe_2O_3, analogous to the solution phase complexes $FeOSOOH^{2+}$ and $FeOSO_2^+$ (Kao, 1979). For example, the kinetically active species may be a surface complex formed by the ligand exchange of $HOSO_2^-$ or SO_3^{2-} with one or two surface hydroxyl groups. Since the zero point of charge for α-Fe_2O_3 is $pH_{zpc} = 8.5$ (Parks and de Bruyn 1962), one would expect that almost all hematite surface hydroxyl groups would be protonated at low pH. Therefore it is highly likely that the predominant surface species are ≡Fe(III)-OSO_2H, $<\equiv Fe(III)>_2OOSOH^+$, ≡Fe(III)$OSO_2^-$, $<\equiv Fe(III)>_2OOSO$, and $\equiv FeOH_2^+$ over the pH range of experiments reported here.

The product, SO_4^{2-}, can also be expected to form complexes with surface ≡Fe(III) similar to solution phase complexes. Sigg and Stumm (1980) have reported intrinsic stability constants for

$\equiv Fe(III)-OSO_3^-$ and $<\equiv Fe(III)>_2OSO_3$ surface complexes on goethite (α-FeOOH). Stumm and co-workers have found a linear free energy relationship between the stability constants of surface complexes and their solution phase analogs (Stumm et al., 1980). This suggests that a comparison of the solution stability constants of $FeSO_3^+$ and $FeSO_4^+$, at the same ionic strength and temperature, may allow one to predict the relative stability of S(IV) versus S(VI) surface complexes with $\equiv Fe(III)$. The stability constant for $FeSO_4^+$ ($Fe^{3+} + SO_4^{2-} \rightleftharpoons FeSO_4^+$) is $10^{2.0}$ M^{-1} (Smith and Martell, 1976). The analogous stability constant for $FeSO_3^+$ is reported by Kao (1979) to be $10^{7.2}$ M^{-1}. Therefore, under the conditions of the experiments reported here, S(IV) will be able to displace S(VI) from surface coordination sites, and no rate inhibition by sulfate should be observed. This is consistent with experimental observations.

4.2 Oxidation of S(IV)

4.2.1 Reaction Stoichiometry

The reaction stoichiometry for oxygenated reactions is presented in equation 4.8:

$$HOSO_2^- + 1/2\ O_2 \xrightarrow[h\nu(\lambda > 330\ nm)]{\alpha\text{-}Fe_2O_3} SO_4^{2-} + H^+ \qquad (4.8)$$

The theoretical stoichiometry was verified experimentally by determining the analytical concentrations of S(IV), $O_2(aq)$, and SO_4^{2-} both before and after irradiation of an air-saturated aqueous

suspension (pH = 2.50) of hematite particles ([α-Fe_2O_3] = 82.5 μM) with initial S(IV) and O_2(aq) concentrations of 0.28 mM and 0.24 mM respectively. Experimental conditions for the stoichiometry experiment are similar to those of other experiments reported here. Results of this experiment give the following experimental stoichiometric coefficients: $\Delta[O_2(aq)]/\Delta[S(IV)] = 0.41$ and $\Delta[S(IV)]/\Delta[S(VI))] = -1.01$. These values are in reasonable agreement with the reaction stoichiometry of equation 4.8. The discrepancy between experimental and theoretical oxygen stoichiometric coefficients (0.41 vs. 0.5) is perhaps due to oxygen leakage into the reactor. Two points can be made regarding the stoichiometry of S(IV) autoxidation: i) all S(IV) is quantitatively converted to SO_4^{2-}, and ii) while hematite and O_2 are both capable of oxidizing S(IV), O_2 is the net stoichiometric oxidant in this system. The last point was reconfirmed in a separate experiment. A deoxygenated solution of S(IV) (0.43 mM) and α-Fe_2O_3 (0.30 mM) was prepared, and was kept oxygen free by continuous sparging of the reactor with nitrogen gas. The reactants were kept in the dark for 30 minutes, during which no detectable $Fe(II)_{aq}$ was produced. Irradiation of the mixture with visible light (λ = 452 nm) for three hours produced 12 μM $Fe(II)_{aq}$. Experiments with oxygenated suspensions containing S(IV) did not produce detectable quantities of $Fe(II)_{aq}$ after similar periods of irradiation. Hematite is thermodynamically capable of oxidizing S(IV), however the rate of oxidation by hematite is slower than by oxygen (Fe(III) catalyzed).

4.2.2 Quantum Yields for Fe(II) Production in Deoxygenated Hematite Suspensions

4.2.2.1 Reductive Dissolution of Hematite

Quantum yield determinations for $Fe(II)_{aq}$ production are potentially useful for identifying the light absorbing species which drive the redox reaction. Several possibilities exist which may be classified into two general categories: i) direct reductive dissolution of the solid by a photo-induced surface reaction producing $Fe(II)_{aq}$, and ii) an aqueous phase photochemical charge transfer reaction involving the reduction of $Fe(III)_{aq}$ to $Fe(II)_{aq}$, which provides a driving force for the dissolution of α-Fe_2O_3. Oxygen was excluded in the quantum yield experiments to permit careful study of the Fe(III)-S(IV) redox reaction without the complications of induced oxidations of S(IV) and $Fe(II)_{aq}$ by O_2. Figure 4.3 illustrates results of one quantum yield determination. The initial rapid increase in $[Fe(II)_{aq}]$, upon illumination, may be due to higher energy surface sites which have greater reactivity than other surface sites. High energy sites could be the result of surface discontinuities (kinks, ledges) which are coordinatively unsaturated relative to other surface sites. The thermal (dark) reaction rate was subtracted from measured rates of illuminated reactions to obtain the true photochemical reaction rates. As seen in Figure 4.3, the rate of hematite reductive dissolution is enhanced significantly by visible light. In the absence of S(IV), no detectable $Fe(II)_{aq}$ was released in a deoxygenated hematite

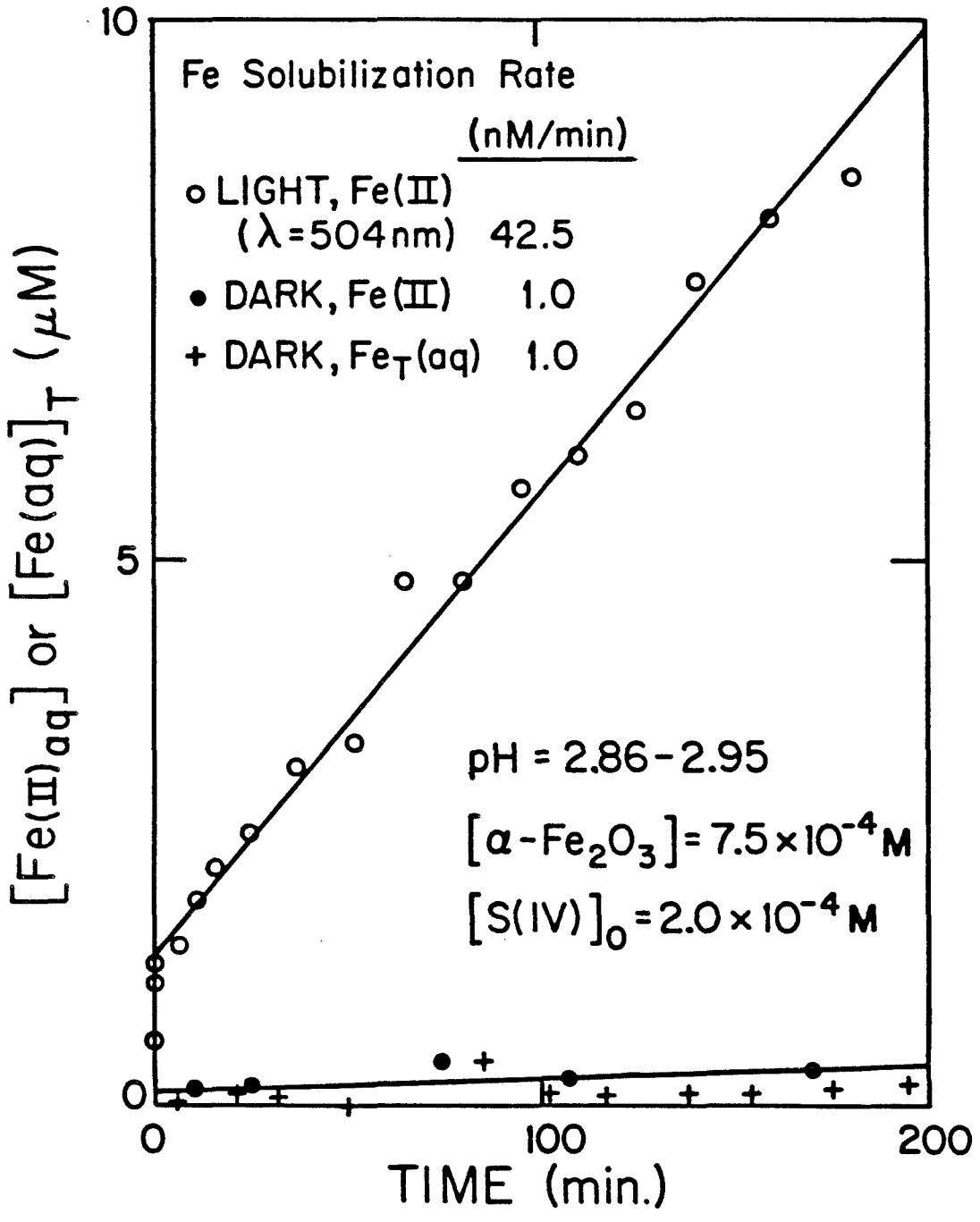

Figure 4.3. Photochemical and thermal solubilization of hematite in deoxygenated aqueous hematite suspensions containing S(IV).

suspension throughout an eight hour illumination (λ = 375 nm) period. Experimental quantum yields for $Fe(II)_{aq}$ production are presented in Table 4.1 and Figures 4.4 and 4.5. Due to light scattering by the hematite particles, the quantum yields presented here should be considered as minimum values for the relevant process. From Figure 4.4 one observes that the quantum yield increases greatly from 420 to 350 nm, corresponding to the region of maximum absorption of aqueous (and probably surface also) Fe(III)-S(IV) complexes (λ = 367 nm). Figure 4.5 illustrates that this increase in quantum yield also corresponds to the lowest energy $O^{2-} \longrightarrow Fe^{3+}$ charge transfer band (λ = 375 nm) within hematite (Tossel et al., 1973).

Childs and Ollis (1980) have pointed out that, together with surface photo-redox reactions, three other general processes may contribute to the net oxidation: i) surface thermal (dark) reactions, ii) aqueous phase thermal (dark) reactions, and iii) aqueous phase photochemical reactions. As previously described (Section 1.1.1), aqueous phase photochemical pathways may involve direct excitation of $SO_2 \cdot H_2O$, $HOSO_2^-$, SO_3^{2-}, $S_2O_5^{2-}$, or metal complexes of S(IV). Aquated SO_2, $HOSO_2^-$, SO_3^{2-}, and $S_2O_5^{2-}$ have absorption maxima at 280, 190, <190, and 255 nm respectively. Aqueous dioxygen has an absorption maximum at a wavelength less than 200 nm. Since the absorption maxima of these species occur at $\lambda < 295$ nm, it is concluded that they are not important light absorbing species in either the system studied or in natural waters. Aqueous

Table 4.1 Experimental quantum yields for aqueous Fe(II) production in deoxygenated hematite suspensions containing S(IV). For all experiments: [hematite] = 0.75 mM, Batch 2; Total [S(IV)] = 0.20 mM; pH = 2.86 - 2.95.

λ (nm)	$\Phi_{Fe(II)}$
350	2.7×10^{-2}
375	1.0×10^{-2}
392	9.5×10^{-3}
416	5.9×10^{-3}
452	4.0×10^{-3}
504	3.3×10^{-3}
585	2.2×10^{-3}
676	1.2×10^{-3}
676	1.3×10^{-3}

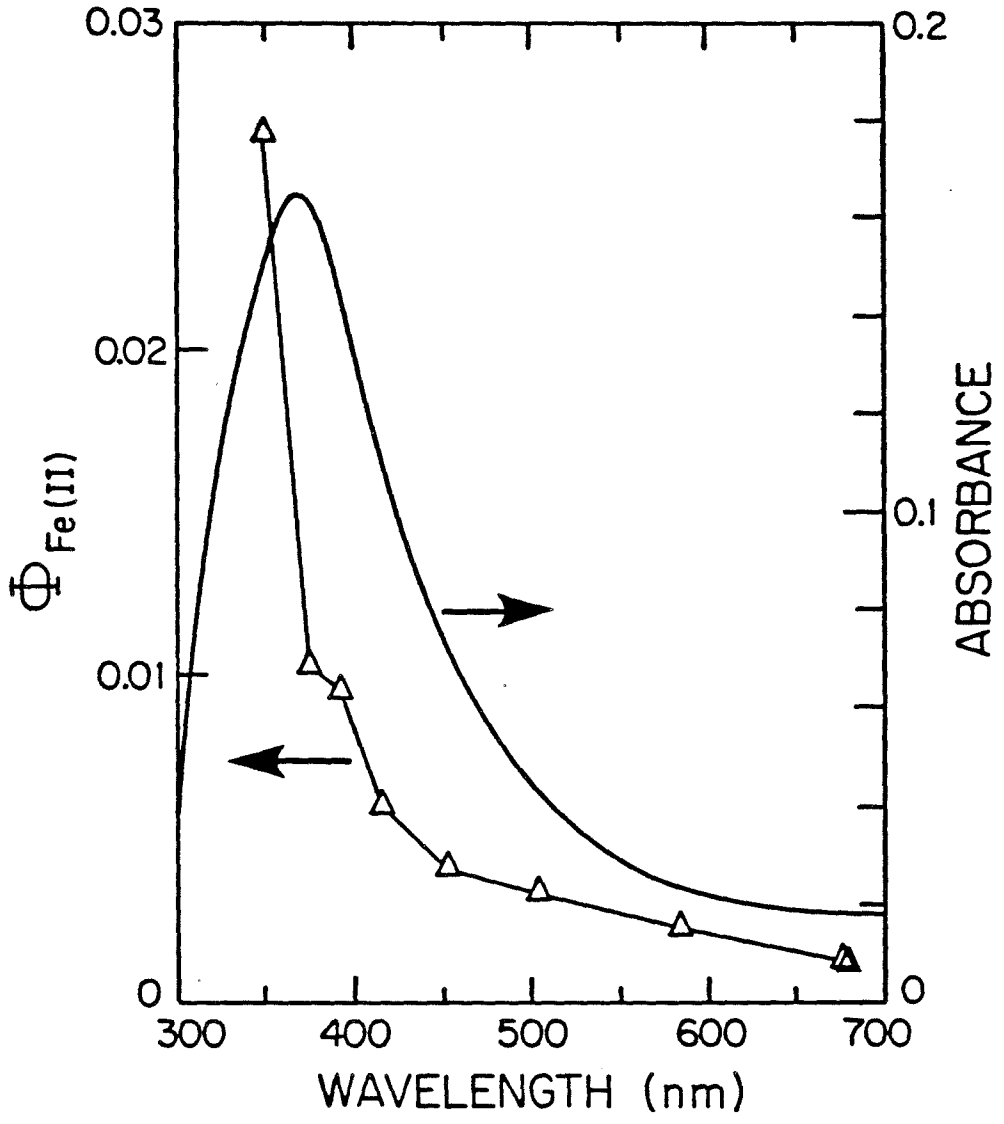

Figure 4.4. i) Experimental quantum yields for aqueous Fe(II) production in deoxygenated hematite suspensions containing S(IV), and ii) charge transfer absorption band of an aqueous Fe(III)-S(IV) complex (λ = 367 nm). For the quantum yields: [hematite] = 0.75 mM, Batch 2; total [S(IV)] = 0.20 mM; pH = 2.86-2.95. For the charge transfer spectrum: aqueous [Fe(III)] = 0.11 mM; total [S(IV)] = 1.0 mM; pH = 2.94; 10 cm path length. This was obtained by subtracting spectra of Fe(III) and S(IV) solutions (aqueous [Fe(III)] = 0.11 mM at pH = 2.90; and total [S(IV)] = 1.0 mM at pH = 2.94) from the charge transfer spectrum.

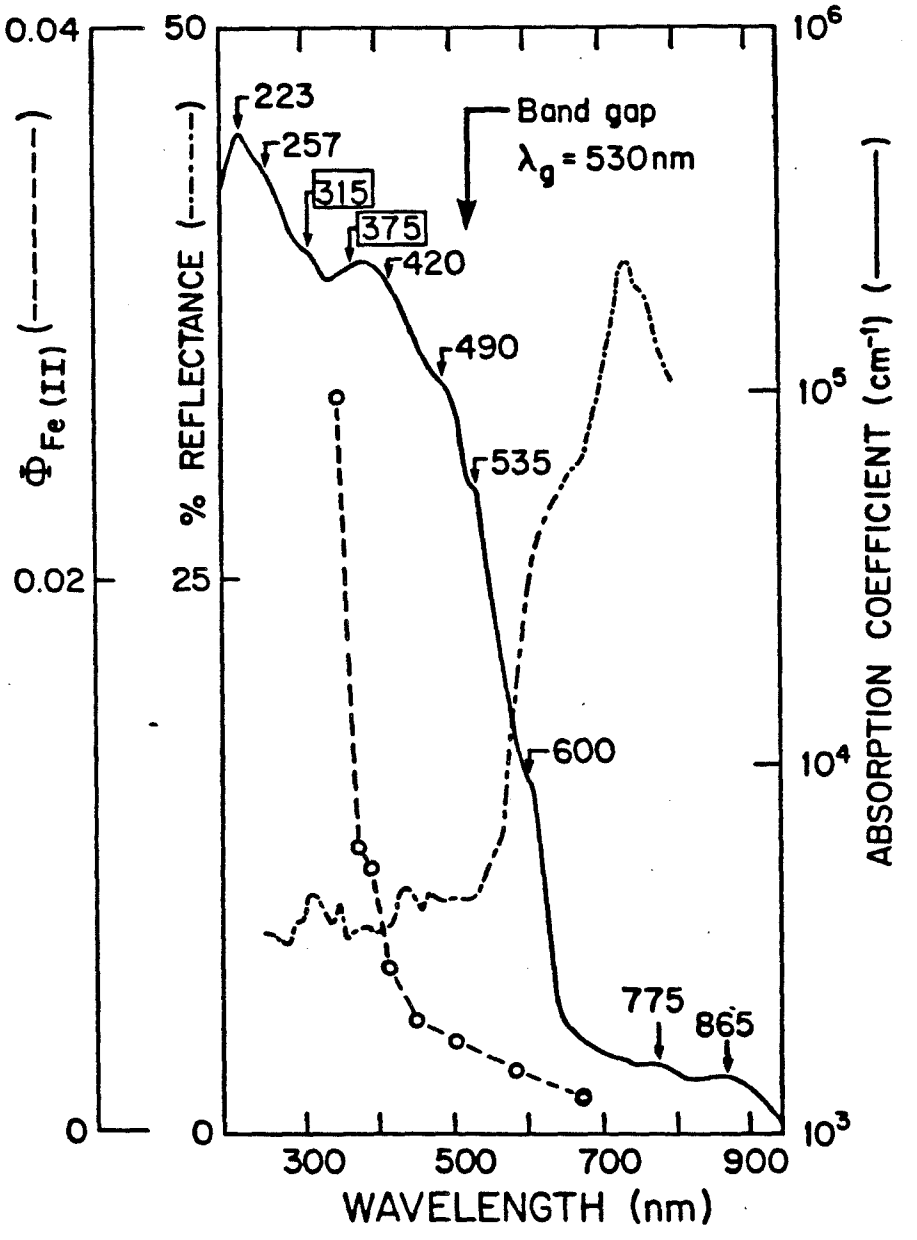

Figure 4.5. i) Experimental quantum yields for aqueous Fe(II) production in deoxygenated hematite suspensions containing S(IV), ii) reflectance spectrum of hematite, and iii) absorption coefficients of hematite, after Marusak et al. (1980). For the quantum yields: [hematite] = 0.75 mM, Batch 2; total [S(IV)] = 0.20 mM; pH = 2.86-2.95. The reflectance spectrum is of dried (120°C) hematite (Batch 2). Absorption coefficients of hematite are for thin films.

Fe(III)-S(IV) complexes exhibit charge transfer absorption bands at wavelengths < 400 nm (Vepřek-Šiška et al., 1974), as illustrated in Figure 4.4. It is likely that the ≡Fe(III)-S(IV) surface complexes have charge transfer absorption bands at approximately the same energies as their analogous aqueous complexes. Absorption coefficients of α-Fe_2O_3, as a function of wavelength, have been measured by Marusak and co-workers (1980), and their results, together with the results of this work, are presented in Figure 4.5. Based on the previous discussion, it appears that the bulk solid, α-Fe_2O_3, and both surface and aqueous Fe(III)-S(IV) complexes are the only chemical species which have absorption bands in the near UV and visible spectrum for this system.

The possibility that photo-induced charge transfer reactions reduce aqueous Fe(III) complexes and thus drive the dissolution of hematite was examined. The rate of $Fe(II)_{aq}$ production from redox reactions of all aqueous phase Fe(III) complexes is limited by the rate at which $Fe(III)_{aq}$ is released to solution by hematite dissolution. The rate of hematite dissolution, in the dark, was measured under conditions identical to those of the quantum yield experiments (Figure 4.3). Under these conditions $d[Fe(aq)]_T \approx 1$ nM/min. However, the rate of $Fe(II)_{aq}$ production in the quantum yield experiments varied from 2.9-47 nM/min, i.e. 2.9-47 times faster than the dissolution rate of hematite. Furthermore, the concentration of ≡Fe(III)-S(IV) surface complexes for the quantum yield experiments was 3.1×10^{-5} M (determined from the

S(IV) adsorption experiments), which greatly exceeded the concentration of all aqueous Fe(III) species. The production of $Fe(II)_{aq}$ in irradiated suspensions of α-Fe_2O_3 containing S(IV) is predominantly due to photo-induced surface redox reactions. Using the total exchange capacity of hematite reported here, and assuming approximately 9 surface hydroxyl groups per 100 $(\text{Å})^2$ of hematite surface (Dana and Ford, 1960; Morimoto et al., 1969), the rate of hematite dissolution in the dark is ca. 0.22 nmole/m^2-min, at pH 2.9 with [S(IV)] = 0.20 mM. This is slightly faster than the rate of hematite dissolution reported by Chang and Matijević (1983). They report a dissolution rate of 0.085 nmole/m^2-min at pH 3.0 in a 0.30 mM solution of EDTA. The slight discrepancy in rates can be explained by noting that a slow, but non-negligible thermal reductive dissolution of hematite is occurring in solutions containing S(IV). This pathway is probably absent in solutions of EDTA.

An experimental rate expression can be formulated for the photo-induced reductive dissolution of hematite. Consider the case of monochromatic light which causes a unimolecular reaction (Balzani and Carassiti, 1970). For the photo-induced reductive dissolution of hematite this would give:

$$\frac{d[Fe(II)_{aq}]}{dt} = \Phi_{Fe(II)} I_o (1-10^{-\varepsilon CL})(A/V) \qquad (4.9)$$

where $d[Fe(II)_{aq}]/dt$ is the average rate of $Fe(II)_{aq}$ production (M/min), $\Phi_{Fe(II)}$ is the experimental quantum yield (dimensionless), I_o is the intensity of light (photon flux) incident to the reactor cell (einstein/min-cm^2), A is the area of the reactor cell exposed to light (cm^2), V is the reactor volume (liter), ε, C are the molar absorptivity ($M^{-1}cm^{-1}$) and concentration (M) respectively of the photochemically reactive Fe(III) species, and L is the light path length. The quantity $(1-10^{-\varepsilon CL})$ represents the fraction of incident light intensity which is absorbed by the reactants. If the photochemically reactive Fe(III) species absorbs virtually all of the incident light ($\varepsilon CL > 1$) equation 4.9 simplifies to:

$$\frac{d[Fe(II)_{aq}]}{dt} \approx \Phi_{Fe(II)} I_o (A/V) \qquad (4.10)$$

Under these conditions the rate of $Fe(II)_{aq}$ production is constant, which is consistent with the experimental observations (Figure 4.3). Values of $\Phi_{Fe(II)}$ are tabulated in Table 4.1. For constant intensity, the rate of $Fe(II)_{aq}$ production can be formulated as:

$$\frac{d[Fe(II)]_{aq}}{dt} = k_1 [S(IV)]_{ADS} \qquad (4.11)$$

where the quantity $[S(IV)]_{ADS}$ is given by the adsorption isotherm

(Equation 4.1).

A conceptual model for the photo-induced oxidation of S(IV) in aqueous suspensions of hematite is presented in Figure 4.6. Two major pathways may lead to the production of $Fe(II)_{aq}$: i) surface redox reactions, both photochemical and thermal (dark), involving ≡Fe(III)-S(IV) surface complexes (reactions (3) and (4) in Figure 4.6), and ii) aqueous phase photochemical and thermal redox reactions (reactions (11) and (12) in Figure 4.6). However, the rate of hematite dissolution (reaction (5) in Figure 4.6) limits the rate at which $Fe(II)_{aq}$ may be produced by aqueous phase pathways (reactions (11) and (12) in Figure 4.6) by limiting the availability of $Fe(III)_{aq}$ for such reactions. The rate of total aqueous iron production ($d[Fe(aq)]_T/dt = d([Fe(III)_{aq}] + [Fe(II)_{aq}])/dt$), in the dark, represents an upper bound to the rate of $Fe(II)_{aq}$ generation from all redox reactions other than the photo-induced surface redox reaction (reactions (4) + (11) + (12) in Figure 4.6). The rate of aqueous iron production, in the dark, has been shown to be far slower than the observed rates of $Fe(II)_{aq}$ production in illuminated suspensions of hematite containing S(IV) (Figure 4.3). The production of $Fe(II)_{aq}$ in irradiated suspensions of hematite containing S(IV) is therefore due to a surface photo-induced reductive dissolution reaction.

The photo-induced surface redox reaction may be due to direct excitation of i) the bulk solid, α-Fe_2O_3, and/or ii) one or more types of surface complexes. From the results of the quantum yield

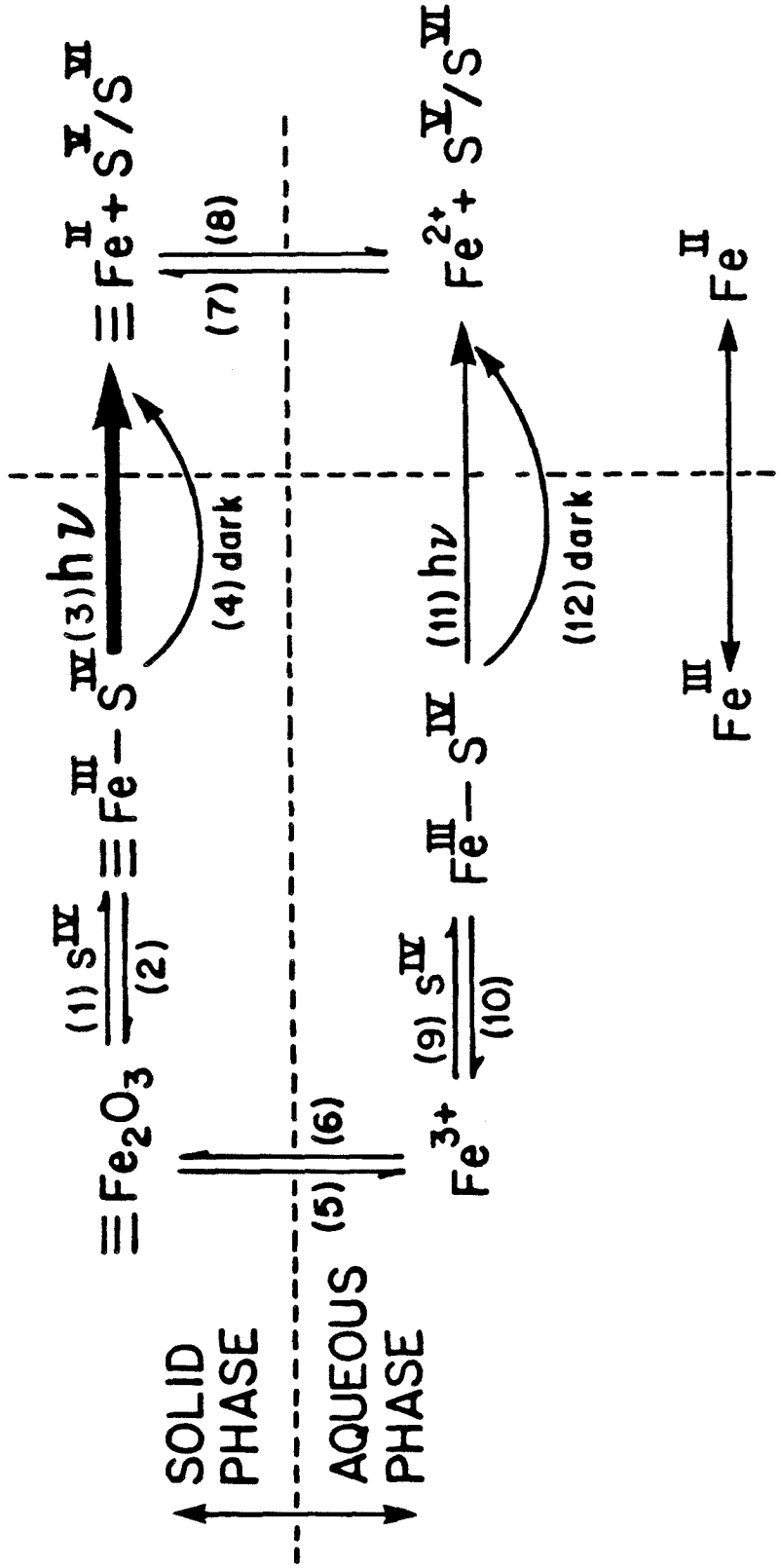

Figure 4.6. Conceptual model of Fe(III) reduction in hematite suspensions containing S(IV).

studies, it appears that both phenomena may be consistent with increased hematite redox reactivity; consequently both pathways will be discussed. Several models could conceivably be invoked to interpret the surface photochemical behavior of α-Fe_2O_3; two models which invoke direct excitation of the bulk solid, and two models which postulate excitation of surface complexes.

Two models which are used to interpret the electronic properties of bulk solids are i) the band model and ii) crystal field theory. From a surface coordination perspective, photo-induced surface redox reactions may be promoted by excitation of charge transfer bands in surface complexes such as: i) $\equiv Fe(III)\text{-}OH \longrightarrow Fe(II)_{aq} + {}^{\bullet}OH$ and/or ii) $\equiv Fe(III)\text{-}S(IV) \longrightarrow Fe(II)_{aq} + S(V)/S(VI)$. The implications and relative merits of these proposed models will be discussed and compared with available data.

4.2.2.2 Excitation of Bulk Solution

Predictions based on the band model suggest that photons with energy greater than the band gap energy of dry hematite ($\lambda < 530$ nm) would be approximately equally efficient at promoting a valence band electron to the conduction band, allowing adsorbed S(IV) to undergo electron transfer to the hole created in the valence band. In the absence of O_2 or other oxidants, this would result in the reduction of α-Fe_2O_3 giving $Fe(II)_{aq}$. As one observes in Figure 4.5, there is a small increase in quantum yield throughout the band gap region. However the region of large increase in quantum yield for $Fe(II)_{aq}$

production ($350 < \lambda < 420$ nm) does not coincide with the bandgap energy (E_G = 2.34 eV, λ_G = 530 nm).

Hydroxylation of surface sites could alter the band gap energy and could possibly cause a shift in the absorption edge of the solid. One of the methods used to determine band gap energies involves extrapolation of the linear portion of the absorption edge of the solid to "background absorbance" (Strehlow and Cook, 1973). Figure 3.2 illustrates that for hematite used in these experiments there is little, if any, shift in the absorption edge due to surface hydroxylation. Reflectance spectra of α-Fe_2O_3, α-FeOOH, and γ-FeOOH (Figure 3.3) illustrate that the shift in absorption edge is only 40-60 nm, despite the fact that hydroxyl groups are present at stoichiometric levels in these solids. Even if the band gap energy for hydroxylated hematite was 2.64 eV (λ_G = 470 nm, a 60 nm shift), it would still remain well outside the range of maximum increase in quantum yield for $Fe(II)_{aq}$ production. This further suggests that the delocalized band model, by itself, may not be the most appropriate model for describing the photo-redox properties of colloidal α-Fe_2O_3. While the band model offers an excellent interpretation to results of surface photochemical reactions on ZnO and TiO_2, it is less successful for α-Fe_2O_3.

The rapid increase in quantum yield between 420 nm and 350 nm does coincide with the lowest energy $O^{2-} \longrightarrow Fe^{3+}$ charge transfer band in hematite (Tossel et al., 1973). Morin's (1959) idea of charge localization on hematite lattice ions is consistent with

these results and the results of studies on the efficiency of current generation by irradiated polycrystalline α-Fe_2O_3 electrodes (McGregor et al., 1979; Kennedy and Frese, 1978). The shapes of current efficiency curves as a function of wavelength of irradiation, at different applied potentials, are quite similar to the shape of the quantum yield curve for $Fe(II)_{aq}$ production reported here (Figure 4.5). The current efficiency curves exhibit maxima located at approximately λ = 360-390 nm, which correlate reasonably well with the peak for the lowest energy $O^{2-} \longrightarrow Fe^{3+}$ lattice charge transfer band (λ = 375 nm). Furthermore, the current efficiency does not increase rapidly in the region corresponding to the band gap energy (λ_G = 530 nm). This further indicates that a model with more localized charge carriers may be appropriate for α-Fe_2O_3. Excitation of the $O^{2-} \longrightarrow Fe^{3+}$ lattice charge transfer band in hematite may create "holes" localized on lattice oxygen (O^-) and electrons localized on lattice iron (Fe^{2+}). The holes then migrate to the surface where electron transfer from adsorbed S(IV) occurs. Note that, in this proposed reaction scheme, the lattice recombination reaction ($O^- + Fe^{2+}$) is likely to limit the yield of the overall reaction. This model is quite similar to the surface ligand to metal charge transfer reaction:

$$\equiv Fe(III)\text{-}OH \longrightarrow \equiv Fe(II) + {}^{\bullet}OH.$$

4.2.2.3 Excitation of Surface Complexes

No data exist on the charge transfer spectra of surface

complexes; however information on solution charge transfer complexes may provide some basis for understanding surface charge transfer complexes. The surface complex, ≡FeOH, could undergo a photo-induced ligand to metal charge transfer reaction ($\equiv FeOH \longrightarrow \equiv Fe(II) + {}^{\bullet}OH$) resulting in the reductive dissolution of hematite. Presumably ${}^{\bullet}OH$ would be scavenged by S(IV) and Fe(II). The surface complex ≡FeOH has solution phase analogs, $FeOH^{2+}$ and $Fe_2(OH)_2^{4+}$, which have charge transfer bands located at 300 nm ($FeOH^{2+} \longrightarrow Fe^{2+} + {}^{\bullet}OH$) and 335 nm respectively (Carey and Langford, 1975; Langford and Carey, 1975; Feeya and David, 1976). These maxima occur at shorter wavelengths than were utilized in any of the experiments reported here, and are <u>not</u> consistent with either these quantum yield studies or with the current efficiency studies (McGregor et al., 1979; Kennedy and Frese, 1978). To the extent that the charge transfer spectrum of the surface species ≡FeOH is similar to its aqueous phase analogs, it is concluded that this is not likely to be the dominant pathway for the photo-induced reduction of α-Fe_2O_3.

Charge transfer excitation of ≡Fe(III)-S(IV) <u>surface</u> complexes is likely to be the predominant pathway for the surface photochemical production of $Fe(II)_{aq}$ in the system studied. From Figure 4.4 one observes that the corresponding aqueous phase Fe(III)-S(IV) complex has a charge transfer band located at λ_{MAX} = 367 nm, which corresponds quite well with the observed increase in quantum yield for $Fe(II)_{aq}$ production. The maxima of charge transfer bands for

≡Fe(III)-S(IV) surface complexes are likely to occur at energies similar to their aqueous phase analogs. Futhermore, ≡Fe(III)-S(IV) surface complexes are the predominant surface species for the experiments reported here. Although the possibility that an $O^{2-} \longrightarrow Fe^{3+}$ lattice charge transfer is the primary photochemical reaction can not be excluded, the ≡Fe(III)-S(IV) photo-induced surface charge transfer reaction is the simplest explanation which is consistent with the experimental results. It is likely to be the dominant pathway for the photo-induced reduction of α-Fe_2O_3. A similar explanation has been suggested for the photo-induced dissolution of lepidocrocite (γ-FeOOH) suspensions containing citrate (Waite, 1983).

In general, it would seem that the relative contributions of bulk solid excitation versus surface complex excitation to the overall rate of photo-induced surface redox reactions will depend on the (surface area)/volume ratio of the solid reactant. As particle dimensions decrease, the relative contribution of surface species to the overall electronic properties, and therefore photochemical properties, of the solid must increase and approach the limiting behavior of aqueous complexes. The role of surface complexes in the overall photochemical reactivity of a solid will become more important as the (surface area)/volume ratio of the solid increases.

Impurities, stoichiometric deficiencies, crystal defects, and surface complexation in general result in the creation of allowed energy levels which may alter the electronic properties of the

solid. Such intermediate energy levels may mediate the electron transfer processes occurring on the surfaces of illuminated transition metal oxides such as α-Fe_2O_3. In particular, surface coordination of ligands such as $HOSO_2^-$, by ligand exchange with surface hydroxyl groups, will alter the electronic band structure of the solid.

There are several mechanisms by which redox reactions may occur on surfaces of illuminated solids. As Gomes et al. (1968) point out, the oxidation of some two or multi-electron reductants on semiconductor solids may occur by sequential-one electron transfers. A possible mechanism for the photo-induced reductive dissolution of hematite involving monodentate surface complexes is:

$$\equiv Fe(III)\text{—}OH_2^+ + HOSO_2^- \rightleftharpoons \equiv Fe(III)\text{—}OS(IV)O_2H + H_2O \qquad (4.12)$$

$$\equiv Fe(III)\text{—}OH_2^+ + SO_3^{2-} \rightleftharpoons \equiv Fe(III)\text{—}OS(IV)O_2^- + H_2O \qquad (4.13)$$

$$\equiv Fe(III)\text{—}OS(IV)O_2H \xrightarrow{h\nu} \equiv Fe(II)\text{-}OS(V)O_2^- + H^+ \qquad (4.14)$$

$$\equiv Fe(III)\text{—}OS(IV)O_2^- \xrightarrow{h\nu} \equiv Fe(II)\text{—}OS(V)O_2^- \qquad (4.15)$$

$$\equiv Fe(II)\text{—}OS(V)O_2^- \overset{H_2O}{\rightleftharpoons} \equiv Fe(II)\text{—}OH_2 + SO_3^{\cdot-} \qquad (4.16)$$

$$\equiv Fe(III)\text{—}OH_2^+ + SO_3^{\cdot-} \rightleftharpoons \equiv Fe(III)\text{—}OS(V)O_2 + H_2O \qquad (4.17)$$

$$\equiv Fe(III)\text{—}OS(V)O_2 \xrightarrow{fast} \equiv Fe(II)\text{—}OS(VI)O_2 \qquad (4.18)$$

$$\equiv Fe(II)\text{—}OS(VI)O_2 \xrightarrow{H_2O} \equiv Fe(II)\text{—}OH_2 + SO_4^{2-} + 2H^+ \qquad (4.19)$$

$$\equiv Fe(II)\text{-}OH_2 \rightleftharpoons Fe(II)_{aq} \qquad (4.20)$$

$$2\ SO_3^{\cdot-} \xrightarrow{H_2O} HOSO_2^- + SO_4^{2-} + H^+ \qquad (4.21)$$

$$2\ SO_3^{\cdot-} \longrightarrow S_2O_6^{2-} \qquad (4.22)$$

and, alternatively, for bidentate complexes (see also Figure 4.7):

$$2\ \equiv Fe(III)-OH_2^+ + HOSO_2^- \rightleftharpoons \langle \equiv Fe(III) \rangle_2 O_2S(IV)OH^+ + 2H_2O \qquad (4.23)$$

$$2\ \equiv Fe(III)-OH_2^+ + SO_3^{2-} \rightleftharpoons \langle \equiv Fe(III) \rangle_2 O_2S(IV)O + 2H_2O \qquad (4.24)$$

$$\langle \equiv Fe(III) \rangle_2 O_2S(IV)OH^+ \xrightarrow{h\nu} \langle \equiv Fe(II), \equiv Fe(III) \rangle O_2S(V)O + H^+ \qquad (4.25)$$

$$\langle \equiv Fe(III) \rangle_2 O_2S(IV)O \xrightarrow{h\nu} \langle \equiv Fe(II), \equiv Fe(III) \rangle O_2S(V)O \qquad (4.26)$$

$$\langle \equiv Fe(II), \equiv Fe(III) \rangle O_2S(V)O \xrightarrow{\text{fast}} \langle \equiv Fe(II) \rangle_2 O_2S(VI)O \qquad (4.27)$$

$$\langle \equiv Fe(II) \rangle_2 O_2S(VI)O \xrightarrow{H_2O} 2\ \equiv Fe(II)-OH_2 + SO_4^{2-} + 2H^+ \qquad (4.28)$$

$$\equiv Fe(II)-OH_2 \rightleftharpoons Fe(II)_{aq} \qquad (4.29)$$

Both reaction mechanisms given above implicitly assume that no oxidant, other than the solid, is present. This implies that the solid is a stoichiometric reactant and not a catalyst. However in most natural waters, and certainly atmospheric water droplets, dissolved oxygen will be present at concentrations approaching 0.25 mM. Oxygen may enter into the reaction scheme in several different ways.

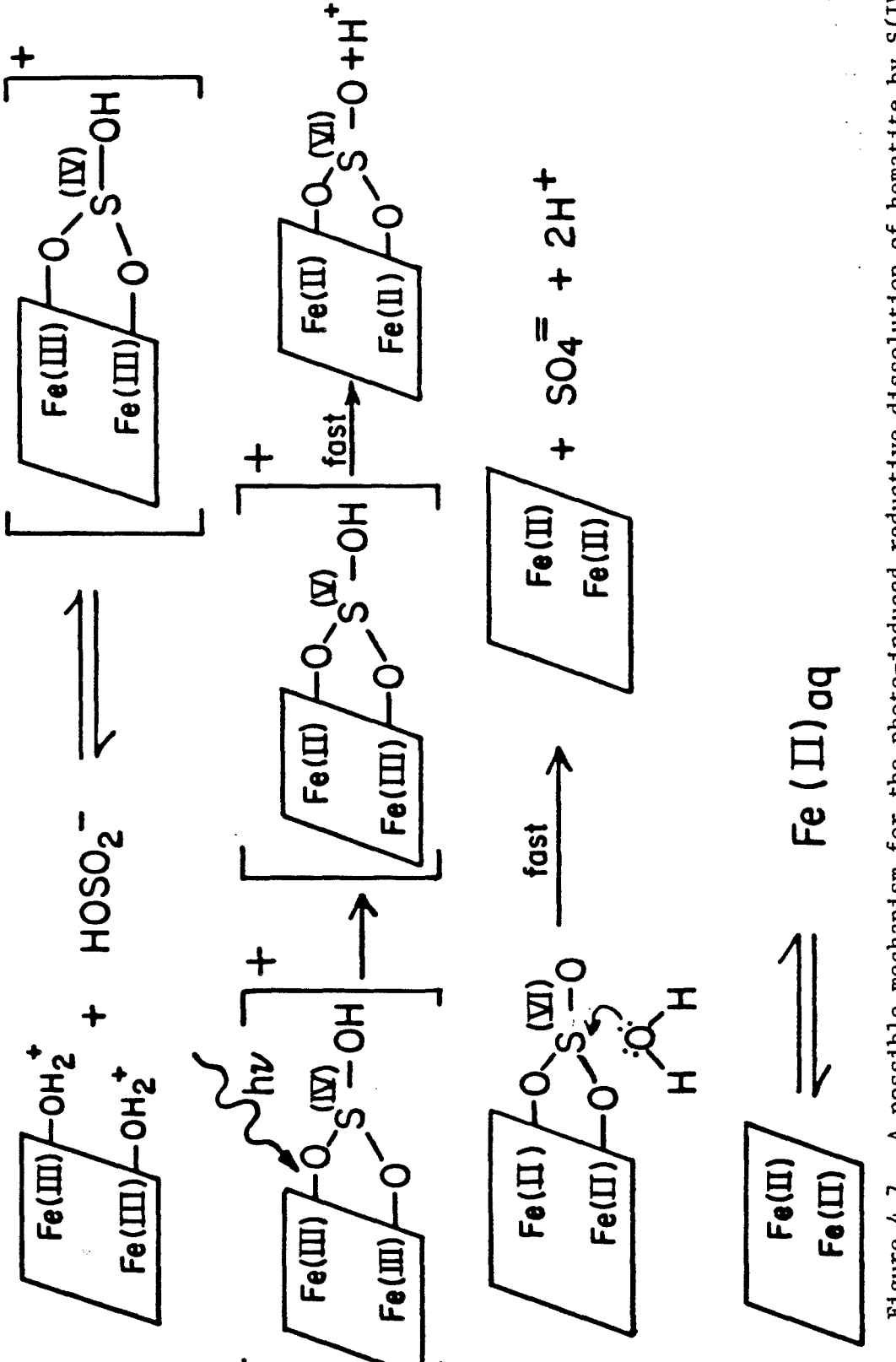

Figure 4.7. A possible mechanism for the photo-induced reductive dissolution of hematite by S(IV).

4.2.3 Effect of Reaction Variables on Rate of S(IV) Oxidation by Molecular Oxygen

4.2.3.1 S(IV)

As shown in Figure 4.8, at low [S(IV)] the reaction exhibits a first-order dependence on [S(IV)], while at high [S(IV)] the reaction rate is zero-order with respect to [S(IV)]. Between these concentration extremes the apparent reaction order with respect to [S(IV)] will vary between zero and one. This observation is consistent with the concept of saturation kinetics that results from the Langmurian adsorption of S(IV) on hematite.

At lower light intensities, the rate of S(IV) oxidation increases with time (Figures 4.9 and 4.10). This autocatalytic behavior strongly suggests that $Fe(II)_{aq}$ is rapidly oxidized to $Fe(III)_{aq}$, thereby increasing the rate of $Fe(III)_{aq}$ catalyzed S(IV) autoxidation. With a rapid Fe(II) autoxidation rate, increasing rates of $Fe(II)_{aq}$ generation will cause increases in $Fe(II)_{aq}$ and, therefore, increases in the rate of $Fe(III)_{aq}$ catalyzed S(IV) autoxidation. This will reduce the length of induction periods observed for S(IV) autoxidations in illuminated hematite suspensions. Results of experiments illustrated in Figures 4.9 and 4.10 support this hypothesis. The rates of S(IV) autoxidation are nearly identical for λ = 375 and 452 nm (Figure 4.9). The explanation is that rates of $Fe(II)_{aq}$ production for λ = 375 and 452 nm, based on quantum yields and measured light intensities, are identical to within 5% for these experiments. Similar autocatalytic

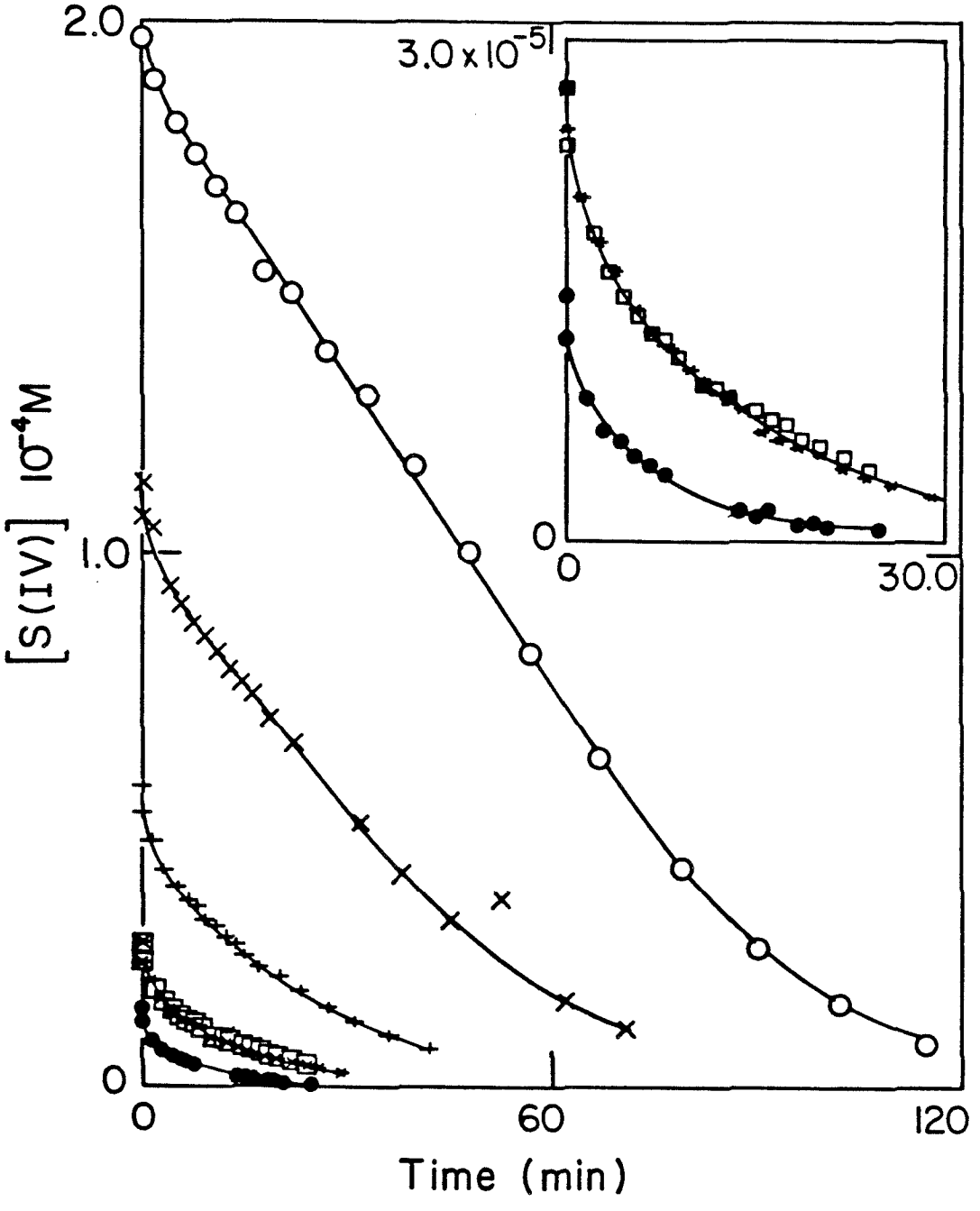

Figure 4.8. Rate of S(IV) autoxidation as a function of [S(IV)]. [hematite] = 82.5 μM, pH = 2.44-2.48, p_{O_2} = 1.0 atm. Insert: expanded scale for low [S(IV)] experiments.

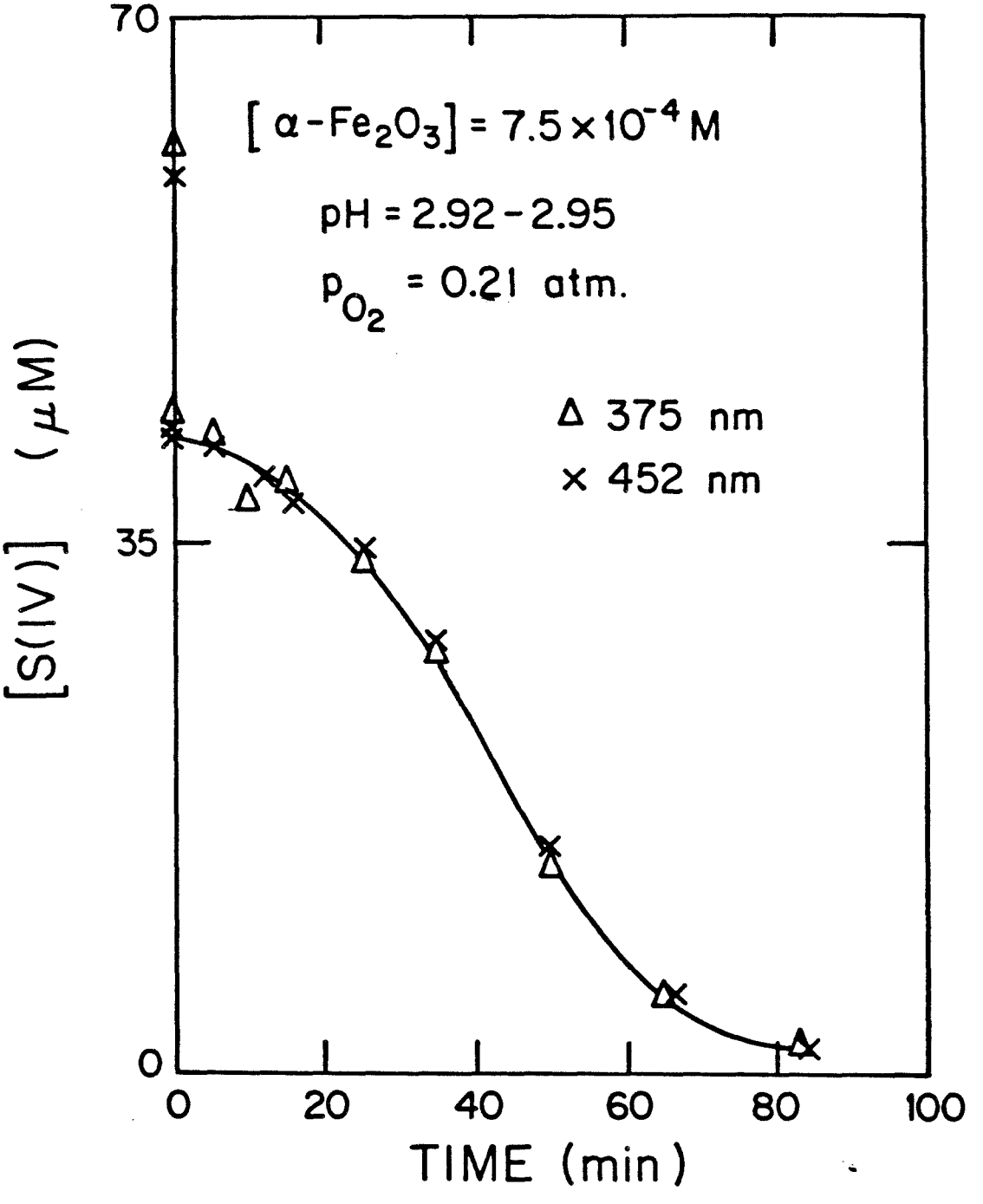

Figure 4.9. Autocatalytic autoxidation of S(IV).

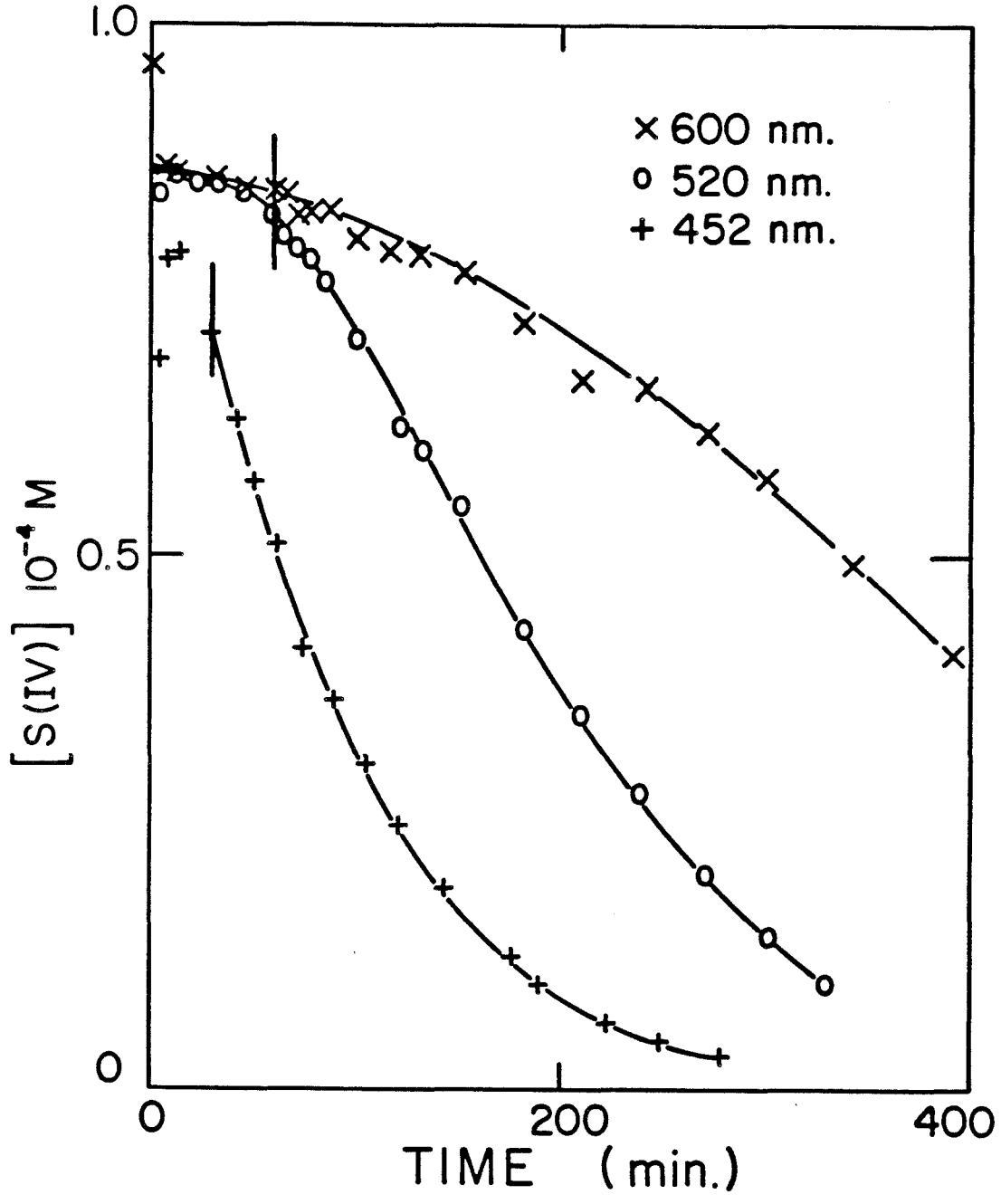

Figure 4.10. Effect of visible light on S(IV) autoxidation. [hematite] = 25 μM, pH = 2.41-2.43, p_{O_2} = 1.0 atm. Vertical lines indicate the time at which reactants were illuminated with monochromatic light.

behavior for S(IV) autoxidation, with λ = 452, 520, and 600 nm, is illustrated in Figure 4.10. Although rates of $Fe(II)_{aq}$ production were not measured for the experiments illustrated in Figure 4.10, the relative rates based on quantum yield experiments are: ν(452 nm) > ν(520 nm) > ν(600 nm). The length of the induction period for experiments illustrated in Figure 4.10 increases with decreasing rates of $Fe(II)_{aq}$ production, lending further support to the hypothesis. Conceivably, the crystal structure of hematite could provide a unique surface coordination environment for S(IV) species and alter the absorption spectrum of adsorbed S(IV), to the extent that illumination of adsorbed S(IV) with visible light would create an excited S(IV) species capable of reacting rapidly with O_2. This possibility was examined by illuminating (λ = 375 nm) a 0.75 mM suspension of α-Al_2O_3 (structurally identical to α-Fe_2O_3) containing S(IV) (60 μM) and O_2 (p_{O2} = 0.21 atm). Throughout the 2.5 hour illumination period no detectable change in [S(IV)] was observed.

4.2.3.2 Total Surface Area

Evidence that S(IV) is oxidized on the surface of hematite is presented in Figure 4.11. The slope of the log-log plot of the pseudo-order rate constant, k_{OBS}, versus [α-Fe_2O_3] (which is proportional to surface area) is essentially one, indicating that the rate determining step involves a surface active species. This is consistent with results of Section 4.2.2, which demonstrated that

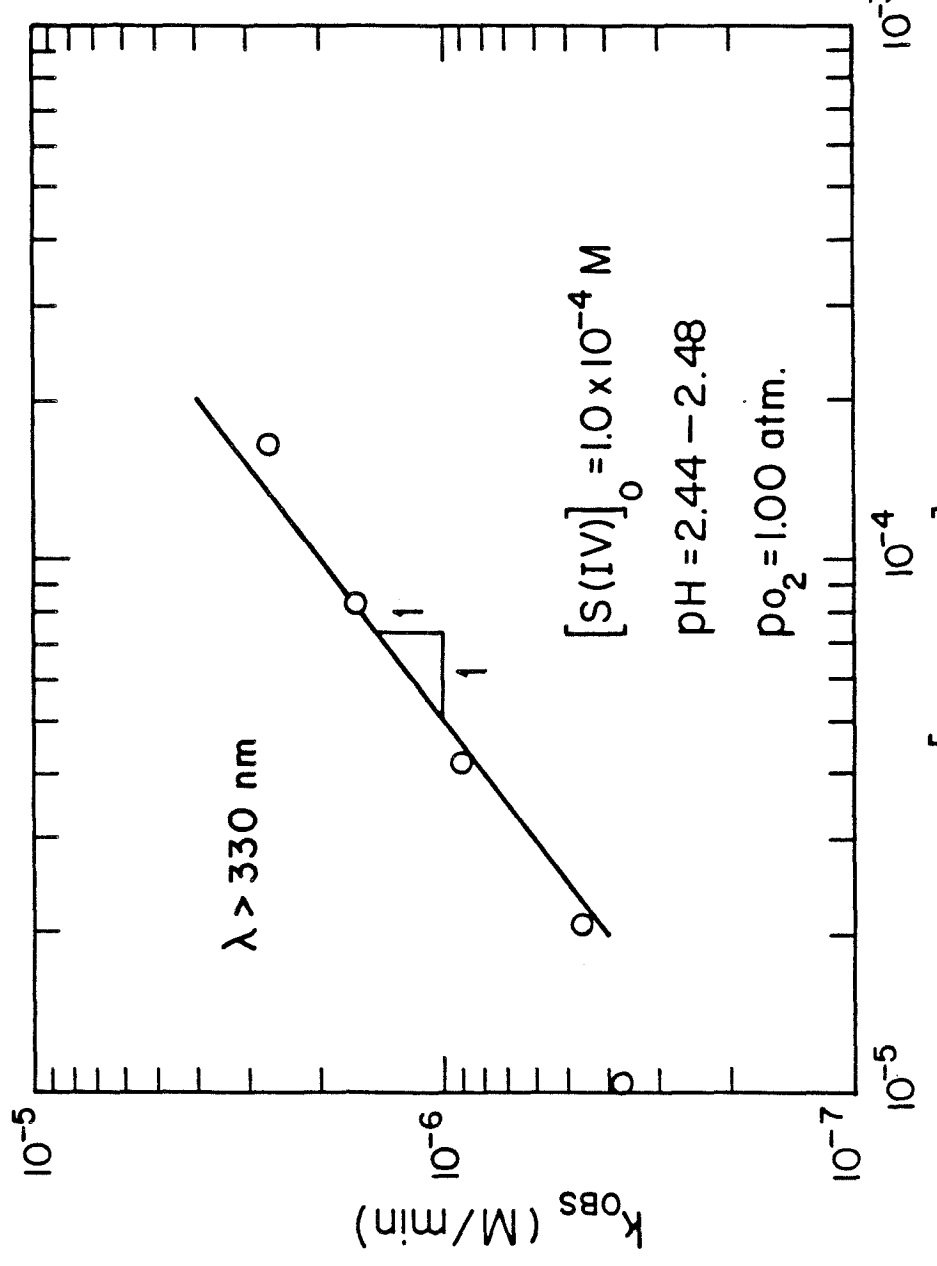

Figure 4.11. Pseudo-order rate constant for S(IV) autoxidation as a function of hematite concentration.

≡Fe(III)-S(IV) surface complexes undergo a photo-induced ligand to metal charge transfer reaction resulting in the reductive dissolution of hematite.

4.2.3.3 Oxygen

From Figure 4.12 one observes that rates of oxygen reduction in illuminated hematite suspensions containing S(IV) also exhibit autocatalytic behavior. This is consistent with the idea that continuous surface photochemical production of $Fe(II)_{aq}$ and oxidation to $Fe(III)_{aq}$ results in increasing $[Fe(III)_{aq}]$ and therefore increasing rates of S(IV) autoxidation and O_2 reduction.

4.2.3.4 pH

In Figure 4.13 results of pH dependence experiments, designed to determine the reactive S(IV) species, are presented. The pH dependence of the normalized rate constants, R, is similar to the distribution diagram of $HOSO_2^-$ for $pK_{a1} = 1.8$ and $pK_{a2} = 7.2$. This suggests that the rate determining step involves $HOSO_2^-$ as the principal reactive species over the pH range of 1 to 3. The reaction appears to proceed via the rapid formation of bisulfite/iron surface complexes formed by ligand exchange with protonated surface hydroxyl groups ($pH_{zpc} = 8.5$ vide supra). Thus a surface reaction producing $\equiv FeOSO_2H$, which subsequently undergoes a rate-determining electron transfer, is also consistent with the observed pH dependence.

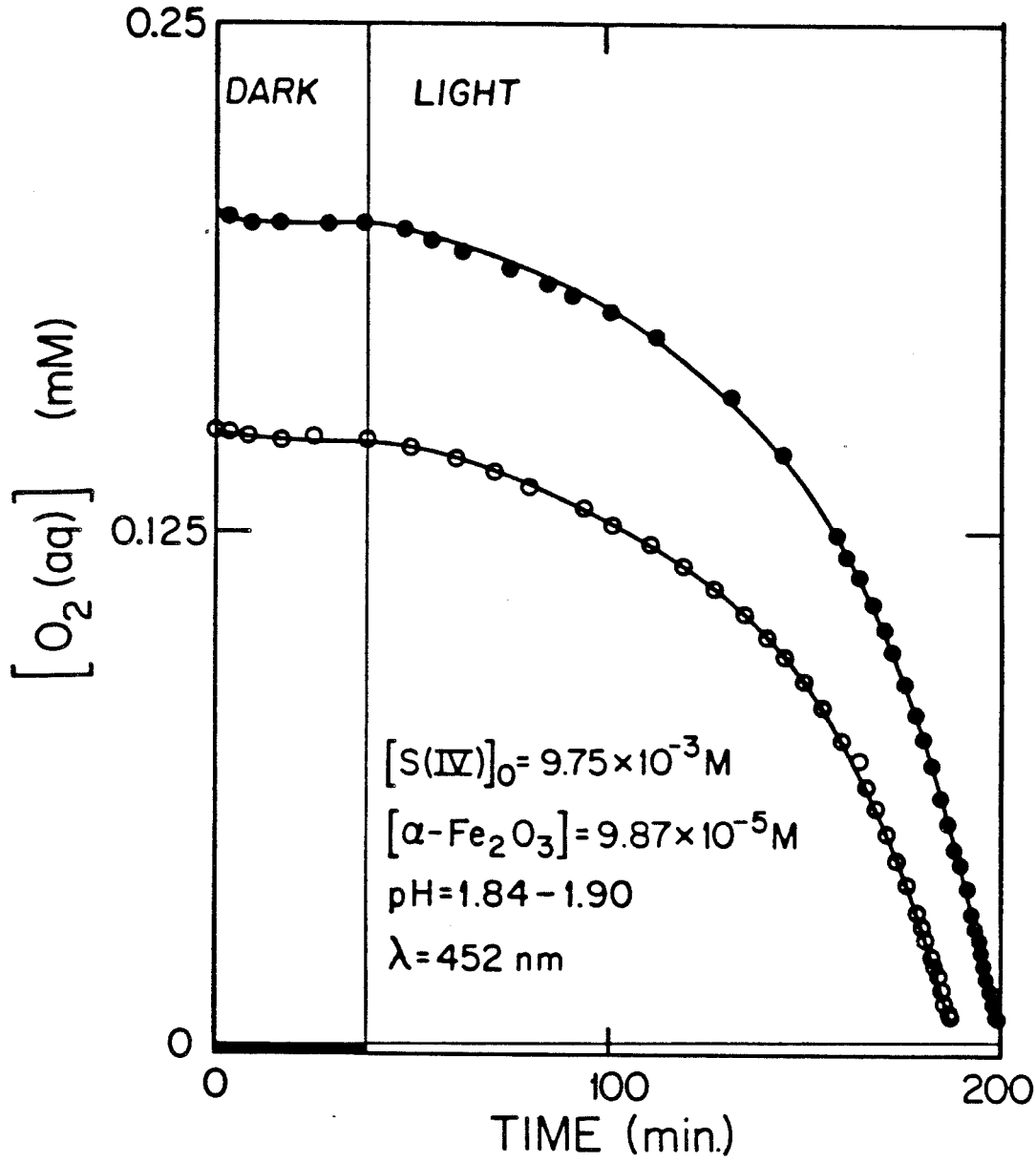

Figure 4.12. Reduction of molecular oxygen by S(IV).

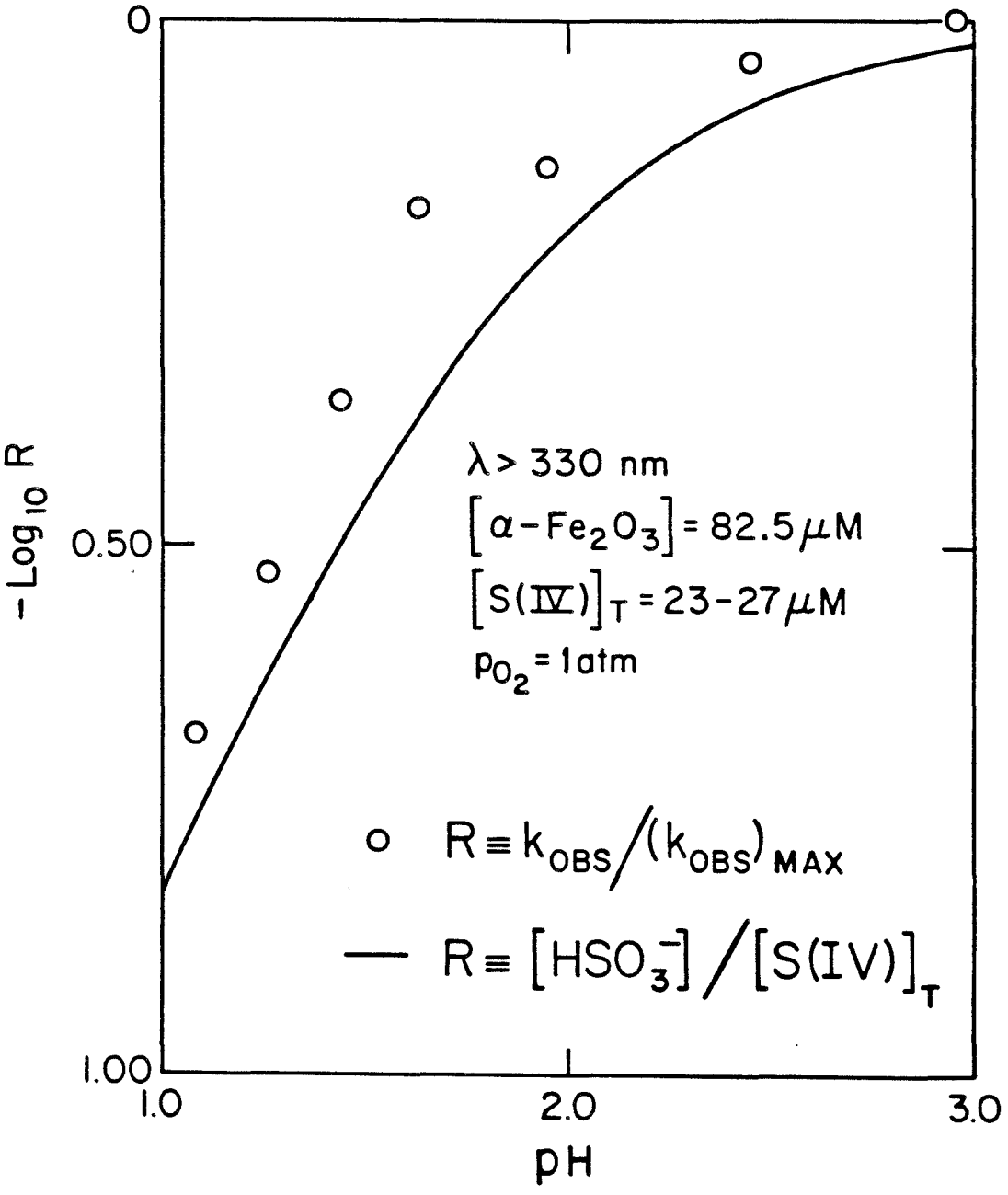

Figure 4.13. Experimental rate constants for S(IV) autoxidation as a function of pH.

4.3 Reaction Model

4.3.1 Kinetic Model for S(IV) Oxidation

4.3.1.1 General Model Description

An overall mechanism consistent with the autocatalytic nature of S(IV) autoxidation in illuminated hematite suspensions appears to involve three general steps: i) production of $Fe(II)_{aq}$ from photo-induced charge transfer reactions involving ≡Fe(III)-S(IV) surface complexes, ii) induced oxidation of $Fe(II)_{aq}$ and S(IV) by O_2, and iii) $Fe(III)_{aq}$ catalyzed autoxidation of S(IV). These processes can be represented by the following stoichiometric reactions:

$$<\equiv Fe(III)>_2 S(IV) \xrightarrow[h\nu]{k_1} 2\ Fe(II)_{aq} + S(VI) \qquad (4.30)$$

$$FeOSO_2H^+ + 3/4\ O_2 \xrightarrow{k_2'} Fe^{3+} + SO_4^{2-} + 1/2\ H_2O \qquad (4.31)$$

$$HOSO_2^- + 1/2\ O_2 \xrightarrow[Fe(III)_{aq}]{k_3} SO_4^{2-} + H^+ \qquad (4.32)$$

Rate expressions corresponding to reactions 4.30 - 4.32 can be formulated as:

$$\nu_1 = k_1[S(IV)]_{ADS} \qquad (4.33)$$

$$\nu_2 = k_2[Fe(II)_{aq}][S(IV)]_{aq}[O_2(aq)] \qquad (4.34)$$

$$\nu_3 = \frac{k_3[Fe(III)_{aq}][S(IV)]_{aq}}{[H^+]} \quad (4.35)$$

These rate expressions (vide infra), together with the S(IV) adsorption isotherm (Equation 4.1), form the basis of the kinetic model used to predict the rate of S(IV) autoxidation in illuminated hematite suspensions.

The model uses a fifth order Runge-Kutta routine to solve the following system of coupled differential equations:

$$\frac{d[Fe(II)_{aq}]}{dt} = \nu_1 - \nu_2 \quad (4.36)$$

$$\frac{d[Fe(III)_{aq}]}{dt} = \nu_2 \quad (4.37)$$

$$\frac{d[S(IV)]_{aq}}{dt} = -1/2\ \nu_1 - \nu_2 - \nu_3 \quad (4.38)$$

$$\frac{d[O_2(aq)]}{dt} = -3/4\ \nu_2 - 1/2\ \nu_3 \quad (4.39)$$

4.3.1.2 Kinetic Model for Hematite Reductive Dissolution

The average rate of $Fe(II)_{aq}$ production can be formulated as:

$$\frac{d[Fe(II)_{aq}]}{dt} = \sum_{\lambda} \Phi(\lambda) \cdot I'_a(\lambda) \quad (4.40)$$

where λ is the wavelength of light (nm), $\Phi(\lambda)$ is the quantum yield, and $I'_a(\lambda)$ is the volume-averaged absorbed light intensity (einstein/L-min). However the absorbed light intensity can be expressed as:

$$I'_a = I'_o(1 - 10^{-\epsilon CL}) \qquad (4.41)$$

where ϵ, C, and L are as previously defined (Section 4.2.2.1), and I'_o is the volume-averaged light intensity incident to the reactor cell. The average rate of $Fe(II)_{aq}$ production (Equation 4.40) is then equated to a first order rate expression (Equation 4.33) to determine, with known $[S(IV)]_{ADS}$ and for fixed intensity, the rate constant k_1.

4.3.1.3 Induced Oxidation of Fe(II) and S(IV)

Although the rate expression for $Fe(II)_{aq}$ oxygenation in the presence of S(IV) has not been determined, numerous investigators have found the rate of $Fe(II)_{aq}$ oxidation to be first order in both $[Fe(II)_{aq}]$ and $[O_2(aq)]$ (Stumm and Lee, 1961; Singer and Stumm, 1970; Kurimura et al., 1968; Tamura et al., 1976; and Goto et al., 1970). The reaction rate is independent of pH for values of pH < 3.5 (Singer and Stumm, 1970). Tamura et al. (1976) and Kurimura et al. (1968) have found the rate of $Fe(II)_{aq}$ oxygenation to be first order in total ligand concentration for ligands such as $H_2PO_4^-$, F^-, and a wide variety of aminocarboxylates. This suggests that the form of the rate expression for the autoxidation of

$Fe(II)_{aq}$, in aqueous S(IV) solutions at low pH, may be reasonably stated as in equation 4.34. Neytzell de Wilde and Taverner (1958) found that, in oxygenated solutions of $Fe(II)_{aq}$/S(IV), the autoxidation kinetics of both $Fe(II)_{aq}$ and S(IV) were very similar. They observed that $Fe(II)_{aq}$ and S(IV) autoxidation kinetics exhibited induction periods of similar time, followed by rapid rates of oxidation. For one experiment at 20°C ($[Fe(II)_{aq}]_o$ = 0.6 mM, [S(IV)] = 1.1 mM, pH = 2.7), they found that 0.4 mM $Fe(II)_{aq}$ was oxidized in less than two minutes. This implies that the half-life of $Fe(II)_{aq}$, under these conditions, is less than two minutes. The half-life of $Fe(II)_{aq}$ at pH = 2.7 (p_{O2} = 0.21 atm), but in the absence of S(IV), is six years (Singer and Stumm, 1970). The accelerated rate of $Fe(II)_{aq}$ autoxidation in solutions of S(IV) has also been observed by Huss et al. (1982).

4.3.1.4 Fe(III) Catalyzed Autoxidation of S(IV)

The $Fe(III)_{aq}$ catalyzed autoxidation of S(IV), represented by reaction 4.32, has been investigated by Aubuchon (1976), and Martin (1984). The rate expression and rate constant (k_3 = 49.2 min^{-1}) reported by Martin (1984) are used for all model calculations.

4.3.2 Model Predictions

The results of a model calculation are presented in Figure 4.14. For this experiment the rate constant for $Fe(II)_{aq}$ production is

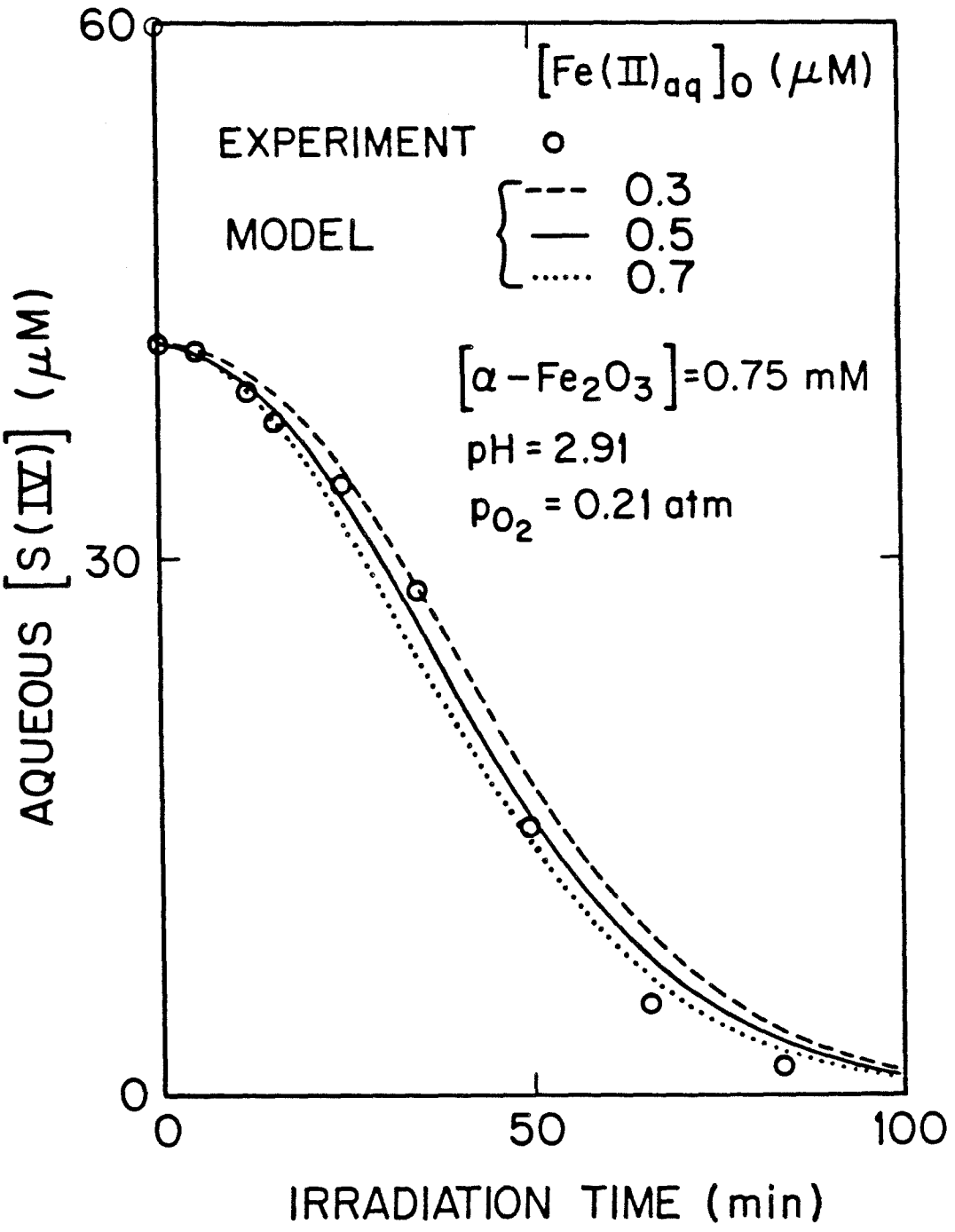

Figure 4.14. Experimental results and model predictions of S(IV) autoxidation rates, with monochromatic illumination. λ = 452 nm, I_o' = 13 μ(einstein)/L-min.

$k_1 = 2.4 \times 10^{-3}$ min^{-1}. The rate constant for $Fe(II)_{aq}$ oxygenation, k_2, was optimized by a nonlinear least squares method in this calculation. Illumination of deoxygenated hematite suspensions, containing S(IV), results in a small, but initially rapid increase in $[Fe(II)_{aq}]$ (0.3 - 0.7 μM), followed by a constant rate of $Fe(II)_{aq}$ production. Therefore, the rate constant for Fe(II) autoxidation, k_2, was optimized, with an initial $[Fe(II)_{aq}]_o$ = 0.5 μM. The value of k_2, determined by this method, is k_2 = 2.5×10^6 $M^{-2}min^{-1}$ which is used for all model calculations. Using the rate expression for $Fe(II)_{aq}$ oxidation (Equation 4.34) to interpret the results of Neytzell de Wilde and Taverner (1958), at 20°C, one estimates $k_2 = 4.6 \times 10^5$ $M^{-2}min^{-1}$, which is a factor of 5.5 smaller than the model optimized value. From Figure 4.14, one observes that the model predictions, albeit with an optimized value of k_2, are in reasonable quantitative aggreement with the corresponding experiment. Further, one notices that the initial $[Fe(II)_{aq}]_o$ has a moderate influence on the rate of S(IV) oxidation for these conditions.

The results of an experiment performed in the immersion well reactor (IWR), utilizing "white light" ($\lambda > 330$ nm), are presented in Figures 4.15 and 4.16 together with the corresponding model predictions. Because of lower $[S(IV)]_{ADS}$, shorter light path length, and greater light intensity, the absorbance of reactants in the IWR experiment is less than that for the experiment which utilized the monochromatic illumination system (MIS). The

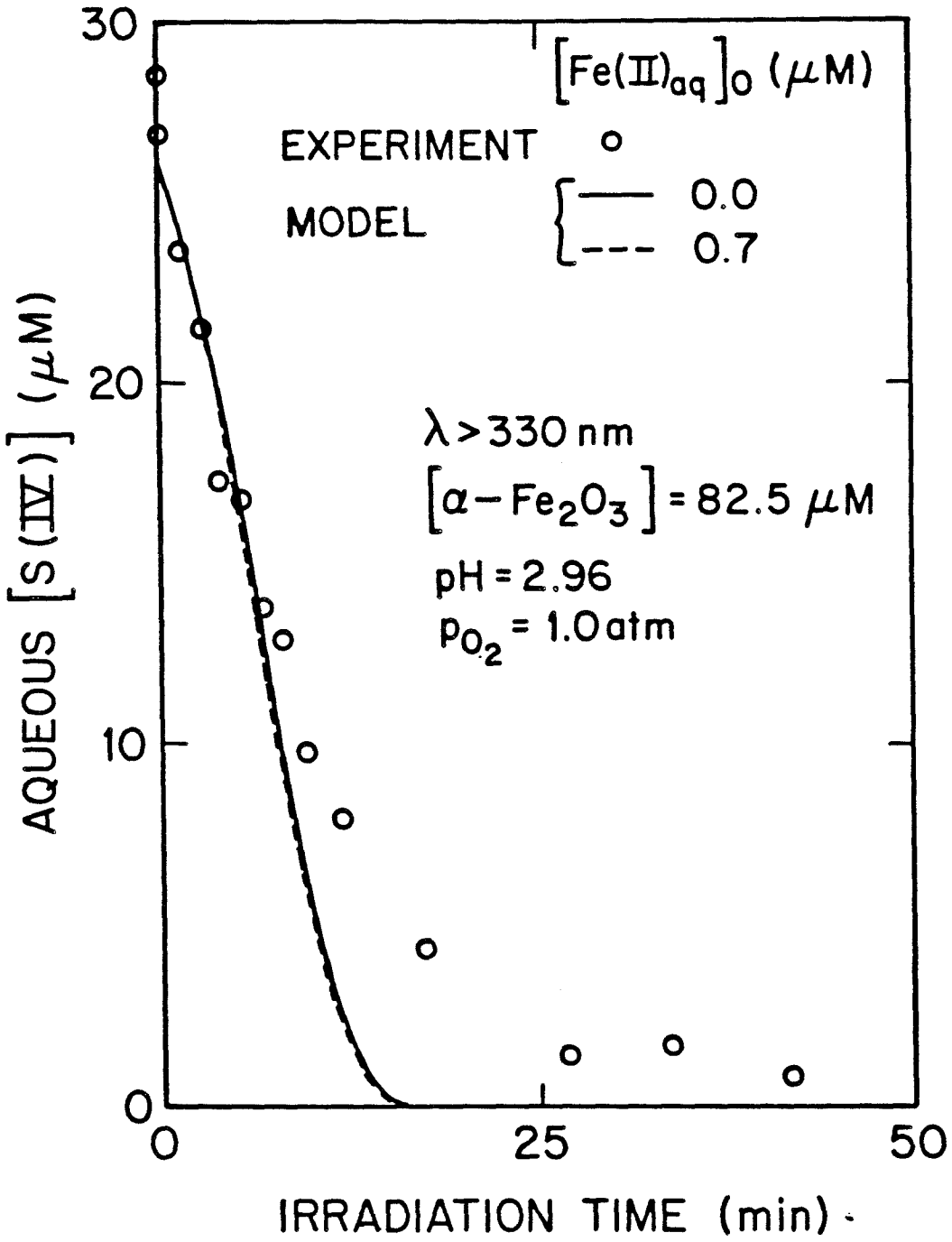

Figure 4.15. Experimental results and model predictions of S(IV) autoxidation rates, with polychromatic illumination.

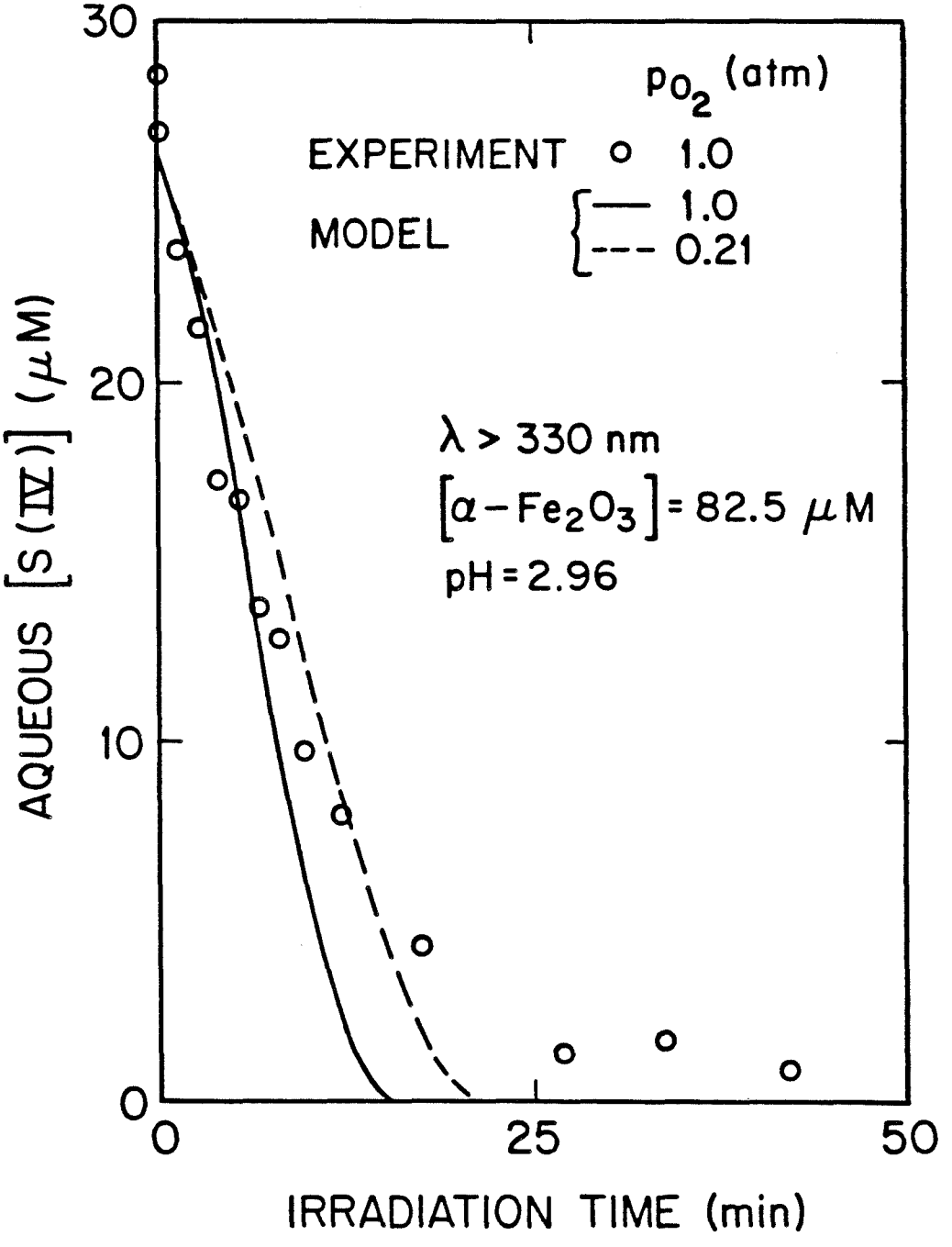

Figure 4.16. Experimental results, and model predictions of S(IV) autoxidation rates for different oxygen partial pressures, with polychromatic illumination.

absorbance, εCL, where ε, C, and L are as previously defined (Section 4.2.2.1), is calculated assuming the Lambert-Beer law is applicable for $[S(IV)]_{ADS}$. Thus, for the IWR experiment, the absorbance can be estimated by scaling for the different $[S(IV)]_{ADS}$ and light path lengths. The volume-averaged light intensities, $I_o'(\lambda)$, were calculated using the manufacturers specified spectral energy distribution of the Hg-vapor lamp, corrected for absorption by the UV filter (Table 3.3). Quantum yields for $Fe(II)_{aq}$ production, corresponding to the spectral distribution of the Hg-vapor lamp, were calculated by linear interpolation between known values. For the fixed intensity of the IWR experiment, $k_1 = 0.96\ min^{-1}$. Due to a higher rate of $Fe(II)_{aq}$ production, initial $[Fe(II)_{aq}]$ does not affect the rate of S(IV) oxidation as significantly for IWR experiments as for MIS experiments (Compare Figures 4.14 and 4.15). From Figures 4.14 - 4.16, one observes that the model predictions are in reasonable quantitative agreement with experimental observations over a wide range of conditions. This suggests that the model may be generally valid for most experiments reported here. A conceptual model of the redox chemistry of oxygenated hematite suspensions containing S(IV) is presented in Figure 4.17.

4.3.3 Band Model Interpretation

Hoffmann (1984) has suggested an alternative mechanism for the autoxidation of S(IV) on illuminated hematite surfaces. The

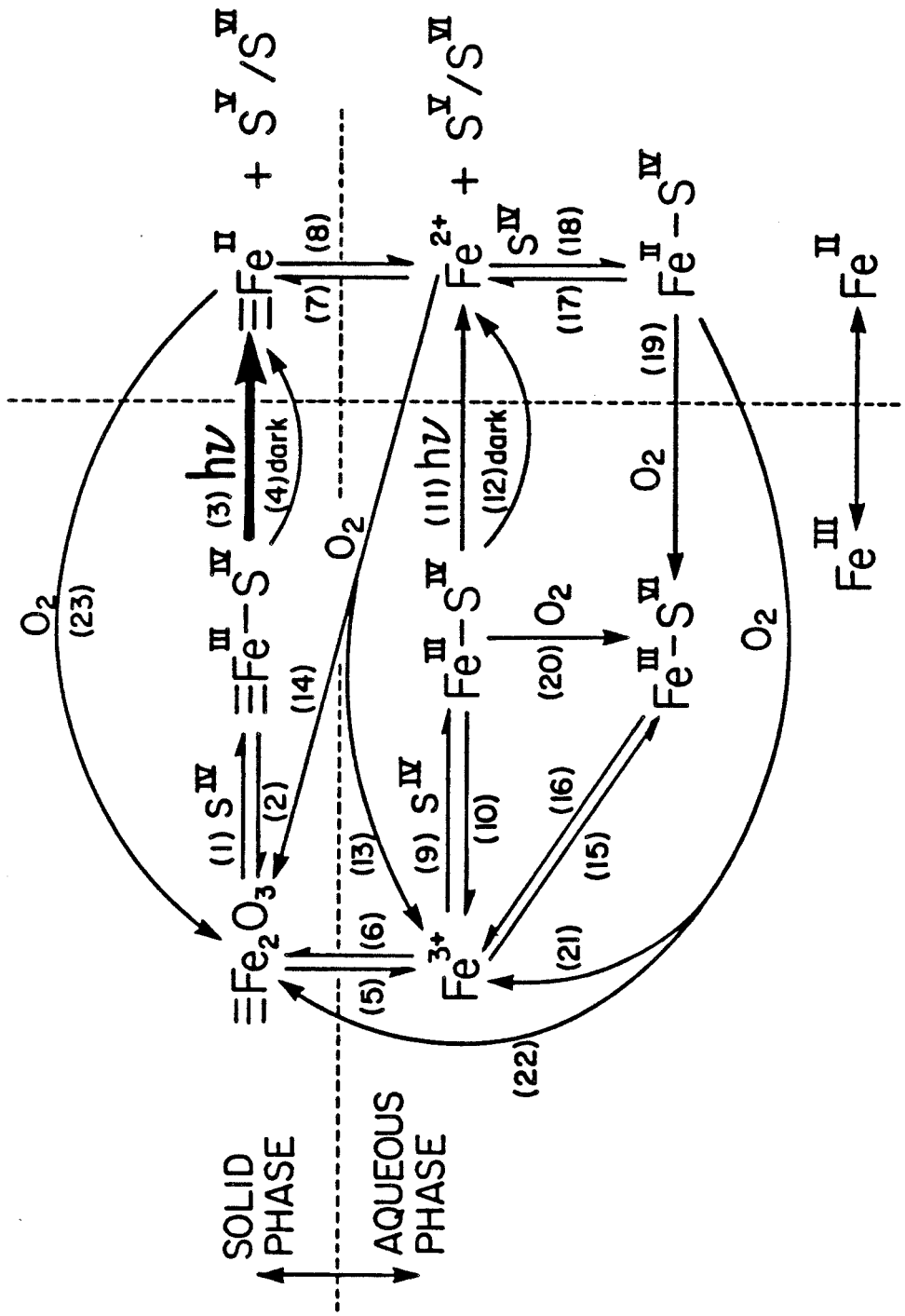

Figure 4.17. Conceptual model of the redox chemistry of oxygenated hematite suspensions containing S(IV).

suggested mechanism postulates that both S(IV) and O_2 are adsorbed on hematite, and that band gap excitation of the solid promotes electron transfer from adsorbed S(IV) to O_2 through the solid. A possible rate expression for this process is:

$$\frac{d[S(IV)]}{dt} = k\theta_{S(IV)}\theta_{O2}X_T \qquad (4.42)$$

(Hoffmann, 1984) where X_T is the molar concentration of surface sites. The quantity θ_i is described by a Langmuir adsorption isotherm:

$$\theta_i = \frac{[i]_{ADS}}{X_T} = \frac{K_i C_i}{1 + \Sigma K_i C_i} \qquad (4.43)$$

where K_i and C_i are the Langmuir adsorption constant (M^{-1}) and molar concentration of aqueous species "i" respectively, and $[i]_{ADS}$ is the molar concentration of adsorbed species "i". Note that a functional relationship between specific surface area and surface site concentration is given in equation 4.2.

For constant intensity of illumination the rate expression can be expressed as:

$$\frac{d[S(IV)]}{dt} = \frac{kK_1K_2[S(IV)]_{aq}[O_2]_{aq}X_T}{(1 + K_1[S(IV)]_{aq} + K_2[O_2]_{aq})^2} \qquad (4.44)$$

(Hoffmann, 1984) where K_1, K_2 are Langmuir adsorption constants

(M^{-1}) for S(IV) and O_2 respectively. The functional form of equation 4.44 does not exclude the possibility of autocatalytic-like behavior. In a limiting case, where $K_1[S(IV)]_{aq} >> 1$, $K_2[O_2]_{aq}$, equation 4.44 takes the form:

$$\frac{d[S(IV)]}{dt} \approx \frac{kK_2[O_2]_{aq}X_T}{K_1[S(IV)]_{aq}} \qquad (4.45)$$

Under these conditions and when $[O_2]_o > [S(IV)]_o/2$, equation 4.45 could predict that the disappearance of S(IV) with time resembles that predicted by an autocatalytic rate expression.

This mechanism (illustrated in Figure 4.18) assumes that the bulk solid is the chromophore, and further requires one of two possible chemical conditions. If the band model is applicable it implies a delocalized network of electrons which facilitate electron transfer from S(IV) to O_2. This is not consistent with the quantum yield studies. A more localized model for bulk solid excitation would require S(IV) and O_2 to adsorb on adjacent surface sites, so that electron transfer from S(IV) to O_2, through the solid lattice, would compete effectively with electron-hole recombination. The co-adsorption of S(IV) and O_2 on adjacent sites is a rather stringent constraint, and unlikely. However, this possibility can not be excluded.

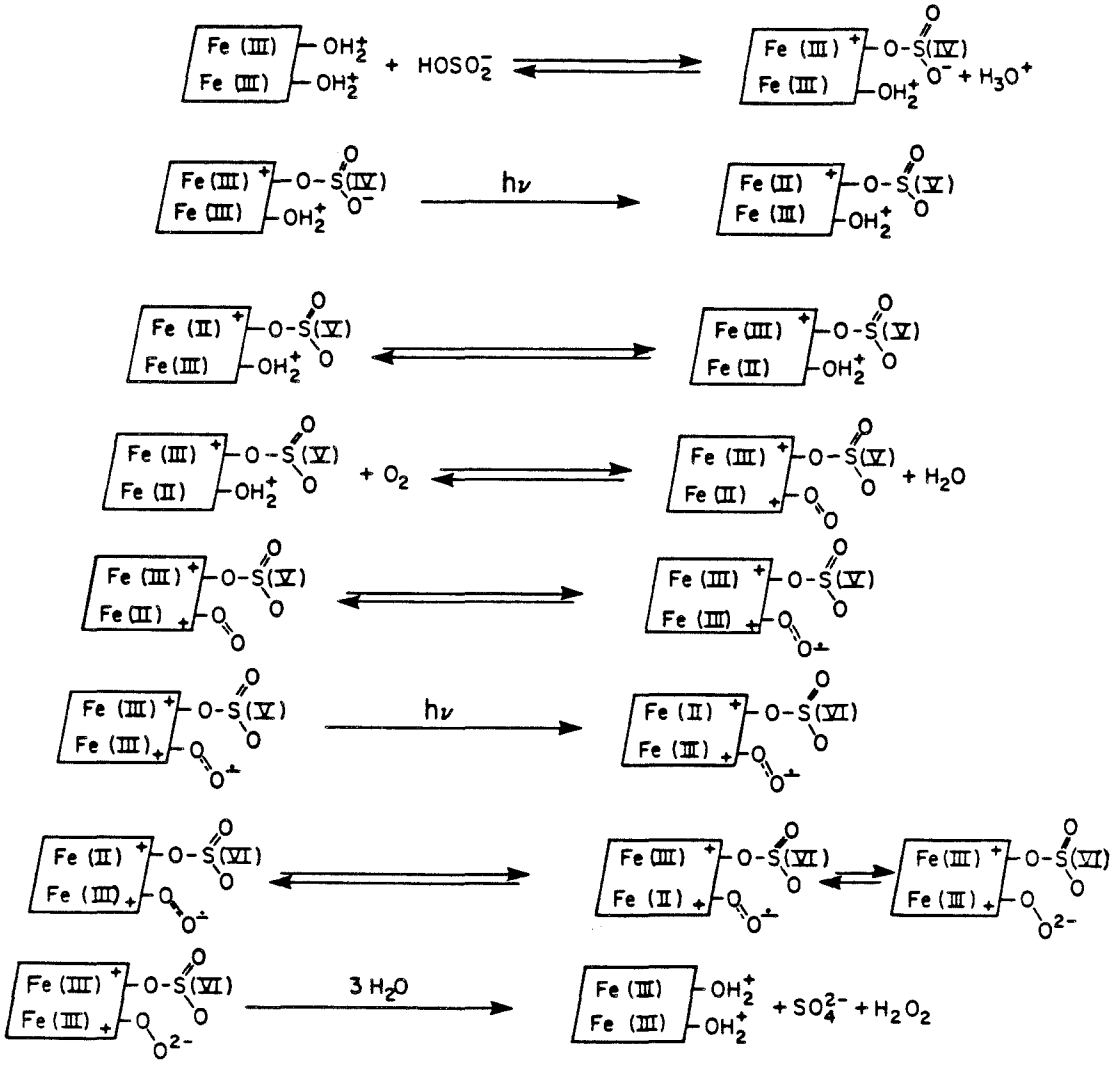

Figure 4.18 A possible mechanism for S(IV) autoxidation in illuminated hematite suspensions. Hoffmann (1984).

CHAPTER 5

SUMMARY AND CONCLUSIONS

5.1 Reductive Dissolution of Hematite

This work demonstrates that ≡Fe(III)-S(IV) surface complexes on α-Fe_2O_3 undergo a photo-induced charge transfer reaction resulting in the reductive dissolution of hematite. An experimental rate expression for the photo-induced reductive dissolution of hematite can be formulated as:

$$\frac{d[Fe(II)]_{aq}}{dt} = \Phi_{Fe(II)} I_o (A/V) \qquad (5.1)$$

Direct excitation of charge transfer bands in ≡Fe(III)-S(IV) surface complexes provide the simplest explanation which is consistent with experimental observations, although excitation of the low energy $O^{2-} \longrightarrow Fe^{3+}$ charge transfer band in the bulk solid cannot be totally excluded.

5.2 S(IV) Oxidation

A reasonable explanation for the autoxidation of S(IV) in illuminated hematite suspensions involves three general processes: i) production of $Fe(II)_{aq}$ from photo-induced ligand to metal charge transfer reactions of ≡Fe(III)-S(IV) surface complexes, ii) oxidation of $Fe(II)_{aq}$ to $Fe(III)_{aq}$ and, iii) the $Fe(III)_{aq}$ catalyzed autoxidation of S(IV). Predictions of a numerical model, based on these processes, agree reasonably well with experiments carried out

under a wide range of conditions. This suggests that the model may have general validity for the results reported here.

5.3 Roles of Surface Photo-redox Reactions in Natural Waters

Illumination of some solids with visible and near UV light is capable of accelerating the rates of their surface redox reactions. Similar processes may possibly play important roles in the atmospheric transformations of SO_2, aldehydes, ketones, and aldehyde addition products (Hoffmann and Jacob, 1984). Photo-induced reductions of iron (hydrous) oxides in surface and atmospheric waters will increase the concentrations of $Fe(II)_{aq}$ and $Fe(III)_{aq}$ above levels which would be predicted to exist in oxygenated waters at equilibrium with the atmosphere. The net effect of surface photo-redox reactions may be to increase the rate of iron cycling in surface and atmospheric waters and to increase the concentrations of iron species which may be preferred for biological uptake. Furthermore, reactions which are catalyzed by $Fe(III)_{aq}$, such as S(IV) autoxidation, may proceed at much higher rates than those predicted by models which constrain $Fe(III)_{aq}$ to be in equilibrium with an iron (hydrous) oxide phase. In addition, photo-induced reductions of Mn(III, IV) and Fe(III) (hydrous) oxides by naturally occurring organics are likely to play important roles in the geochemical cycling of these elements.

The overall reaction rate for a given surface photo-chemical reaction of interest in natural waters will depend on: i) the

relative abundance of the solid in natural waters, ii) the wavelength dependent quantum yield of surface complexes and/or of the solid for the given chemical reaction, and iii) the wavelength dependent light intensity in the water of interest.

The band model has proven to be a useful model for understanding the electronic properties of some solids. In order to assess the potential of a wide variety of naturally occurring solids for participating in surface photochemical reactions, an examination of the band gap energies of some well characterized solids may be useful, provided one realizes that the band theory may not be the most appropriate model for the electronic properties of all solids. Table 5.1 provides a listing of band gap energies for some binary compound semiconductors (Strehlow and Cook, 1973). Within the framework of band theory, for a solid to participate in surface photochemical reactions of interest in natural waters, its band gap energy must be constrained to values less than 4.20 eV, which corresponds to light of wavelength 295 nm. The minimum energy required to "activate" the solid may be altered by surface coordination, stoichiometric deficiencies, impurities, and crystal defects, all of which may introduce energy levels within the "band gap." Of the solids listed in Table 5.1, Fe(III) and Mn(IV) oxides are capable of being "activated" by visible light, are very insoluble, and therefore are likely to exhibit surface photo-redox activity in natural waters. Some of the transition metal sulfides may also exhibit photo-induced corrosion reactions. Solids with

Table 5.1. Band gap energies of some binary semiconductor compounds. Data are from Strehlow and Cook (1973).

Compound	Band gap, E_G (eV)	Wavelength of light, λ_G, equivalent to E_G (nm)
MgO	7.77	160
CaO	7.7	161
ZnO	3.35	370
PbO	2.76	499
SiO_2	11.0	113
TiO_2 (rutile)	3.0-3.3	376-413
β-MnO_2 (rutile)	0.26	4769
β-PbO_2	1.7	729
$PbBr_2$	3.2	387
Al_2O_3	9.5-9.9	125-131
α-Fe_2O_3 (hematite)	2.34	530
Cu_2S	1.2-1.9	653-1034
α-MnS	6.2	200
ZnS	3.7-3.9	318
CdS	2.4	517
β-HgS	0.54	2298
α-HgS	2.0	620
PbS	0.41	3026
FeS_2	1.2	1034

large band gap energies, such as Al_2O_3, SiO_2, and their naturally occurring analogs, are not likely to be active participants in surface photochemical reactions in natural waters.

Iron and manganese are major components of the earth's crust and oxy-hydroxides of Fe(III) and Mn(III,IV) are participants in many of the important chemical transformations occurring in natural waters (Morgan and Stumm, 1964). The oxygenation reactions of Mn(II) and Fe(II) have been well studied (Morgan and Stumm, 1964; Sung, 1980; Davies, 1984). More recently, reactions involving the reduction of Fe(III), and Mn(III,IV) oxides have been studied (Theis and Singer, 1974; Stone, 1983). However, the role of light in these redox reactions is not well understood.

Sunda et al. (1983), and Miles and Brezonik (1981) have shown that "humic acids" are capable of reducing Mn(III,IV) oxides and Fe(III), and that the rate of these reactions is greatly accelerated upon irradiation of the reactants with visible light. As Sunda et al. (1983) point out, photo-induced reduction of Mn(III,IV) oxides could explain, in part, the vertical distribution of Mn in the open ocean.

Manganese profiles in the ocean exhibit definite maxima in the photic zone (Klinkhammer and Bender, 1980). Only approximately 1% of the Mn in the upper 25 meters is present in particulate form (Landing and Bruland, 1980), and the dissolved manganese decreases rapidly below the photic zone with a concomitant increase in particulate concentrations. Photo-induced reductions of Mn(III,IV)

(hydrous) oxides by organics in the photic zone are a possible explanation for this phenomenon. In natural waters, organics will most likely be adsorbed onto particles such as metal oxides. Therefore, photo-induced reductions of Mn(III,IV) and Fe(III) (hydrous) oxides by naturally occurring organics are likely to play important roles in the geochemical cycling of these elements and in their availability to aquatic organisms. Investigations of well-defined model systems are needed to further understand the mechanisms of these photochemical surface redox reactions.

A study of the photo-induced redox reactions between γ-MnOOH, γ-FeOOH (or α-FeOOH) and selected model organics, such as benzoic acids, would provide insight into the mechanisms of corresponding reactions occurring in natural waters. The choice of these specific solids is based on the observations that γ-MnOOH is the end product of Mn(II) oxidation in lakewaters (Stumm and Morgan, 1981); and that γ-FeOOH (lepidocrocite) and α-FeOOH (goethite) are representative of the final products of Fe(II) oxygenation and Fe(III) hydrolysis in lake waters respectively. Organic compounds such as catechol, various dihydroxybenzoic acids, and gallic acid are reasonable representatives of the more complex "humic substances."

Of specific interest is the role of light in the reaction. A likely possibility is that light absorption by a surface complex promotes ligand to metal electron transfer, with subsequent desorption of the oxidized organic and lattice detachment and desorption of the reduced metal.

Additionally, the kinetics of $Fe(II)_{aq}$ autoxidation in the presence of S(IV) oxyanions should be investigated in detail, because of its importance in the redox chemistry of iron and sulfur in hydrometeors.

LITERATURE CITED

Agren, A. (1954) Acta Chemica Scan. 8, 266-279.

Atkinson, R. J., R. L. Parfitt, and R. St. C. Smart (1970) J. Chem. Soc., Faraday Trans. 1 70, 1472-1479.

Atkinson, R. J., A. M. Posner, and J. P. Quirk (1967) J. Phys. Chem. 71, 550.

Aubuchon, C. S. (1976) "The Rate of Iron Catalyzed Oxidation of Sulfur-Dioxide by Oxygen in Water," Ph.D. Thesis, The Johns Hopkins University.

Bäckstrom, H. L. J. (1934) Z. Phys. Chem. (Leipzig) 25B, 122-138.

Bahnemann, D., A. Henglein, and L. Spanhel (1984) Faraday Discuss. Chem. Soc. 78.

Balzani, V., and V. Carassiti (1970) Photochemistry of Coordination Compounds, Academic Press, 11-12.

Bard, A. J. (1979) J. Photochemistry 10, 59-75.

Bassett, H., and W. G. Parker (1951) J. Chem. Soc. (Lon.) 1540-1560.

Becker, W. G., and A. J. Bard (1983) J. Phys. Chem. 87:24, 4888-4893.

Becquerel, E. (1839) Compt. Rend. 9, 561.

Bedarida, F., F. Flamini, O. Grubessi, and G. M. Pedemonte (1973) Am. Mineralogist 58, 794-795.

Bedarida, F., and G. M. Pedemonte (1971) Am. Mineralogist 56, 1469-1473.

Boyce, S. D., M. R. Hoffmann, P. A. Hong, and L. M. Moberly (1983) Environ. Sci. Technol. 17, 602-611.

Brimblecombe, P., and D. J. Spedding (1974) Atmos. Environ. 8, 937-945.

Calvert, J. G. (1956) Photoactivated Surface Reactions, Report No. 15, Air Pollution Foundation, Los Angeles, CA, 91-109.

Calvert, J. G., and W. R. Stockwell (1984) in SO_2, NO and NO_2 Oxidation Mechanisms, Acid Precip. Ser., Vol. 3, J. G. Calvert, ed., Ann Arbor Sci., Chp. 1, 1-62.

Calvert, J. G., F. Su, J. W. Bottenheim, and O. P. Strausz (1978) Atmos. Environ. 12, 197-226.

Calvert, J. G., K. Theurer, G. T. Rankin, and W. MacNevin (1954) J. Am. Chem. Soc. 76, 2575-2578.

Carey, J. H., and C. H. Langford (1975) Can. J. Chem. 53, 2436-2440.

Carlyle, D. W. (1972) J. Am. Chem. Soc. 94, 4525-4529.

Carlyle, D. W. (1971) Inorg. Chem. 10, 761-764.

Chang, H. C., and E. Matijevic (1983) J. Colloid Interface Sci. 92:2, 479-488.

Childs, L. P., and D. F. Ollis (1980) J. Catal. 66, 383-390.

Collienne, R. H. (1983) Limnology & Oceanography 28:1, 83-100.

Cotton, F. A., and G. Wilkinson (1962) Advanced Inorganic Chemistry, 2nd ed., John Wiley and Sons, Inc.

Dana, E. S., and W. E. Ford (1960) A Textbook on Mineralogy, John Wiley and Sons, Inc., NY.

Davies, S. H. R. (1984) Ph.D. Thesis, California Institute of Technology.

El-Wakil, A. M., M. S. Soliman, and A. B. Farag (1983) Z. Naturforsch. 38b, 858-860.

Erickson, R. E., L. M. Yates, R. L. Clark, and D. McEwen (1977) Atmos. Environ. 11, 813-817.

Feeya, D., and P. G. David (1976) J. Phys. Chem. 80:6, 579-583.

Foster, P. M. (1969) Atmos. Environ. 3, 157-175.

Frank, S. N., and A. J. Bard (1977) J. Phys. Chem. 81, 1484-1488.

Freiberg, J. (1975) Atmos. Environ. 9, 661-672.

Fukasawa, T., M. Iwatsuki, S. Kawabuko, and K. Niyazaki (1980) Anal. Chem. 52, 1784-1787.

Fuzzi, S. (1978) Atmos. Environ. 12, 1439-1442.

Gerischer, H. (1977) J. Electroanal. Chem. 82, 133-143.

Gerischer, H. (1979) in Light-Induced Charge Separation in Biology and Chemistry, H. Gerischer and J. J. Katz, eds., Berlin: Dahlem Konferenzen, 61-86.

Gerischer, H. (1980) Far. Discuss. Chem. Soc. 70, 137-151.

Gerischer, H. (1983) J. Electroanal. Chem. 150, 553-569.

Golding, R. M. (1960) J. Chem. Soc., 3711-3716.

Gomes, W. P., T. Freund, and S. R. Morrison (1968) J. Electrochem. Soc. 115, 818-823.

Goodeve, C. F. (1938) Trans. Far. Soc. 34, 570-579.

Goto, K., H. Tamura, and M. Nagayama (1970) J. Inorg. Nucl. Chem. 9, 963.

Grauer, R., and W. Stumm (1982) Colloid and Polymer Sci. 260, 959-970.

Gravelle, P. C., F. Juillet, P. Meriaudeau, and S. J. Teichner (1971) Faraday Discuss. Chem. Soc. 52, 140-148.

Haber, F., and O. H. Wansbrough-Jones (1931) Z. Phys. Chem. 18B, 103-123.

Harbour, J. R., and M. L. Hair (1977) J. Phys. Chem. 81:18, 1791-1793.

Hayon, E., E. Treinin, and J. Wilf (1972) J. Am. Chem. Soc. 94, 47-57.

Hingston, F. J. (1981) in Adsorption of Inorganics at Solid-Liquid Interfaces, M. A. Anderson and A. J. Rubin, eds., Ann Arbor Sci., Chp. 2, 51-90.

Hingston, F. J., A. M. Posner, and J. P. Quirk (1971) Faraday Discuss. Chem. Soc. 52, 334-342.

Hoffmann, M. R., and S. D. Boyce (1983) in Trace Atmospheric Constituents, Adv. Environ. Sci. & Technology, Vol. 12, S. E. Schwartz, ed., John Wiley & Sons, Chp. 3, 147-189.

Hoffmann, M. R., and D. J. Jacob (1984) in SO_2, NO and NO_2 Oxidation Mechanisms, Acid Precip. Ser., Vol. 3, J. G. Calvert, ed., Ann Arbor Sci., Chp. 3, 101-172.

Hoffmann, M. R. (1984) personal communication.

Huie, R. E., and P. Neta (1984) J. Phys. Chem., in press.

Humphrey, R. C., M. H. Ward, and W. Hinze (1970) Anal. Chem. 42:7, 698-702.

Huss, A., P. K. Lim, and C. A. Eckert (1978) J. Am. Chem. Soc. 100, 6252-6253.

Hutchinson, G. E. (1957) A Treatise on Limnology, Volume 1, Part 2, John Wiley & Sons.

Karraker, D. G. (1963) J. Phys. Chem. 67, 871-874.

Kautek, W., and H. Gerischer (1982) Surf. Sci., 46-60.

Kennedy, J. H., and K. W. Frese (1978) J. Electrochem. Soc. 125:5, 709-714.

Klinkhammer, G. P., and M. L. Bender (1980) Earth & Plan. Sci. Lett. 46, 361-384.

Kunen, S. M., A. C. Lazrus, G. L. Kok, and B. G. Heikes (1983) J. Geophys. Res. 88, 3671-3674.

Kurimura, Y., R. Ochiai, and N. Matsuura (1968) Bull. Chem. Soc. Japan 41, 2234-2239.

Kutal, C. (1983) J. Chem. Educ. 60:10, 882-887.

Landing, W. M., and K. W. Bruland (1980) Earth & Plan. Sci. Lett. 49, 45-56.

Langford, C. H., and J. H. Carey (1975) Can J. Chem. 53, 2430-2435.

Latimer, W. M. (1952) Oxidation Potentials, Prentice-Hall Inc.

Lever, A. B. P. (1974) J. Chem. Ed. 51:9, 612-616.

Liljestrand, H. M., and J. J. Morgan (1981) Environ. Sci. Technol. 15, 333-339.

Luňák, S., and J. Vepřek-Šiška (1976) Coll. Czech. Chem. Comm. 41, 3495-3503.

Maahs, H. G. (1983) Atmos. Environ. 17, 341-345.

Markham, M. C., and K. J. Laidler (1953) J. Phys. Chem. 57, 363-369.

Martin, L. R. (1984) in SO_2, NO, and NO_2 Oxidation Mechanisms, Acid Precip. Ser., Vol. 3, J. G. Calvert, ed., Ann Arbor Sci., Chp. 2, 63-100.

Marusak, L. A., R. Messier, and W. B. White (1980) J. Phys. Chem. Solids 41, 981-984.

Matijević, E., and P. Scheiner (1978) J. Colloid & Interface Sci. 63:3, 509-524.

McArdle, J. V., and M. R. Hoffmann (1983) J. Phys. Chem. 87, 5425-5429.

McGregor, K. G., M. Calvin, and J. W. Otvos (1979) J. Appl. Phys. 50:1, 369-373.

McMahon, J. W. (1969) Limnol. Oceanogr. 14, 357-367.

Miles, C. J., and P. L. Brezonik (1981) Environ. Sci. Technol. 15:9, 1089-1095.

Morgan, J. J., and W. Stumm (1964) "The Role of Multivalent Metal Oxides in Limnological Transformations, as Examplified by Iron and Manganese," Proceedings of the Second Conference on Water Pollution Research, Pergamon, Elmsford, NY.

Morimoto, T., T. Nagao, and F. Tokuda (1969) J. Phys. Chem. 73:1, 243-248.

Morin, F. J. (1959) in Semiconductors, ACS Mono. No. 140, N. B. Hannay, ed., Chp. 14, 600-633.

Morrison, S. R. (1980) Electrochemistry at Semiconductor and Oxidized Metal Electrodes, Plenum Press, NY.

Motschi, H. (1984) Colloids & Surfaces 9, 333-347.

Muller, H. (1932) Mikrochemie 12, 307-314.

Munger, J. W., D. J. Jacob, J. M. Waldman, and M. R. Hoffmann (1983) J. Geophys. Res. 88, 5109-5121.

Murray, J. W. (1979) in Marine Minerals, Vol. 6, R. G. Burns, ed., Minerological Society of America, Chp. 2, 47-98.

Neytzell de Wilde, F. G., and L. Taverner (1958) 2nd U.N. International Conference on the Peaceful Uses of Atomic Energy Proceedings, Vol. 3, 303-317.

Parfitt, R. L., and R. St. C. Smart (1977) J. Chem. Soc., Faraday Trans. 1 73, 796-802.

Parks, G. A., and P. L. de Bruyn (1962) J. Phys. Chem. 66, 967-973.

Penkett, S. A., B. M. R. Jones, K. A. Bruce, and A. E. J. Eggleton (1979) Atmos. Environ. 13, 123-137.

Rand, M. C., A. E. Greenberg, M. J. Taras, and M. A. Franson, eds. (1976) Standard Methods, 14th ed., 496-498.

Rubin, T. R., J. G. Calvert, G. T. Rankin, and W. MacNevin (1953) J. Am. Chem. Soc. 75, 2850-2853.

Schindler, P. (1981) in Adsorption of Inorganics at the Solid-Liquid Interfaces, M. A. Anderson and A. J. Rubin, eds., Ann Arbor Sci., Chp. 1, 1-50.

Sidebottom, H. W., C. C. Badcock, G. E. Jackson, J. G. Calvert, G. W. Reinhart, and E. K. Damon (1972) Environ. Sci. Technol. 6, 72-79.

Sidhu, P. S., R. G. Gilkes, R. M. Cornell, and J. P. Quirk (1981) Clays and Clay Minerals 29:4, 269-276.

Sigg, L., and W. Stumm (1980) Colloids and Surfaces 2, 101-117.

Singer, P. C., and W. Stumm (1970) Science 167, 3921.

Skoog, D. A., and D. M. West (1969) Fundamentals of Analytical Chemistry, 2nd ed., 414-416.

Smith, R. M., and A. E. Martell (1976) Critical Stability Constants, Plenum Press, NY.

Stone, A. T. (1983) "The Reduction and Dissolution of Mn(III) and Mn(IV) Oxides by Organics," Ph.D. Thesis, California Institute of Technology, Pasadena, CA.

Strehlow, W. H., and E. L. Cook (1973) J. Phys. Chem. Ref. Data 2, 163-199.

Strömberg, A., O. Gropen, R. Wahlgren, and O. Lindqvist (1983) Inorg. Chem. 22, 1129-1133.

Stumm, W., R. Kummert and L. Sigg (1980) Croatica Chemica Acta 53, 291-312.

Stumm, W., and G. F. Lee (1961) Ind. Eng. Chem. 53, 143.

Stumm, W. and J. J. Morgan (1981) Aquatic Chemistry, John Wiley & Sons, Inc.

Sunda, W. G., S. A. Huntsman, and G. R. Harvey (1983) Nature 301, 234-236.

Sung, W. (1980) "Catalytic Effects of the γ-FeOOH (Lepidocrocite) Surface on the Oxygenation Removal Kinetics of Fe(II) and Mn(II)," Ph.D. Thesis, California Institute of Technology, Pasadena, CA.

Tamura, H., K. Goto, T. Yotsuyanagi, and M. Nagayama (1974) Talanta 21, 314-318.

Tamura, H., K. Goto, and M. Nagayama (1976) J. Inorg. Nucl. Chem. 38, 113-117.

Taylor, D. D., and R. C. Flagan (1981) ACS Symposium Series No. 167 Atmospheric Aerosol: Source/Air Quality Relationships, E. S. Macias and P. K. Hopke, eds., 157-172.

Theis, T. L., and P. C. Singer (1974) Environ. Sci. & Technol. 8, 569.

Tossel, J. A., D. J. Vaughan, and K. H. Johnson (1973) Nature 244, 42-45.

Valentine, J. S. (1973) Chem. Rev. 73, 235-245.

Vepřek-Šiška, J. and S. Luňák (1974) Z. Naturforschung 29B, 689-690.

Vepřek-Šiška, J., S. Luňák, and A. El-Wakil (1974) Z. Naturforsch. 29b, 812-813.

Vogel, A. I. (1961) Quantitative Inorganic Analysis, p. 370.

Waite, T. D. (Dec. 1983) Ph.D. Thesis, Massachusetts Institute of Technology, Boston, MA.

Waldman, J. M., J. W. Munger, D. J. Jacob, R. C. Flagan, J. J. Morgan, and M. R. Hoffmann (1982) Science 218, 677-680.

Weast, R. C., and M. J. Astle, eds., (1980-81) CRC Handbook of Chemistry and Physics, Chemical Rubber Pub. Co., 61st ed.

Wegner, E. E., and A. W. Adamson (1966) J. Am. Chem. Soc. 88, 394-404.

Zepp, R. G., and M. Cline (1977) Environ. Sci. Technol. 11, 359-366.

A. EXPERIMENTAL DATA

Experiment Number 102282

$[S(IV)]_T = 2.09 \times 10^{-4}$ M

$[\alpha\text{-}Fe_2O_3] = 8.25 \times 10^{-5}$ M

Hematite batch 1

pH = 2.48

p_{O2} = 1.0 atm.

$\lambda > 330$ nm

I = Not available

hν + reactants: 0.0 min.

Time (min)	[S(IV)], (M)
0.0	2.09×10^{-4}
9.5	1.52×10^{-4}
20.5	1.14×10^{-4}
32.6	7.47×10^{-5}
48.2	3.52×10^{-5}
62.2	1.60×10^{-5}
85.3	7.53×10^{-6}

Experiment Number 110482

$[S(IV)]_T = 9.25 \times 10^{-5}$ M

$[\alpha\text{-}Fe_2O_3] = 8.25 \times 10^{-5}$ M

Hematite batch 1

pH = 2.45

p_{O2} = 1.0 atm.

$\lambda > 330$ nm

I = not available

hν + reactants: 0.0 min.

Time (min)	[S(IV)], (M)
0.0	8.93×10^{-5}
2.0	7.88×10^{-5}
5.3	6.81×10^{-5}
10.5	6.17×10^{-5}
20.7	4.23×10^{-5}
26.7	3.32×10^{-5}
32.5	2.29×10^{-5}
38.6	1.76×10^{-5}

Experiment Number 112982

$[S(IV)]_T = 1.09 \times 10^{-4}$ M

$[\alpha\text{-}Fe_2O_3] = 8.25 \times 10^{-5}$ M

Hematite batch 1

pH = 2.43

p_{O2} = 1.0 atm.

$\lambda > 330$ nm

I = not available

hν + reactants: 0.0 min.

Time (min)	[S(IV)], (M)
0.0	1.05×10^{-4}
4.3	9.18×10^{-5}
8.0	7.75×10^{-5}
11.3	6.72×10^{-5}
14.0	5.68×10^{-5}
18.8	4.19×10^{-5}
23.6	2.92×10^{-5}
29.4	1.70×10^{-5}
33.2	1.17×10^{-5}
37.4	8.75×10^{-6}
41.4	5.61×10^{-6}

Experiment Number 120182

$[S(IV)]_T = 1.18 \times 10^{-4}$ M

$[\alpha\text{-}Fe_2O_3] = 8.25 \times 10^{-5}$ M

Hematite batch 1

pH = 2.42

N_2 flow, $P_{O2} = 0$

$\lambda > 330$ nm

I = not available

hν + reactants: 0.0 min.

Time (min)	[S(IV)], (M)
0.0	1.09×10^{-4}
1.4	1.07×10^{-4}
5.9	1.01×10^{-4}
9.8	9.84×10^{-5}
13.8	9.06×10^{-5}
17.6	8.69×10^{-5}
21.7	8.04×10^{-5}
25.5	7.53×10^{-5}
29.3	6.90×10^{-5}
33.3	5.54×10^{-5}
39.4	5.59×10^{-5}
45.0	4.69×10^{-5}
56.5	3.41×10^{-5}
64.3	2.58×10^{-5}
74.1	1.70×10^{-5}

Experiment Number 120782

$[S(IV)]_T = 1.11 \times 10^{-4}$ M

$[\alpha\text{-}Fe_2O_3] = 1.64 \times 10^{-4}$ M

Hematite batch 1

pH = 2.44

p_{O2} = 1 atm.

$\lambda > 330$ nm

I = not available

hν + reactants: 0.0 min.

Time (min)	[S(IV)], (M)
0.0	1.04×10^{-4}
2.5	8.89×10^{-5}
5.4	8.01×10^{-5}
7.7	7.14×10^{-5}
10.3	6.46×10^{-5}
12.6	5.94×10^{-5}
15.0	5.22×10^{-5}
18.1	4.59×10^{-5}
20.6	4.15×10^{-5}
23.7	3.57×10^{-5}
29.2	2.75×10^{-5}
34.1	2.02×10^{-5}
41.7	1.29×10^{-5}
47.5	8.44×10^{-6}
52.2	5.63×10^{-6}
56.6	4.23×10^{-6}

Experiment Number 120882

$[S(IV])_T = 1.08 \times 10^{-4}$ M

$[\alpha\text{-}Fe_2O_3] = 4.14 \times 10^{-5}$ M

Hematite batch 1

pH = 2.45

pO_2 = 1 atm.

$\lambda > 330$ nm

I = not available

hν + reactants: 0.0 min

Time (min)	[S(IV)], (M)
0.0	1.03×10^{-4}
2.5	9.54×10^{-5}
7.5	9.03×10^{-5}
12.5	8.56×10^{-5}
19.2	8.01×10^{-5}
25.1	7.42×10^{-5}
31.1	6.86×10^{-5}
57.0	4.72×10^{-5}
62.5	4.32×10^{-5}
68.0	3.91×10^{-5}
73.9	3.44×10^{-5}
79.8	3.13×10^{-5}
86.3	2.85×10^{-5}
92.4	2.53×10^{-5}

36.8	6.31×10^{-5}
42.7	5.88×10^{-5}
40.3	5.38×10^{-5}
98.9	2.33×10^{-5}
134.9	1.10×10^{-5}

Experiment Number 121482

$[S(IV)]_T = 1.05 \times 10^{-4}$

$[\alpha\text{-}Fe_2O_3] = 2.07 \times 10^{-5}$ M

Hematite batch 1

pH = 2.46

p_{O2} = 1 atm

$\lambda > 330$ nm

I = not available

hν + reactants: 0.0 min.

Time (min)	[S(IV)], (M)
0.0	9.90×10^{-5}
2.0	9.55×10^{-5}
14.8	8.85×10^{-5}
27.9	8.27×10^{-5}
41.0	7.35×10^{-5}
53.9	7.03×10^{-5}
66.9	6.51×10^{-5}
80.0	5.95×10^{-5}
93.0	5.15×10^{-5}
106.0	4.55×10^{-5}
118.8	4.05×10^{-5}
132.8	3.42×10^{-5}
145.1	2.83×10^{-5}
166.9	2.14×10^{-5}
190.0	1.43×10^{-6}
233.7	6.20×10^{-6}

Experiment Number 121582

$[S(IV)]_T = 1.13 \times 10^{-4}$ M

$[\alpha\text{-}Fe_2O_3] = 8.25 \times 10^{-5}$ M

Hematite batch 1

pH = 2.47

p_{O2} = 1 atm.

$\lambda > 330$ nm

I = not available

hν + reactants: 0.0 min.

Time (min)	[S(IV)], (M)
0.0	1.07×10^{-4}
1.5	1.05×10^{-4}
3.9	9.38×10^{-5}
5.6	9.05×10^{-5}
7.4	8.71×10^{-5}
9.1	8.46×10^{-5}
11.0	8.17×10^{-5}
12.8	7.84×10^{-5}
14.5	7.57×10^{-5}
16.2	7.37×10^{-5}
18.6	6.90×10^{-5}
22.1	6.46×10^{-5}
31.9	4.96×10^{-5}
37.9	4.00×10^{-5}
44.9	3.12×10^{-5}
52.4	3.52×10^{-5}
62.0	1.61×10^{-5}
70.8	1.08×10^{-5}

Experiment Number 011083

$[S(IV)]_T = 1.05 \times 10^{-4}$ M

$[\alpha\text{-}Fe_2O_3] = 1.04 \times 10^{-5}$ M

Hematite batch 1

pH = 2.46

p_{O2} = 1 atm

$\lambda > 330$ nm

I = not available

hν + reactants: 0.0 min.

Time (min)	[S(IV)], (M)
0.0	1.02×10^{-4}
1.1	1.02×10^{-4}
15.1	9.64×10^{-5}
30.0	9.14×10^{-5}
45.0	8.70×10^{-5}
59.9	8.21×10^{-5}
75.3	7.64×10^{-5}
110.5	6.43×10^{-5}
130.1	5.70×10^{-5}
150.5	5.04×10^{-5}
176.3	3.35×10^{-5}
200.1	2.56×10^{-5}
230.5	1.64×10^{-6}
260.0	9.68×10^{-6}
300.1	4.98×10^{-6}

Experiment Number 011283

$[S(IV)]_T = 1.97 \times 10^{-4}$ M

$[\alpha\text{-}Fe_2O_3] = 8.25 \times 10^{-5}$ M

Hematite batch 1

pH = 2.48

p_{O2} = 1 atm.

$\lambda > 330$ nm

I = not available

hν + reactants: 0.0 min.

Time (min)	[S(IV)], (M)
0.0	1.97×10^{-4}
1.8	1.89×10^{-4}
5.1	1.81×10^{-4}
8.0	1.75×10^{-4}
11.0	1.69×10^{-4}
14.0	1.64×10^{-4}
18.0	1.53×10^{-4}
22.0	1.49×10^{-4}
27.1	1.38×10^{-4}
33.1	1.30×10^{-4}
40.0	1.17×10^{-4}
48.0	1.01×10^{-5}
56.9	8.13×10^{-5}
66.9	6.17×10^{-5}
79.0	4.12×10^{-5}
90.1	2.61×10^{-5}
102.0	1.57×10^{-5}
114.9	8.09×10^{-6}

Experiment Number 012583

$[S(IV)]_T = 5.63 \times 10^{-5}$ M

$[\alpha\text{-}Fe_2O_3] = 8.25 \times 10^{-5}$ M

Hematite batch 1

pH = 2.45

p_{O2} = 1 atm.

$\lambda > 330$ nm

I = not available

hν + reactants: 0.0 min.

Time (min)	[S(IV)], (M)
0.0	5.14×10^{-5}
1.2	4.61×10^{-5}
3.0	4.07×10^{-5}
5.1	3.75×10^{-5}
6.6	3.49×10^{-5}
7.7	3.39×10^{-5}
13.5	2.67×10^{-5}
15.0	2.46×10^{-5}
16.9	2.26×10^{-5}
20.0	2.07×10^{-5}
23.0	1.80×10^{-5}
27.1	1.50×10^{-5}

9.1	3.13×10^{-5}
10.6	3.02×10^{-5}
12.1	2.81×10^{-5}
31.0	1.22×10^{-5}
36.0	9.58×10^{-6}
42.0	7.02×10^{-6}

Experiment Number 012683

$[S(IV)]_T = 2.72 \times 10^{-5}$ M

$[\alpha\text{-}Fe_2O_3] = 8.25 \times 10^{-5}$ M

Hematite batch 1

pH = 2.44

p_{O2} = 1 atm.

$\lambda > 330$ nm

I = not available

hν + reactants: 0.0 min.

Time (min)	[S(IV)], (M)
0.0	2.38×10^{-5}
2.1	1.84×10^{-5}
3.3	1.62×10^{-5}
4.5	1.47×10^{-5}
5.7	1.35×10^{-5}
6.7	1.25×10^{-5}
7.8	1.21×10^{-5}
8.9	1.10×10^{-6}
10.8	8.27×10^{-6}
11.9	9.22×10^{-6}
12.9	8.67×10^{-6}
14.9	7.88×10^{-6}
16.2	7.30×10^{-6}
17.4	6.99×10^{-6}
18.6	6.08×10^{-6}
20.0	5.71×10^{-6}
22.0	5.08×10^{-6}
24.0	4.30×10^{-6}

Experiment Number 013183

$[S(IV)]_T = 2.73 \times 10^{-5}$ M

$[\alpha\text{-}Fe_2O_3] = 8.25 \times 10^{-5}$ M

Hematite batch 1

pH = 2.45

p_{O2} = 1 atm.

$\lambda > 330$ nm

I = not available

hν + reactants: 0.0 min.

Time (min)	[S(IV)], (M)
0.0	2.46×10^{-5}
1.2	2.06×10^{-5}
2.6	1.79×10^{-5}
3.9	1.61×10^{-5}
5.4	1.39×10^{-5}
7.0	1.25×10^{-5}
8.3	1.15×10^{-5}
9.9	1.02×10^{-5}
11.3	9.37×10^{-6}
12.6	8.57×10^{-6}
14.0	7.92×10^{-6}
15.4	6.52×10^{-6}
16.8	5.10×10^{-6}
18.2	5.57×10^{-6}
20.0	5.15×10^{-6}
21.8	4.32×10^{-6}
23.8	3.83×10^{-6}
25.8	3.33×10^{-6}
28.9	2.64×10^{-6}

Experiment Number 020183

$[S(IV)]_T = 1.46 \times 10^{-5}$ M

$[\alpha\text{-}Fe_2O_3] = 8.25 \times 10^{-5}$ M

Hematite batch 1

pH = 2.45

p_{O2} = 1 atm.

$\lambda > 330$ nm

I = not available

hν + reactants: 0.0 min.

Time (min)	[S(IV)], (M)
0.0	1.21×10^{-5}
1.5	8.45×10^{-6}
3.0	6.60×10^{-6}
4.3	5.92×10^{-6}
5.5	4.98×10^{-6}
6.6	4.43×10^{-6}
7.9	3.98×10^{-6}
9.2	5.00×10^{-6}
10.3	4.96×10^{-6}
13.8	1.79×10^{-6}
15.0	1.57×10^{-6}
16.2	1.73×10^{-6}
17.3	9.76×10^{-6}
18.4	9.76×10^{-7}
19.6	1.01×10^{-7}
20.7	8.81×10^{-7}
24.7	6.70×10^{-7}

Experiment Number 020283

$[S(IV)]_T = 3.32 \times 10^{-5}$ M

$[\alpha\text{-}Fe_2O_3] = 8.25 \times 10^{-5}$ M

Hematite batch 1

pH = 2.45

p_{O2} = 0 atm.

$\lambda > 330$ nm

I = not available

hν + reactants: 0.0 min.

Time (min)	[S(IV)], (M)
0.0	2.95×10^{-5}
1.2	2.93×10^{-5}
4.0	2.45×10^{-5}
7.9	2.19×10^{-5}
14.1	1.84×10^{-5}
17.1	1.84×10^{-5}
21.3	1.50×10^{-5}
34.1	9.47×10^{-6}
42.3	7.28×10^{-6}
58.1	3.45×10^{-6}
68.0	2.10×10^{-6}
79.3	2.21×10^{-7}
88.1	6.94×10^{-7}
100.4	6.14×10^{-7}

Experiment Number 020783

$[S(IV)]_T = 1.38 \times 10^{-5}$ M

$[\alpha\text{-}Fe_2O_3] = 1.04 \times 10^{-5}$ M

Hematite batch 1

pH = 2.40

p_{O2} = 1 atm.

$\lambda > 330$ nm

I = not available

hν + reactants: 0.0 min.

Time (min)	[S(IV)], (M)
0.0	1.29×10^{-5}
3.4	1.13×10^{-5}
7.9	1.06×10^{-5}
11.9	1.02×10^{-5}
17.7	9.58×10^{-6}
23.2	9.27×10^{-6}
31.0	8.65×10^{-6}
42.9	7.58×10^{-6}
62.1	6.33×10^{-6}
101.6	4.68×10^{-6}

Experiment Number 020883

$[S(IV)]_T = 8.00 \times 10^{-6}$ M

$[\alpha\text{-}Fe_2O_3] = 1.04 \times 10^{-5}$ M

Hematite batch 1

pH = 2.43

p_{O2} = 1 atm.

$\lambda > 330$ nm

I = not available

hν + reactants: 0.0 min.

Time (min)	[S(IV)], (M)
0.0	6.62×10^{-6}
3.5	5.79×10^{-6}
7.3	5.62×10^{-6}
11.5	5.00×10^{-6}
16.9	5.27×10^{-6}
23.0	4.41×10^{-6}
32.2	4.52×10^{-6}
42.4	3.95×10^{-6}
61.4	3.31×10^{-6}
103.0	2.77×10^{-6}

Experiment Number 020983

$[S(IV)]_T = 2.91 \times 10^{-6}$ M

$[\alpha\text{-}Fe_2O_3] = 1.04 \times 10^{-5}$ M

Hematite batch 1

pH = 2.43

p_{O2} = 1 atm.

$\lambda > 330$ nm

I = not available

hν + reactants: 0.0 min.

Time (min)	[S(IV)], (M)
0.0	2.61×10^{-6}
3.4	2.13×10^{-6}
8.2	1.99×10^{-6}
12.3	1.69×10^{-6}
17.6	1.64×10^{-6}
23.4	1.55×10^{-6}
31.1	1.40×10^{-6}
42.6	9.59×10^{-7}
61.4	7.69×10^{-7}
90.8	6.94×10^{-7}

Experiment Number 021483

$[S(IV)]_T = 6.19 \times 10^{-6}$ M

$[\alpha\text{-}Fe_2O_3] = 8.25 \times 10^{-5}$ M

Hematite batch 1

pH = 2.44

p_{O2} = 1 atm.

$\lambda > 330$ nm

I = not available

hν + reactants: 0.0 min.

Time (min)	[S(IV)], (M)
1.65	3.56×10^{-6}
3.05	1.99×10^{-6}
4.20	1.67×10^{-6}
5.40	1.18×10^{-6}
8.00	5.32×10^{-7}
9.30	5.12×10^{-7}

Experiment Number 030883

$[S(IV)]_T = 4.20 \times 10^{-5}$ M

$[\alpha\text{-}Fe_2O_3] = 8.25 \times 10^{-5}$ M

Hematite batch 1

pH = 1.95

p_{O2} = 1 atm.

$\lambda > 330$ nm

I = not available

hν + reactants: 0.0 min.

Time (min)	[S(IV)], (M)
0.0	2.54×10^{-5}
1.6	1.99×10^{-5}
3.0	1.73×10^{-5}
4.4	1.63×10^{-5}
5.8	1.52×10^{-5}
7.4	1.33×10^{-5}
9.0	1.22×10^{-5}
12.0	1.04×10^{-5}
16.0	8.81×10^{-6}
21.1	6.31×10^{-6}
27.1	4.94×10^{-6}
34.0	4.47×10^{-6}
42.0	4.27×10^{-6}
51.1	1.52×10^{-6}
61.2	5.33×10^{-7}

Experiment Number 030983

$[S(IV)]_T = 2.85 \times 10^{-5}$ M

$[\alpha\text{-}Fe_2O_3] = 8.25 \times 10^{-5}$ M

Hematite batch 1

pH = 2.96

p_{O2} = 1 atm.

$\lambda > 330$ nm

I = not available

hν + reactants: 0.0 min.

Time (min)	[S(IV)], (M)
0.0	2.69×10^{-5}
1.3	2.36×10^{-5}
2.7	2.15×10^{-5}
3.9	1.73×10^{-5}
5.3	1.67×10^{-5}
6.8	1.37×10^{-5}
8.1	1.29×10^{-5}
9.7	9.76×10^{-6}
12.0	7.94×10^{-6}
17.5	4.38×10^{-6}
27.1	1.35×10^{-6}
33.9	1.69×10^{-6}
42.0	8.72×10^{-7}

Experiment Number 031583

$[S(IV)]_T = 2.64 \times 10^{-5}$ M

$[\alpha\text{-}Fe_2O_3] = 8.25 \times 10^{-5}$ M

Hematite batch 1

pH = 3.38-3.13

p_{O2} = 1 atm.

$\lambda > 330$ nm

I = not available

hν + reactants: 0.0 min.

Time (min)	[S(IV)], (M)
0.0	2.40×10^{-5}
1.0	2.20×10^{-5}
2.5	1.88×10^{-5}
3.8	1.65×10^{-5}
5.2	1.43×10^{-5}
6.6	1.24×10^{-5}
8.3	9.73×10^{-6}
11.7	7.60×10^{-6}
14.1	4.65×10^{-6}
16.2	4.68×10^{-6}
18.0	3.05×10^{-6}
21.0	2.71×10^{-6}
25.6	1.04×10^{-6}
30.1	2.00×10^{-6}

10.0	8.17×10^{-6}
36.1	1.26×10^{-6}

Experiment Number 031683

$[S(IV)]_T = 2.94 \times 10^{-5}$ M

$[\alpha\text{-}Fe_2O_3] = 8.25 \times 10^{-5}$ M

Hematite batch 1

pH = 1.63

p_{O2} = 1 atm.

$\lambda > 330$ nm

I = not available

hν + reactants: 0.0 min.

Time (min)	[S(IV)], (M)
0.0	2.64×10^{-5}
1.3	2.11×10^{-5}
2.9	1.93×10^{-5}
4.2	1.84×10^{-5}
5.5	1.78×10^{-5}
7.0	1.57×10^{-5}
8.7	1.50×10^{-5}
10.1	1.42×10^{-5}
12.0	1.29×10^{-5}
14.1	1.07×10^{-5}
19.1	9.08×10^{-6}
24.0	7.48×10^{-6}
29.8	5.89×10^{-6}
37.0	3.08×10^{-6}
45.0	2.36×10^{-6}
54.1	1.74×10^{-6}
65.2	7.64×10^{-7}
77.1	4.26×10^{-7}

Experiment Number 030783

$[S(IV)]_T = 6.36 \times 10^{-5}$ M

$[\alpha\text{-}Fe_2O_3] = 0$

Hematite batch 1

pH = 2.45

p_{O2} = 1 atm.

$\lambda > 330$ nm

I = not available

hν + reactants: 0.0 min.

Time (min)	[S(IV)], (M)
0.0	6.36×10^{-5}
1.8	6.06×10^{-5}
16.5	5.78×10^{-5}
31.5	5.75×10^{-5}
48.3	5.71×10^{-5}
61.1	5.68×10^{-5}
79.5	5.65×10^{-5}
107.4	5.56×10^{-5}
143.2	5.42×10^{-5}
180.0	5.31×10^{-5}
223.7	5.16×10^{-5}
301.8	4.89×10^{-5}
348.2	4.74×10^{-5}
415.0	4.64×10^{-5}

Experiment Number 032883

$[S(IV)]_T = 2.96 \times 10^{-5}$ M

$[\alpha\text{-}Fe_2O_3] = 8.25 \times 10^{-5}$ M

Hematite batch 1

pH = 1.44

p_{O2} = 1 atm.

$\lambda > 330$ nm

I = not available

hν + reactants: 0.0 min.

Time (min)	[S(IV)], (M)
0.0	2.46×10^{-5}
1.5	2.11×10^{-5}
2.8	1.99×10^{-5}
4.1	1.89×10^{-5}
5.7	1.75×10^{-5}
15.3	1.24×10^{-5}
19.1	1.06×10^{-5}
27.0	7.79×10^{-6}
31.2	7.06×10^{-6}
38.1	5.40×10^{-6}

7.1	1.67×10^{-5}
8.6	1.63×10^{-5}
10.0	1.42×10^{-5}
12.1	1.37×10^{-5}
45.3	4.65×10^{-6}
54.1	3.34×10^{-6}
65.3	2.48×10^{-6}
78.2	1.50×10^{-6}
90.0	9.22×10^{-7}

Experiment Number 032983

$[S(IV)]_T = 2.89 \times 10^{-5}$ M

$[\alpha\text{-}Fe_2O_3] = 8.25 \times 10^{-5}$ M

Hematite batch 1

pH = 1.26

p_{O2} = 1 atm.

$\lambda > 330$ nm

I = not available

hν + reactants: 0.0 min.

Time (min)	[S(IV)], (M)
0.0	2.44×10^{-5}
1.1	2.16×10^{-5}
2.9	2.06×10^{-5}
4.4	1.94×10^{-5}
6.0	1.84×10^{-5}
7.5	1.77×10^{-5}
9.1	1.66×10^{-5}
12.1	1.58×10^{-5}
16.35	1.38×10^{-5}
21.1	1.24×10^{-5}
27.1	1.10×10^{-5}
39.1	8.20×10^{-6}
50.1	6.71×10^{-6}
61.0	5.26×10^{-6}
72.2	4.04×10^{-6}
83.1	3.16×10^{-6}
96.6	2.22×10^{-6}
111.2	1.48×10^{-6}

Experiment Number 033083

$[S(IV)]_T = 2.71 \times 10^{-5}$ M

$[\alpha\text{-}Fe_2O_3] = 8.25 \times 10^{-5}$ M

Hematite batch 1

pH = 1.08

p_{O2} = 1 atm.

$\lambda > 330$ nm

I = not available

hν + reactants: 0.0 min.

Time (min)	[S(IV)], (M)
0.0	2.35×10^{-5}
1.3	2.10×10^{-5}
3.0	2.00×10^{-5}
4.4	1.91×10^{-5}
6.0	1.82×10^{-5}
7.5	1.82×10^{-5}
9.1	1.77×10^{-5}
11.8	1.65×10^{-5}
16.0	1.49×10^{-5}
21.3	1.35×10^{-5}
27.2	1.19×10^{-5}
34.0	1.02×10^{-5}
42.0	9.64×10^{-6}
52.5	8.04×10^{-6}
61.0	7.47×10^{-6}
72.3	6.26×10^{-6}
83.0	4.81×10^{-6}
95.2	4.34×10^{-6}
108.0	3.34×10^{-6}

Experiment Number 081683

$[S(IV)]_T = 8.68 \times 10^{-5}$ M

$[\alpha\text{-}Fe_2O_3] = 2.46 \times 10^{-5}$ M

Hematite batch 1

pH = 2.42

p_{O2} = 1 atm.

λ = 452 nm

I = not available

hν + reactants: 30.0 min.

Time (min)	[S(IV)], (M)
3.0	6.99×10^{-5}
7.7	7.84×10^{-5}
13.6	7.96×10^{-5}
29.6	7.22×10^{-5}
43.3	6.34×10^{-5}
51.4	5.68×10^{-5}
62.9	5.13×10^{-5}
74.8	4.12×10^{-5}
90.8	3.64×10^{-5}
105.5	3.03×10^{-5}
121.9	2.48×10^{-5}
143.9	1.87×10^{-5}
176.1	1.23×10^{-6}
190.0	9.77×10^{-6}
223.0	6.09×10^{-6}
249.7	4.60×10^{-6}
278.6	3.18×10^{-6}

Experiment Number 082383

$[S(IV)]_T = 9.44 \times 10^{-5}$ M

$[\alpha\text{-}Fe_2O_3] = 2.46 \times 10^{-5}$ M

Hematite batch 1

pH = 2.43

p_{O2} = 1 atm.

λ = 520 nm

I = not available

hν + reactants: 60.0 min.

Time (min)	[S(IV)], (M)
0.0	9.44×10^{-5}
3.2	8.43×10^{-5}
6.6	8.66×10^{-5}
12.0	8.60×10^{-5}
21.8	8.51×10^{-5}
30.7	8.51×10^{-5}
45.3	8.42×10^{-5}
60.0	8.21×10^{-5}
65.0	8.00×10^{-5}
71.2	7.93×10^{-5}
75.5	7.83×10^{-5}
85.5	7.57×10^{-5}
99.7	7.03×10^{-5}
123.5	6.21×10^{-5}
132.6	5.98×10^{-5}
151.0	5.48×10^{-5}
181.8	4.30×10^{-5}
209.5	3.50×10^{-5}
239.8	2.76×10^{-5}
270.0	2.01×10^{-5}
302.2	1.43×10^{-5}
330.3	9.92×10^{-6}

Experiment Number 082583

$[S(IV)]_T = 9.59 \times 10^{-5}$ M

$[\alpha\text{-}Fe_2O_3] = 2.46 \times 10^{-5}$ M

Hematite batch 1

pH = 2.41

p_{O2} = 1 atm.

λ = 600 nm

I = not available

hν + reactants: 60.0 min.

Time (min)	[S(IV)], (M)
0.0	9.59×10^{-5}
3.5	8.48×10^{-5}
6.0	8.65×10^{-5}
100.1	7.98×10^{-5}
116.8	7.86×10^{-5}
131.0	7.82×10^{-5}

13.7	8.64×10^{-5}
29.0	8.55×10^{-5}
46.1	8.47×10^{-5}
59.6	8.43×10^{-5}
65.1	8.42×10^{-5}
71.6	8.22×10^{-5}
77.2	8.22×10^{-5}
86.6	8.25×10^{-5}
152.3	7.86×10^{-5}
181.8	7.18×10^{-5}
210.1	6.65×10^{-5}
242.3	6.60×10^{-5}
270.6	6.15×10^{-5}
300.5	5.74×10^{-5}
343.1	4.93×10^{-5}
391.5	4.09×10^{-5}

Experiment Number 100783

$[S(IV)]_T = 9.75 \times 10^{-3}$ M

$[\alpha\text{-}Fe_2O_3] = 2.05 \times 10^{-4}$ M

Hematite batch 2

pH = 1.84-1.90

$[O_2(aq)]_o = 2.05 \times 10^{-4}$ M

λ = 452 nm

I = not available

$h\nu$ + reactants: 39.0 min.

Time (min)	$[O_2(aq)]$, (M)
0.0	2.05×10^{-4}
4.2	2.03×10^{-4}
10.0	2.01×10^{-4}
17.2	2.01×10^{-4}
29.5	2.01×10^{-4}
38.2	2.01×10^{-4}
49.0	1.99×10^{-4}
56.0	1.97×10^{-4}
63.2	1.94×10^{-4}
75.3	1.90×10^{-4}
85.0	1.86×10^{-4}
91.5	1.83×10^{-4}
101.0	1.79×10^{-4}
111.9	1.73×10^{-4}
131.5	1.58×10^{-4}
144.5	1.44×10^{-4}
158.3	1.24×10^{-4}
161.1	1.19×10^{-4}
164.1	1.14×10^{-4}
167.3	1.07×10^{-4}
169.9	1.01×10^{-4}
172.1	9.56×10^{-5}
175.1	8.78×10^{-5}
177.9	8.00×10^{-5}
179.8	7.44×10^{-5}
182.0	6.75×10^{-5}
184.3	5.97×10^{-5}
186.3	5.31×10^{-5}
187.6	4.69×10^{-5}
189.1	4.34×10^{-5}
190.6	3.75×10^{-5}
192.2	3.13×10^{-5}
193.0	2.81×10^{-5}
193.9	2.50×10^{-5}
194.7	2.19×10^{-5}
195.5	1.88×10^{-5}
196.3	1.56×10^{-5}
197.1	1.25×10^{-5}
197.9	9.38×10^{-6}
198.7	6.25×10^{-6}
199.6	5.72×10^{-6}

Experiment Number 101083

$[S(IV)]_T = 9.75 \times 10^{-3}$ M

$[\alpha\text{-}Fe_2O_3] = 9.87 \times 10^{-5}$ M

Hematite batch 2

pH = 1.86

$[O_2(aq)]_o = 1.51 \times 10^{-4}$ M

λ = 452 nm

I = not available

$h\nu$ + reactants: 39.0 min.

Time (min)	$[O_2(aq)]$, (M)
0.0	1.51×10^{-4}
4.3	1.50×10^{-4}
9.2	1.49×10^{-4}
159.5	7.41×10^{-5}
164.0	6.88×10^{-5}
165.6	6.25×10^{-5}

17.5	1.48×10^{-4}
25.5	1.49×10^{-4}
39.0	1.48×10^{-4}
50.4	1.46×10^{-4}
61.5	1.43×10^{-4}
71.3	1.40×10^{-4}
80.0	1.36×10^{-4}
93.8	1.31×10^{-4}
101.4	1.27×10^{-4}
111.1	1.22×10^{-4}
119.7	1.17×10^{-4}
127.1	1.11×10^{-4}
134.8	1.05×10^{-4}
140.5	9.94×10^{-5}
144.9	9.44×10^{-5}
149.8	8.84×10^{-5}
154.5	8.19×10^{-5}
168.0	5.69×10^{-5}
170.7	5.09×10^{-5}
173.2	4.47×10^{-5}
175.5	3.84×10^{-5}
178.1	3.13×10^{-5}
179.2	2.81×10^{-5}
180.3	2.50×10^{-5}
181.8	2.03×10^{-5}
182.4	1.88×10^{-5}
183.3	1.56×10^{-5}
184.3	1.25×10^{-5}
185.3	9.38×10^{-6}
186.0	7.03×10^{-6}
186.7	6.44×10^{-6}
263.0	7.31×10^{-6}
305.0	6.88×10^{-6}

Experiment Number 012684

$[\text{salicylate}]_T = 9.84 \times 10^{-3}$ M

$[\alpha\text{-}Fe_2O_3] = 5.00 \times 10^{-4}$

Hematite batch 2

pH = 5.49-5.57

$p_{O2} = 0.21$ atm.

$\lambda = 452$ nm

I = not available

hν + reactants: 47.0 min.

Time (min)	$[Fe(II)_{aq}]$, (M)
3.0	Not detectable
44.4	Not detectable
51.3	Not detectable
60.0	Not detectable
69.5	Not detectable
82.1	Not detectable
90.0	Not detectable
100.4	Not detectable
112.3	Not detectable
121.2	Not detectable
130.6	Not detectable
141.1	Not detectable

Experiment Number 020384

$[S(IV)]_T = 4.54 \times 10^{-5}$ M

$[\alpha\text{-}Fe_2O_3] = 1.00 \times 10^{-4}$ M

Hematite batch 2

[Superoxide dismutase] = 10 ug/L

pH = 7.46-7.65

$p_{O2} = 0.21$ atm.

$\lambda = 452$ nm

I = not available

[EDTA] = 5.0 μM

hν + reactants: 0.0 min.

Time (min)	[S(IV)], (M)
0.0	4.54×10^{-5}
0.5	4.44×10^{-5}
9.4	3.95×10^{-5}
28.2	3.18×10^{-5}
37.0	2.89×10^{-5}
48.3	2.54×10^{-5}
56.6	2.25×10^{-5}
79.5	1.72×10^{-5}
90.2	1.51×10^{-5}
99.4	1.32×10^{-5}
109.6	1.08×10^{-5}
119.1	9.33×10^{-6}
173.4	4.60×10^{-6}

69.5	1.94×10^{-5}

Experiment Number 020684

$[S(IV)]_T = 4.34 \times 10^{-5}$ M

$[\alpha\text{-}Fe_2O_3] = 1.00 \times 10^{-4}$ M

Hematite batch 2

pH = 7.42-7.55

$p_{O2} = 0.21$ atm.

$\lambda = 452$ nm

I = not available

hν + reactants: 0.0 min.

Time (min)	[S(IV)], (M)
0.0	4.34×10^{-5}
0.2	4.15×10^{-5}
5.0	3.98×10^{-5}
15.1	3.63×10^{-5}
24.0	3.37×10^{-5}
35.0	2.96×10^{-5}
45.0	2.56×10^{-5}
55.0	2.17×10^{-5}
65.0	1.87×10^{-5}
75.4	1.62×10^{-5}
90.4	1.33×10^{-5}
105.4	1.13×10^{-5}
129.5	8.45×10^{-6}
165.3	5.95×10^{-6}
178.0	5.27×10^{-6}

Experiment Number 020884

$[S(IV)]_T = 4.12 \times 10^{-5}$ M

$[\alpha\text{-}Fe_2O_3] = 1.00 \times 10^{-4}$ M

Hematite batch 2

[Catalase] = 10.5 ug/L

pH = 7.45-7.53

$p_{O2} = 0.21$ atm.

$\lambda = 452$ nm

I = not available

[EDTA] = 5.0 μM

hν + reactants: 0.0 min.

Time (min)	[S(IV)], (M)
0.0	4.12×10^{-5}
0.5	4.36×10^{-5}
10.1	3.54×10^{-5}
20.0	2.98×10^{-5}
31.9	2.44×10^{-5}
40.0	2.06×10^{-5}
50.0	1.82×10^{-5}
59.9	1.65×10^{-5}
74.3	1.43×10^{-5}
95.0	1.20×10^{-5}
106.5	1.11×10^{-5}
120.0	9.64×10^{-6}
143.6	7.51×10^{-5}
227.5	4.01×10^{-5}

Experiment Number 021084

$[S(IV)]_T = 4.38 \times 10^{-5}$ M

$[\alpha\text{-}Fe_2O_3] = 1.00 \times 10^{-4}$ M

Hematite batch 2

[Mannitol] = 10 μM

pH = 7.35-7.42

$p_{O2} = 0.21$ atm.

$\lambda = 452$ nm

I = not available

[EDTA] = 5.0 μM

hν + reactants: 0.0 min.

Time (min)	[S(IV)], (M)
0.0	4.38×10^{-5}
0.5	4.25×10^{-5}
10.0	3.57×10^{-5}
60.1	1.89×10^{-5}
75.1	1.45×10^{-5}
90.0	1.15×10^{-5}

20.1	3.15×10^{-5}
30.1	2.58×10^{-5}
40.0	2.45×10^{-5}
50.0	2.19×10^{-5}
110.1	8.66×10^{-6}
130.2	6.89×10^{-6}
150.0	5.42×10^{-6}
170.0	4.07×10^{-6}
190.5	3.49×10^{-6}

Experiment Number 021484

$[S(IV)]_T = 2.16 \times 10^{-4}$ M

$[\alpha\text{-}Fe_2O_3] = 1.00 \times 10^{-4}$

Hematite batch 2

pH = 2.43-2.46

$p_{O2} = 2.36 \times 10^{-4}$ atm.

Mλ = 452 nm

I = not available

hν + reactants: 0.0 min.

Time (min)	[S(IV)], (M)
0.0	1.72×10^{-4}
0.4	1.76×10^{-4}
8.0	1.64×10^{-4}
13.3	1.63×10^{-4}
23.0	1.59×10^{-4}
32.2	1.58×10^{-4}
44.5	1.53×10^{-4}
64.1	1.40×10^{-4}
89.5	1.27×10^{-4}
108.8	1.16×10^{-4}
127.3	1.05×10^{-5}
148.9	9.06×10^{-5}
171.8	7.60×10^{-5}
198.0	5.92×10^{-5}

Experiment Number 030784

$[S(IV)]_T = 1.89 \times 10^{-5}$ M

$[\alpha\text{-}Fe_2O_3] = 7.57 \times 10^{-4}$ M

Hematite batch 2

pH = 2.94

$p_{O2} = 0.21$ atm.

λ = 452 nm

I = 14.5 μE/L-min.

hν + reactants: 10.2 min.

Time (min)	[S(IV)], (M)
0.2	7.26×10^{-6}
4.8	6.45×10^{-6}
9.8	5.38×10^{-6}
15.1	4.74×10^{-6}
25.0	3.69×10^{-6}
49.8	1.94×10^{-6}
65.0	1.43×10^{-6}
80.0	1.16×10^{-6}

Experiment Number 030884

$[S(IV)]_T = 2.13 \times 10^{-5}$ M

$[\alpha\text{-}Fe_2O_3] = 7.57 \times 10^{-4}$ M

Hematite batch 2

pH = 2.95-2.96

$p_{O2} = 0.21$ atm.

λ = 375 nm

I = 4.9 μE/L min.

hν + reactants: 10.1 min.

Time (min)	[S(IV)], (M)
2.7	9.47×10^{-6}
5.7	8.85×10^{-6}
9.9	7.82×10^{-6}
14.9	7.17×10^{-6}
34.1	4.24×10^{-6}
50.0	2.55×10^{-6}
64.1	1.99×10^{-6}
24.1	5.66×10^{-6}

Experiment Number 031384

$[S(IV)]_T = 5.99 \times 10^{-5}$ M

$[\alpha\text{-}Fe_2O_3] = 7.50 \times 10^{-4}$ M

Hematite batch 2

pH = 2.90-2.92

p_{O2} = 0.21 atm.

λ = 452 nm

I = 13.0 μE/L min.

hν + reactants: 10.3 min.

Time (min)	[S(IV)], (M)
0.2	4.20×10^{-5}
5.1	4.15×10^{-5}
12.1	3.93×10^{-5}
15.8	3.77×10^{-5}
24.7	3.42×10^{-5}
34.7	2.82×10^{-5}
49.7	1.49×10^{-6}
65.8	4.98×10^{-6}
83.7	1.57×10^{-6}

Experiment Number 031484

$[S(IV)]_T = 6.13 \times 10^{-5}$ M

$[\alpha\text{-}Fe_2O_3] = 7.50 \times 10^{-4}$ M

Hematite batch 2

pH = 2.93

p_{O2} = 0.21 atm.

λ = 375 nm

I = 5.2 μE/L min.

hν + reactants: 10.4 min.

Time (min)	[S(IV)], (M)
0.2	4.35×10^{-5}
5.2	4.18×10^{-5}
9.7	3.77×10^{-5}
14.8	3.90×10^{-5}
25.1	3.37×10^{-5}
34.8	2.78×10^{-5}
49.7	1.35×10^{-6}
64.7	5.02×10^{-6}
82.6	1.97×10^{-6}

Experiment Number 032384

$[S(IV)]_T = 2.01 \times 10^{-4}$ M

$[\alpha\text{-}Fe_2O_3] = 7.50 \times 10^{-4}$ M

Hematite batch 2

pH = 2.88-2.90

N_2 flow, p_{O2} = 0 atm.

λ = 452 nm

I = 11.9 μE/L min.

hν + reactants: 10.0 min.

Time (min)	$[Fe(II)_{aq}]$, (M)
0.1	1.10×10^{-6}
5.1	1.55×10^{-6}
10.0	1.99×10^{-6}
15.1	2.30×10^{-6}
25.0	2.95×10^{-6}
35.0	3.41×10^{-6}
50.0	4.22×10^{-6}
65.0	4.88×10^{-6}
80.0	5.69×10^{-6}
100.0	6.63×10^{-6}
120.0	7.28×10^{-6}
140.5	8.01×10^{-6}
160.1	9.00×10^{-6}
180.2	9.89×10^{-6}
200.0	1.03×10^{-5}

Experiment Number 032684

$[S(IV)]_T = 2.01 \times 10^{-4}$ M

$[\alpha\text{-}Fe_2O_3] = 7.50 \times 10^{-4}$ M

Hematite batch 2

pH = 2.87-2.92

N_2 flow, p_{O2} = 0 atm.

λ = 504 nm

I = 12.6 μE/L min.

hν + reactants: 10.0 min.

Time (min)	$[Fe(II)_{aq}]$, (M)
0.4	1.31×10^{-6}
6.6	1.47×10^{-6}
11.3	1.89×10^{-6}
15.8	2.18×10^{-6}
25.0	2.50×10^{-6}
36.6	3.11×10^{-6}
52.1	3.32×10^{-6}
65.3	4.82×10^{-6}
80.1	4.82×10^{-6}
95.1	5.68×10^{-6}
110.0	5.98×10^{-6}
125.0	6.39×10^{-6}
140.9	7.58×10^{-6}
160.3	8.16×10^{-6}
181.3	8.54×10^{-6}
200.0	8.49×10^{-6}

Experiment Number 032784

$[S(IV)]_T = 2.01 \times 10^{-4}$ M

$[\alpha\text{-}Fe_2O_3] = 7.50 \times 10^{-4}$ M

Hematite batch 2

pH = 2.88

N_2 flow, p_{O2} = 0 atm.

λ = 585 nm

I = 11.9 μE/L min.

hν + reactants: 10.0 min.

Time (min)	$[Fe(II)_{aq}]$, (M)
0.2	7.26×10^{-7}
5.4	1.02×10^{-6}
10.4	1.18×10^{-6}
16.8	1.38×10^{-6}
25.0	1.49×10^{-6}
35.0	2.03×10^{-6}
50.0	2.46×10^{-6}
65.0	2.91×10^{-6}
80.0	3.09×10^{-6}
95.0	3.62×10^{-6}
110.1	3.94×10^{-6}
126.5	4.32×10^{-6}
140.0	4.75×10^{-6}
165.1	5.61×10^{-6}
181.5	5.36×10^{-6}
200.0	5.46×10^{-6}

Experiment Number 032884

$[S(IV)]_T = 2.01 \times 10^{-4}$ M

$[\alpha\text{-}Fe_2O_3] = 7.50 \times 10^{-4}$ M

Hematite batch 2

pH = 2.86-2.94

N_2 flow, p_{O2} = 0 atm.

λ = 676 nm

I = 3.7 μE/L min.

hν + reactants: 10.0 min.

Time (min)	$[Fe(II)_{aq}]$, (M)
0.3	2.83×10^{-7}
7.0	2.15×10^{-7}
11.0	3.17×10^{-7}
16.5	5.30×10^{-7}
25.1	4.28×10^{-7}
35.3	4.71×10^{-7}
50.0	6.07×10^{-7}
80.7	7.26×10^{-7}
96.5	8.80×10^{-7}
109.4	8.88×10^{-7}
122.0	9.82×10^{-7}
198.0	1.42×10^{-6}
303.9	1.63×10^{-6}
359.3	1.62×10^{-6}

66.6	6.92×10^{-7}
385.3	1.63×10^{-6}

Experiment Number 040284

$[S(IV)]_T = 2.01 \times 10^{-4}$ M

$[\alpha\text{-}Fe_2O_3] = 7.50 \times 10^{-4}$ M

Hematite batch 2

pH = 2.86-2.92

N_2 flow, p_{O2} = 0 atm.

λ = 392 nm

I = 5.2 μE/L min.

hν + reactants: 11.0 min.

Time (min)	$[Fe(II)_{aq}]$, (M)
0.3	8.87×10^{-7}
5.3	1.12×10^{-6}
10.5	1.51×10^{-6}
15.8	1.89×10^{-6}
24.4	2.26×10^{-6}
34.0	2.76×10^{-6}
50.7	3.65×10^{-6}
64.0	4.28×10^{-6}
79.7	5.02×10^{-6}
94.2	5.60×10^{-6}
109.0	5.18×10^{-6}
127.0	6.62×10^{-6}
139.0	7.19×10^{-6}
159.0	7.98×10^{-6}
179.0	8.45×10^{-6}
199.0	9.07×10^{-6}

Experiment Number 040384

$[S(IV)]_T = 2.01 \times 10^{-4}$ M

$[\alpha\text{-}Fe_2O_3] = 7.50 \times 10^{-4}$ M

Hematite batch 2

pH = 2.90-2.95

N_2 flow, p_{O2} = 0 atm.

λ = 350 nm

I = 0.86 μE/L min.

hν + reactants: 10.1 min.

Time (min)	$[Fe(II)_{aq}]$, (M)
0.1	4.04×10^{-7}
0.3	4.21×10^{-7}
6.3	6.07×10^{-7}
10.2	6.92×10^{-7}
15.3	9.38×10^{-7}
25.4	1.28×10^{-6}
36.3	1.35×10^{-6}
49.9	1.82×10^{-6}
64.9	2.29×10^{-6}
82.0	2.52×10^{-6}
101.9	3.07×10^{-6}
115.5	3.39×10^{-6}
126.2	3.59×10^{-6}
146.0	3.96×10^{-6} [a]
164.2	4.30×10^{-6}
179.4	4.53×10^{-6}
204.1	5.20×10^{-6}

Experiment Number 040484

$[S(IV)]_T = 2.01 \times 10^{-4}$ M

$[\alpha\text{-}Fe_2O_3] = 7.50 \times 10^{-4}$ M

Hematite batch 2

pH = 2.88

N_2 flow, p_{O2} = 0 atm.

λ = 676 nm

I = 1.5 μE/L min.

hν + reactants: 17.0 min.

Time (min)	$[Fe(II)_{aq}]$, (M)
0.1	1.83×10^{-7}
6.3	2.94×10^{-7}
23.4	3.28×10^{-7}
34.5	3.61×10^{-7}
103.8	5.73×10^{-7}
123.9	8.19×10^{-7}
142.6	6.50×10^{-7}
156.3	7.43×10^{-7}

48.6	3.87×10^{-7}
60.4	4.46×10^{-7}
74.1	5.22×10^{-7}
92.0	7.60×10^{-7}
170.7	6.58×10^{-7}
187.9	8.53×10^{-7}
197.0	7.26×10^{-7}
264.9	1.01×10^{-6}

Experiment Number 040984

$[S(IV)]_T = 2.01 \times 10^{-4}$ M

$[\alpha\text{-}Fe_2O_3] = 7.50 \times 10^{-4}$ M

Hematite batch 2

pH = 2.90-2.95

N_2 flow, $p_{O2} = 0$ atm.

λ = dark

I = 0 μE/L min.

Time (min)	$[Fe(II)_{aq}]$, (M)
10.1	1.35×10^{-7}
25.0	1.78×10^{-7}
74.4	3.90×10^{-7}
107.2	2.20×10^{-7}
202.3	3.31×10^{-7}
229.3	3.05×10^{-7}
254.5	4.76×10^{-7}
275.9	4.76×10^{-7}
300.6	4.41×10^{-7}
317.5	4.59×10^{-7}
345.7	4.67×10^{-7}
394.3	4.93×10^{-7}
561.7	6.29×10^{-7}
627.1	5.78×10^{-7}

Experiment Number 041084

$[S(IV)]_T = 2.01 \times 10^{-4}$ M

$[\alpha\text{-}Fe_2O_3] = 7.50 \times 10^{-4}$ M

Hematite batch 2

pH = 2.86-2.92

N_2 flow, $p_{O2} = 0$ atm.

λ = 416 nm

I = 12.9 μE/L min.

hν + reactants: 19.0 min.

Time (min)	$[Fe(II)_{aq}]$, (M)
0.2	6.63×10^{-7}
10.4	1.50×10^{-6}
27.1	2.07×10^{-6}
40.0	2.82×10^{-6}
53.8	3.48×10^{-6}
65.0	4.88×10^{-6}
78.8	4.70×10^{-6}
89.4	5.10×10^{-6}
104.2	5.56×10^{-6}
117.1	6.16×10^{-6}
133.9	6.60×10^{-6}
146.9	7.44×10^{-6}
157.3	7.44×10^{-6}
177.6	8.14×10^{-6}
195.3	8.61×10^{-6}

Experiment Number 041184

$[S(IV)]_T = 2.01 \times 10^{-4}$ M

$[\alpha\text{-}Fe_2O_3] = 7.50 \times 10^{-4}$ M

Hematite batch 2

pH = 2.87-2.93

N_2 flow, $p_{O2} = 0$ atm.

λ = 375 nm

I = 4.1 μE/L min.

hν + reactants: 10.0 min.

Time (min)	$[Fe(II)_{aq}]$, (M)
0.2	5.27×10^{-7}
6.8	1.09×10^{-6}
14.6	1.43×10^{-6}
80.0	4.31×10^{-6}
97.1	4.95×10^{-6}
114.2	5.71×10^{-6}

24.3	1.89×10^{-6}	122.6	5.67×10^{-6}
33.1	2.25×10^{-6}	135.1	6.16×10^{-6}
43.2	2.80×10^{-6}	155.1	6.77×10^{-6}
53.3	3.30×10^{-6}	167.0	7.35×10^{-6}
65.2	3.61×10^{-6}	280.0	9.89×10^{-6}

Experiment Number 042384

$[S(IV)]_T = 2.01 \times 10^{-4}$ M

$[\alpha\text{-}Fe_2O_3] = 7.50 \times 10^{-4}$ M

Hematite batch 2

pH = 2.92-2.93

N_2 flow, $p_{O2} = 0$ atm.

λ = dark

I = 0 μE/L min.

Time (min)	$[Fe(aq)]_T$, (M)	Time (min)	$[Fe(aq)]_T$, (M)
5.5	2.94×10^{-8}	138.4	7.88×10^{-8}
21.3	7.17×10^{-8}	154.6	8.58×10^{-8}
31.8	5.77×10^{-8}	175.5	1.21×10^{-7}
50.3	8.13×10^{-9}	195.6	1.57×10^{-7}
85.2	3.83×10^{-8}	214.6	2.13×10^{-7}
102.2	7.88×10^{-8}	231.4	2.98×10^{-7}
117.0	7.17×10^{-8}	266.9	2.20×10^{-7}
138.4	7.88×10^{-8}	359.7	3.33×10^{-7}
		439.4	4.39×10^{-7}

Experiment Number 042484

$[S(IV)]_T = 0$

$[\alpha\text{-}Fe_2O_3] = 7.50 \times 10^{-4}$

Hematite batch 2

pH = 2.94

N_2 flow, $p_{O2} = 0$ atm.

λ = 375 nm

I = 3.8 μE/L min.

hν + reactants: 0.0 min.

Time (min)	$[Fe(II)_{aq}]$, (M)	Time (min)	$[Fe(II)_{aq}]$, (M)
0.0	Not detectable	129.5	Not detectable
4.1	Not detectable	148.2	Not detectable
28.0	Not detectable	160.3	Not detectable
41.4	Not detectable	174.0	Not detectable
52.9	Not detectable	187.2	Not detectable
70.4	Not detectable	208.4	Not detectable
89.2	Not detectable	224.3	Not detectable
106.4	Not detectable	486.0	Not detectable

Experiment Number 062784 - Adsorption

pH = 2.92-2.96

λ = dark

Hematite batch 2

$p_{O2} = 0.21$ atm.

I = 0

Total [S(IV)], (M)	$[\alpha\text{-}Fe_2O_3]$, (M)	$[S(IV)]_{aq}$, (M)	$[S(IV)]_{ADS}$, (M)
2.69×10^{-6}	7.50×10^{-4}	1.2×10^{-7}	2.57×10^{-6}
5.58×10^{-6}	7.50×10^{-4}	5.1×10^{-7}	5.07×10^{-6}

8.38×10^{-6}	7.49×10^{-4}	1.9×10^{-7}	8.19×10^{-6}
1.15×10^{-5}	7.49×10^{-4}	4.5×10^{-7}	1.11×10^{-5}
1.44×10^{-5}	7.49×10^{-4}	2.0×10^{-6}	1.25×10^{-5}
1.73×10^{-5}	7.49×10^{-4}	3.4×10^{-6}	1.39×10^{-5}
2.02×10^{-5}	7.48×10^{-4}	4.9×10^{-6}	1.53×10^{-5}
2.30×10^{-5}	7.48×10^{-4}	7.0×10^{-6}	1.60×10^{-5}
2.97×10^{-5}	7.48×10^{-4}	1.3×10^{-5}	1.71×10^{-5}
6.88×10^{-5}	7.45×10^{-4}	4.8×10^{-5}	2.08×10^{-5}
1.23×10^{-4}	7.40×10^{-4}	1.0×10^{-4}	2.34×10^{-5}
2.07×10^{-4}	7.34×10^{-4}	1.8×10^{-4}	3.11×10^{-5}
3.70×10^{-4}	7.21×10^{-4}	3.3×10^{-4}	3.77×10^{-5}
1.25×10^{-3}	6.52×10^{-4}	1.2×10^{-3}	4.50×10^{-5}
			* (5.07×10^{-5})

* corrected for dilution